Underpotential Deposition at Single Crystal Surfaces of Au, Pt, Ag and Other Materials

Enrique Herrero,† Lisa J. Buller,‡ and Héctor D. Abruña*

Department of Chemistry and Chemical Biology, Baker Laboratory, Cornell University, Ithaca, New York 14853-130

Received April 17, 2000

Contents

I. Introduction

The study of the structure and dynamics of deposition of metal adsorbates on solid surfaces is of both fundamental and technological importance.[1−4] The early stages of adsorption/deposition along with the growth mechanism (e.g. nucleation and growth) can dictate the structure and properties of the deposited layer. Metal adatoms and other adsorbates at submonolayer coverage are believed to have electronic properties that can deviate significantly from those of the bulk material. In addition, the adsorbate layer may also alter the electronic properties of the substrate material itself. Such variations in electronic properties have been studied extensively in terms of their fundamental aspects as well as in their application to catalytic systems.[5,6] In addition, small metal clusters have been employed as models for solid surfaces, particularly with regards to electronic structure and chemisorptive properties.[1−4,7]

The adsorption and deposition of metal atoms on foreign metal substrates represents a very attractive family of systems for study because the strong adatom/substrate bonding can control the growth behavior and the resulting structures, especially as a function of surface coverage. Particularly attractive is the study of such systems by electrochemical means, especially within the context of underpotential deposition (UPD).[8−15] This refers to the electrodeposition of metal monolayer(s) on a foreign metal substrate at potentials that can be significantly less negative than that for deposition on the same metal surface as the adsorbate. Such phenomena allow for the precise and reproducible control of the surface coverage and for the study of coverage-dependent properties including the structure of the metallic adlayer and its electronic properties.

Early UPD studies were carried out mostly on polycrystalline electrode surfaces.[8] This was due, at least in part, to the difficulty of preparing and maintaining single-crystal electrodes under well-defined (and controlled) conditions of surface structure and cleanliness. Although some studies on metal single crystal were carried out, these typically in-

† Current address: Department of Physical Chemistry, Universidad de Alicante, Ap. Correos 99, E-03080, Alicante, Spain.
‡ Current address: Madison, WI.

10.1021/cr9600363 CCC: $36.00
Published on Web 06/09/2001

Enrique Herrero was born in Salamanca, Spain, in 1967. He received his B.S. in Chemistry from the University of Alicante (Spain) in 1990. His graduate thesis dealt with the oxidation of methanol, formic acid, and CO on platinum single crystals and was completed in 1995 at the University of Alicante under the direction of Prof. Juan M. Feliu. During this time he spent one year working with Prof. Andrzej Wieckowski at the University of Illinois at Urbana-Champaign. In 1996 he went on to a postdoctoral appointment in the group of Prof. Héctor D. Abruña in the Chemistry Department at Cornell University, where he worked on metal deposition on single crystals. He is currently an assistant professor at the University of Alicante.

Lisa Buller received a B.S. in Chemistry from the University of Wisconsin—Madison in 1992. She obtained a Ph.D. in Chemistry from Cornell University in 1997 under the direction of Prof. H. D. Abruña. Her thesis work dealt with electrochemical and X-ray studies of metal deposition onto single crystals. She is currently an assistant professor at the University of Wisconsin—Platteville.

volved the use of ultrahigh vacuum systems and transfer protocols. A wealth of information emerged from these studies; however, due to their inherent ex-situ nature they also raised some questions, especially in cases involving weakly adsorbed species, as to the precise nature/identity of the surface under study.

The advent of procedures and protocols for the preparation and cleaning of single-crystal surfaces, even of very reactive metals such as platinum, revolutionized the field, and numerous studies on single-crystal electrodes emerged.

In addition, the study and applications of UPD processes evolved from one that was mostly the domain of electrochemists to one that is now pursued in numerous disciplines including chemistry, physics, and materials science. The precise and deliberate control of surface coverage and, in some cases, structure (especially when single-crystal substrates

Héctor D. Abruña received B.S. and M.S. degrees in Chemistry from Rensselaer Polytechnic Institute in 1975 and 1976, respectively. He received a Ph.D. in Chemistry from the University of North Carolina in Chapel Hill in 1980 under the direction of R. W. Murray and T. J. Meyer. He was a postdoctoral associate under A. J. Bard at the University of Texas at Austin from 1980 to 1981. He began his academic career as an Assistant Professor in the Chemistry Department at the University of Puerto Rico in 1982. In 1983 he moved to Cornell University, where he is currently the Emile M. Chamot Professor of Chemistry. Prof. Abruña is an avid runner and prodigious consumer of espresso.

are employed) made these systems especially appealing for addressing issues related to interfacial reactivity including corrosion (and its inhibition), electrocatalysis, and others. Moreover, these systems could also serve as models to study and test predictions from theoretical models of surface structure and growth.

Although electrochemical techniques are extremely valuable for the control and measurement of thermodynamic parameters such as potential, charge, and coverage, structural (and other) conclusions derived from such measurements are of an indirect nature and dependent on the model employed. The advent of in-situ techniques eliminated much of the uncertainties involved and, as a result, generated a great deal of interest, especially when coupled to studies on single-crystal surfaces, and the techniques offered the opportunity of characterizing these systems under active electrochemical control. Of particular importance were the application of spectroscopic techniques such as FT-IR, Raman, and second-harmonic generation (SHG). The development of in-situ structural techniques based on either X-ray based methods (such as grazing incidence X-ray scattering, surface SEXAFS, and X-ray standing waves, among others) or scanned probe microcopies (STM, AFM, and related methods) further enhanced the ability to examine surfaces and surface structure at unprecedented levels of detail.

In this review we examine the underpotential deposition of metal mono- and multilayers on single-crystal electrode surfaces. The intent is to provide a broad overview of the types of systems that have been investigated and try to derive some general observations, where appropriate. We make use of not only electrochemical studies but also information derived from other techniques (especially in-situ). Although we have tried to make reference to a significant number of publications, the intent is not to be all-inclusive and we apologize for the unavoidable omissions.

We explored various strategies for presenting the material and have opted for one based on the identity of the metal substrate. We have placed most of our emphasis on platinum, gold, and silver electrodes since the vast majority of studies on well-defined single-crystal surfaces have been on these systems.

We hope that the material presented in this review will be a valuable reference source not only to electrochemists but also to the entire UPD community.

II. UPD on Gold Surfaces

1. Cu UPD on Au(*h*,*k*,*l*) Electrodes

The UPD of Cu on Au(*h*,*k*,*l*) electrodes has been studied extensively over the past, using virtually all techniques available to surface electrochemists including pure electrochemical methods (voltammetry,[12−18] chronocoulometry,[19−24] chronoamperometry,[25] ring-disk[26]), in situ STM,[27−39] AFM,[40−42] X-ray techniques (surface scattering,[43−48] SEXAFS/XANES,[44,49−57] and X-ray standing waves[58]), EQCM[44,59−61] and SHG,[62] and ex-situ UHV techniques[63−68] (LEED, AES, and RHEED). In addition to these investigations, theoretical models have been applied to Cu UPD on Au(111) electrodes,[66,69−77] which, although initially were at odds with experimental findings, were found to be consistent with them upon a reevaluation of experimental results, especially STM and AFM. All of these studies have provided a detailed knowledge, although still not complete, of these systems, especially for Cu UPD on Au(111) electrodes in sulfuric acid media. In fact, Cu UPD on Au(111) has been one of the most widely studied systems and is also a paramount example of the effects of anions and surface structure on UPD behavior as well as on surface electrochemistry.

A. Cu UPD on Au(111) in Sulfuric Acid Media

The cyclic voltammogram of Cu UPD on Au(111) shows two well-defined and sharp pairs of peaks (Figure 1), corresponding to two different adsorption/desorption processes. The pair of peaks (deposition/stripping) at high underpotentials has a broad shoulder, whereas the deposition peak at low underpotentials splits in two on high-quality Au(111) single crystals.[18,32] The peak currents for the deposition and stripping processes exhibit a marked sweep rate dependence, being proportional to the scan rate for values below 5 mV·s^{-1}.[32] However, at higher scan rates, the peak currents follow a $v^{1/2}$ dependence.[25] This behavior is the result of very slow charge-transfer kinetic processes with instantaneous nucleation and growth kinetics.[25] The splitting of the second deposition peak is the result of two different nucleation processes, one taking place on surface defects and the other on well-ordered (111) terraces;[18] thus, the dependence on the surface quality of the electrode is evident.

Two different coulometric charge values have been reported for the copper underpotential process on Au(111): one around 460 μC·cm^{-2} [32,59,60,63] and another around 350 μC·cm^{-2}.[19,20,26,66] The difference between these values is likely the result of different measurement criteria, since in arriving at the value of 350 μC·cm^{-2} a charge of zero was assigned for a potential in the middle of the broad shoulder of the first peak. The addition of the charge that would correspond to the broad shoulder would give a charge value that is very close to 450 μC·cm^{-2}. The theoretical value (based on the surface atom density) necessary for the deposition of a fully discharged monolayer of copper would be 440 μC·cm^{-2}. Out of the total charge for the copper UPD processes, about 2/3 corresponds to the first deposition peak.[19,20,25,26,32,64]

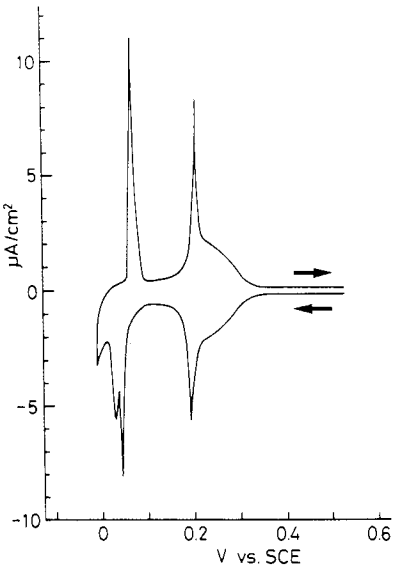

Figure 1. Cyclic voltammogram for a Au(111) electrode in 0.05 M H_2SO_4 + 1 mM $CuSO_4$. Scan rate: 1 mV·s^{-1}. Reproduced with permission from ref 32. Copyright 1991 Elsevier Sequoia SA.

Taking the electrochemical results as a point of departure, one would expect, a priori, that two different copper ad-structures would be present, one after the first deposition peak with an intermediate copper coverage (ca. 2/3) and one after the second deposition peak with a coverage close to 1. The first determinations of the structure of the Cu adlayers were done in UHV by Kolb and co-workers.[63−65] RHEED and LEED revealed two different structures that were interpreted as a $(\sqrt{3} \times \sqrt{3})R30°$ honeycomb structure with $\Theta_{Cu} = 0.67$ after the first deposition peak and a (1×1) structure ($\Theta_{Cu} = 1$) after the second deposition peak. AES measurements also indicated that (bi)sulfate adsorption on the Cu adlayers was stronger than that on the bare Au(111) electrode, in agreement with radiotracer[78,79] and FTIR[80] measurements on Cu UPD on polyoriented gold.

The first in-situ measurements on this system were done by SEXAFS, which confirmed the Cu-(1×1) structure[49,50] (Figure 2). This structure was later observed by STM[34] and AFM.[40,41] SEXAFS measurements provided an accurate determination of the Cu−Cu distance in this structure (2.92 ± 0.03,[50] 2.89 ± 0.03 Å[54]). This value is the same as the Au−Au distance (within the error of the experiment) in the (111) direction (2.92 Å), implying that the Cu-(1×1) adlayer is commensurate with the Au(111) sub-

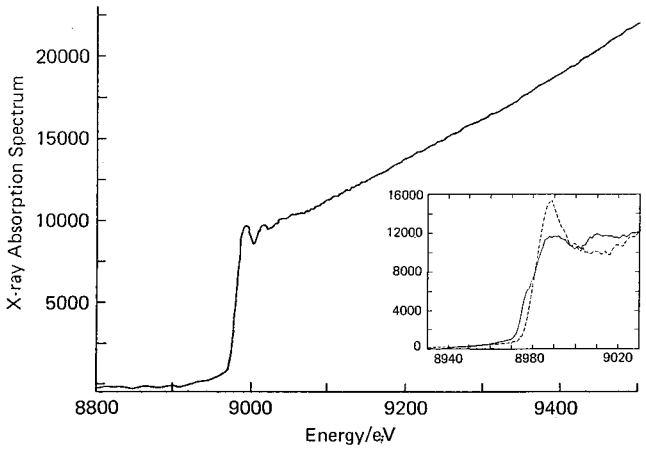

Figure 2. X-ray absorption spectra around the Cu Kα edge for CU UPD on Au(111) at +0.13 V vs Ag/AgCl. Reproduced with permission from ref 50. Copyright 1988 American Chemical Society.

strate,[50,54] as SHG results also suggest.[62] In this structure, Cu adatoms probably sit on 3-fold hollow sites, as derived from the polarization dependence of the SEXAFS[50] or by estimating the number of gold nearest neighbors.[54] SEXAFS spectra also indicate the existence of oxygen (likely arising) from (bi)-sulfate on top of the Cu adlayer.[49,54] The amount of (bi)sulfate coadsorbed on the Cu adlayer has been measured with EQCM[44,59,60] and chronocoulometry.[19,20] Results from both techniques indicate that the coverage of (bi)sulfate is the same as the maximum obtained for a clean Au(111) electrode,[19,20,24,44,59,60] although the EQCM studies[44,59−61] yield values for clean Au(111) electrodes ($\Theta_{anions} \approx 0.33$) that are significantly higher than those obtained with chronocoulometry,[81] STM,[82−84] or radiotracer[81] measurements ($\Theta_{anions} \approx 0.20$). Chronocoulometric[20,24] results also suggested that the Cu adlayer was completely discharged, whereas XANES[49,54] indicated that the oxidation state of copper was approximately +1. These two apparently contradictory results are probably a consequence of the formation of a Au−Cu polar bond (or a surface dipole) in which the Cu atom has a charge deficiency.[20,24] In this way, the complete redox reaction for the adsorption of a Cu monolayer can be written as

$$\text{Au}-\text{(bi)sulfate} + \text{Cu}^{2+} + 2\text{e}^- \leftrightarrow \text{Au}^{\delta-}-\text{Cu}^{\delta+}-\text{(bi)sulfate} \quad (1)$$

Assuming that the (bi)sulfate coverage is approximately the same on the clean and Cu-covered Au(111), the net contribution of the (bi)sulfate to the total charge would be negligible. Therefore, 440 $\mu C \cdot cm^{-2}$ of charge is expected to be transferred for the complete UPD process, in good agreement with the experimental results.[32,59,60,63]

The determination of the structure after the first UPD peak was more difficult and was, for some time, controversial. The first STM[27,28,32−34] and AFM[40] images showed a $(\sqrt{3} \times \sqrt{3})R30°$ structure (Figure 3), in which the maxima were interpreted as Cu adatoms. On the basis of this structure, the total Cu coverage was 0.33. In some cases, this structure

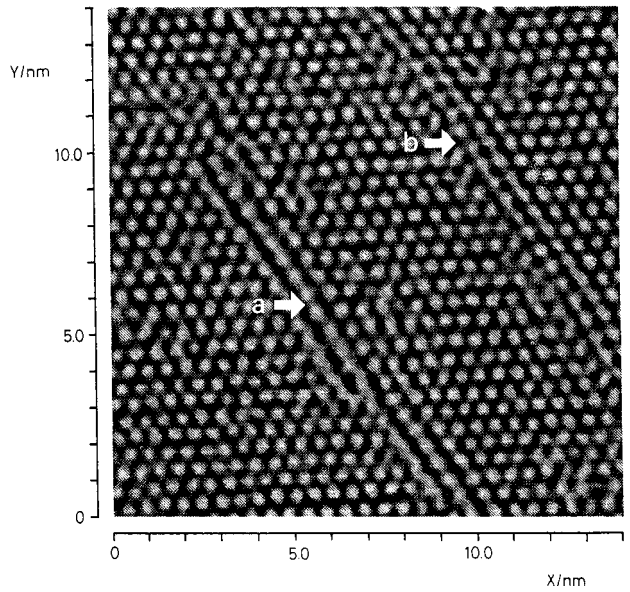

Figure 3. STM image of the $(\sqrt{3} \times \sqrt{3})R30°$ structure for Cu UPD on Au(111) at +0.15 V vs SCE showing two different phase boundaries. Reproduced with permission from ref 32. Copyright 1991 Elsevier Sequoia SA.

evolved with time to form a "(5 × 5)" structure,[27,28,34] induced by the presence of chloride contamination form the reference electrode.[29,41] The $\Theta_{Cu} = 0.33$ was in clear disagreement with the results from chronocoulometry and EQCM, which indicated that the Cu coverage in the adlayer at these potentials was 0.67 and the (bi)sulfate coverage value was 0.33.[19,20,24,44,59,60] Also theoretical calculations predicted the formation of a honeycomb $(\sqrt{3} \times \sqrt{3})R30°$ structure,[69−74] similar to that found in UHV.[63−65] This apparent contradiction was reconciled by Toney et al. using X-ray reflectance spectroscopy.[43] They found that the Cu adlayer, at intermediate coverage values, has a honeycomb $(\sqrt{3} \times \sqrt{3})R30°$ structure in which $\Theta_{Cu} = 0.67$ and with (bi)sulfate anions occupying the centers of the honeycomb ($\Theta_{anion} = 0.33$) (Figure 4) in agreement with the coverage values found with chronocoulometry and EQCM. This meant that the scanning probe techniques (STM, AFM) were not imaging the Cu adatoms but the (bi)sulfate anions that occupied the centers of the honeycomb and protruded well above the Cu plane.[43] Recent SEXAFS measurements also support the honeycomb model.[56] As was the case for the Cu-(1 × 1) structure, XANES clearly suggested that the oxidation state of the Cu adatoms after the first UPD peak is approximately +1,[54] again probably as a result of a polar bond or surface dipoles, in agreement with the results obtained with ring-disk electrodes.[25] For this structure, it has been proposed that the Cu adatoms occupy on-top positions.[45]

Once the structure of the adlayer was resolved, the features in the cyclic voltammogram could be explained. In the initial steps, the first Cu adatoms are randomly deposited on the electrode surface, together with some (bi)sulfate anions. At this stage, Cu adatoms are quite mobile on the electrode surface, as the lack of atomic resolution in STM images would indicate.[32] This part of the process corresponds to the broad shoulder prior to the first UPD peak. At a

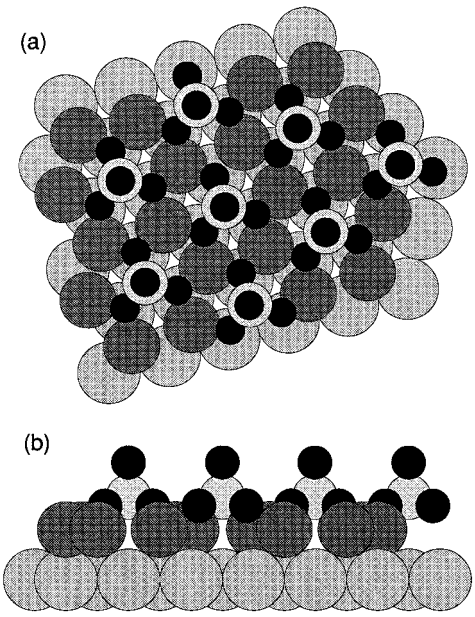

Figure 4. Interfacial structure of the Cu UPD on Au(111) after the first UPD peak: (a) top view; (b) side view. Reproduced with permission from ref 43. Copyright 1995 The American Physical Society.

sulfate coverage of ca. 0.05, the adlayer undergoes a first-order phase transition to form a honeycomb ($\sqrt{3} \times \sqrt{3})R30°$, giving rise to the first UPD peak.[72] Finally, the adlayer transforms to a Cu-(1×1) structure with (bi)sulfate adsorbed on top of the copper adlayer.

B. Influence of Anions on the Cu UPD on Au(111)

The studies of Cu UPD on Au(111) in chloride-containing solutions exemplify the effects of anions in UPD processes in general. STM measurements in sulfuric acid media revealed how trace amounts of chloride (from contamination) induced the transformation of the $(\sqrt{3} \times \sqrt{3})R30°$ to a (5×5) structure.[27,28,32,34] The observed transformation took place even when the bisulfate concentration was much higher than the chloride concentration (ca. 10^4 times higher), a consequence of the high affinity that chloride anions have for copper. This behavior is reflected in the voltammetric profile in the presence of chloride (Figure 5). The voltammogram shows two pairs of peaks, as in the case of sulfuric acid, but the pair at high underpotentials is reversible and appears at potentials that are more positive than in sulfuric acid. The second pair of peaks almost overlaps with bulk Cu deposition.

After the first deposition peak, STM measurements showed the formation of a "(5×5)" structure.[29,33,35,36] Careful measurements indicated that this structure was not a real (5×5) but probably an incommensurate structure, with Cu−Cu distances between those for a (4×4) and a (5×5) structure[29] (Figure 6). Ex-situ LEED analysis also indicated the presence of a distorted (4×4) structure.[67] There were also signs of compression in these structures when the potential was scanned in the negative direction.[33] Chronocuolometric results indicated that the ratio of copper to chloride in the adlayer for these structures

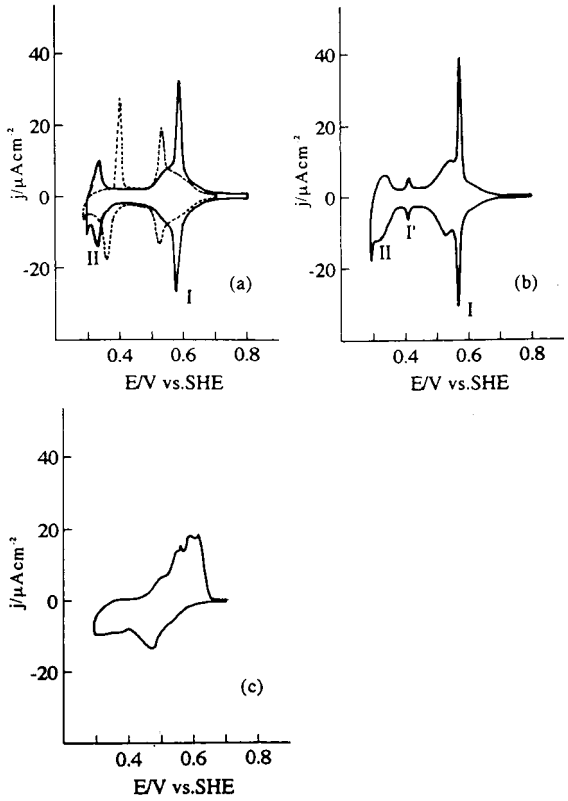

Figure 5. Voltammetric profiles of Cu UPD on Au(111): (a) 0.05 M H_2SO_4 + 1 mM $CuSO_4$ + 0.1 mM KCl; (b) 0.05 M H_2SO_4 + 1 mM $CuSO_4$ + 0.1 mM KBr; (c) 0.05 M H_2SO_4 + 1 mM $CuSO_4$ + 0.1 mM KI. The broken curve on (a) is for 0.05 M H_2SO_4 + 1 mM $CuSO_4$, given for comparison. Scan rate: 5 mV·s^{-1}. Reproduced with permission from ref 36. © 1994 Elsevier Science SA.

was equal to 1.[24] Therefore, a bilayer structure was proposed in which chloride is adsorbed on the copper and where the Cu and the chloride coverage are equal to 0.62.[24,29] SEXAFS measurements indicated that the copper adatoms are packed in registry with the top layer of chloride ions[57] (Figure 7). The distances in the proposed structure are quite similar to those found in solid CuCl.[85]

At potentials negative of the second peak, the "(5×5)" is still visible, and STM images showed a long-range corrugation.[29,33,36] It has been proposed that chloride anions are desorbed at these potentials;[33,36] however, chronocoulometry indicated that the chloride surface concentration remained stable over the entire potential range of Cu UPD[23,24] for chloride concentrations above 10^{-4} M.

At chloride concentrations below 10^{-5} M, a (2×2) structure is seen at potentials below +0.14 V vs SCE (Figure 6). This coincides with the appearance, in the cyclic voltammogram, of an additional peak at this potential. For this structure, the Cu coverage is 0.75 and the chloride concentration is 0.25, again in agreement with the chronocoulometric results.[23]

In perchloric acid media, the situation is quite similar to that found at low chloride concentrations in acid media, since perchlorate solutions almost always have a residual chloride concentration that is around 10^{-6} M. Thus, two structures are observed: a "(5×5)" structure at high underpotentials and the (2×2) structure at potentials lower than

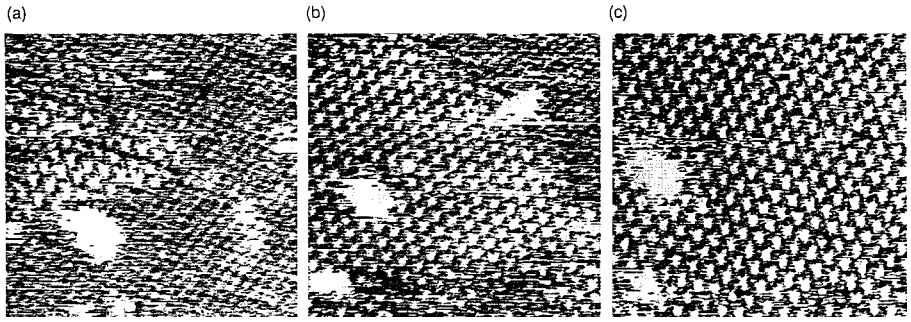

Figure 6. Series of three STM images of Cu UPD on Au(111) in 0.1 M $HClO_4$ + 0.01 M $Cu(ClO_4)_2$ solution containing trace amounts of Cl^- ions (ca. 10^{-6} M) successively recorded over the same area (110 × 100 Å^2) at time intervals of 25 s. Upon a change of the potential from +0.3 to +0.13 V vs SCE at the beginning of image (a) the transformation of the "(5 × 5)" structure into the (2 × 2) structure via an island growth of the (2 × 2) phase is observed. Reproduced with permission from ref 29. Copyright 1995 Elsevier Science BV.

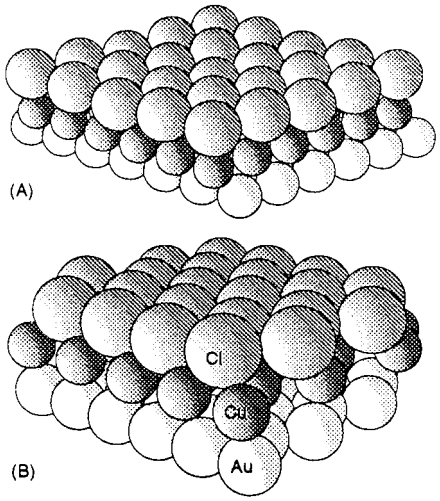

Figure 7. Model for the bilayer structure formed by the copper and chloride ions at the Au(111) surface: (A) copper adsorbed in registry with the Au(111) substrate; (B) copper adsorbed in registry with the top layer of chloride ions. Reproduced with permission from ref 57. Copyright 1995 Elsevier Science Ltd.

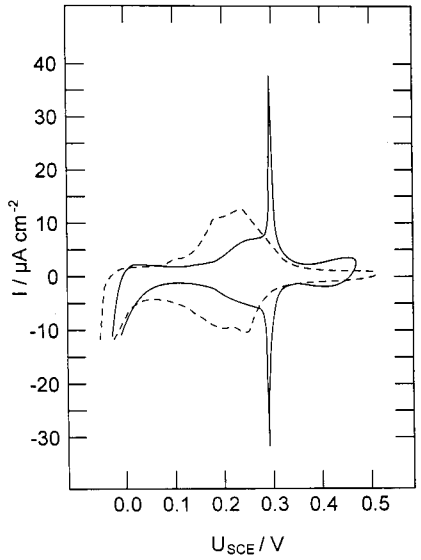

Figure 8. Cyclic voltammogram for a Au(100) electrode in 0.01 M H_2SO_4 + 1 mM $CuSO_4$ without (dashed line) and with the addition of 0.1 mM HCl. Scan rate: 2 mV·s^{-1}. Reproduced with permission from ref 30. Copyright 1995 The American Physical Society.

+0.14 V vs SCE.[29] The (2 × 2) structure has also been observed by AFM.[40]

In the presence of bromide or iodide, the behavior is very similar to that found in the presence of chloride (Figure 5), with a bilayer structure predicted.[21,22,24] For bromide solutions, STM measurements identified two different structures; at high underpotentials a $(\sqrt{7} \times \sqrt{7})R19.1°$ structure ($\Theta_{Cu} = 0.42$)[35] is observed, and after a peak at +0.12 V vs SHE the surface structure is (4 × 4) ($\Theta_{Cu} = 0.56$).[35,36,39] These results are at odds with chronocoulometric results[21,22,24] and with recent X-ray scattering studies.[46,47] In these studies, an ordered hexagonal bromide adlayer is formed at the onset of copper deposition and undergoes a phase transition to form a (4 × 4) commensurate structure ($\Theta_{Cu} = 0.56$) at the peak at +0.32 V vs Ag/AgCl. This bromide adlayer remains stable until the bulk deposition of copper begins.[47] Copper is deposited between the gold surface and the bromide layer.[47] In the presence of iodide, the surface structure is (3 × 3).[35,36]

As a general trend for all the Cu−halide systems, the structures of these adlayers are governed by the halide−halide and the Cu−halide interactions in contrast to the Cu−(bi)sulfate adlayers in which the Cu−Au interaction is dominant. However, clearly all interactions contribute to the UPD processes.

Cu UPD on Au(111) has also been studied in the presence of some organic additives, such as crystal violet,[33,86] coumarin,[87] thiourea,[88] Nafion films,[89] and thiols.[90]

C. Cu UPD on Au(100) and -(110) Electrodes

On Au(100) electrodes and in sulfuric acid media, Cu UPD occurs in a relatively broad peak[17,28,30] (Figure 8). At low bisulfate concentrations (<1 mM), the deposition peak splits into two.[17] STM[30] and AFM[42] studies demonstrated that the surface structure, after the deposition peak, is a pseudomorphic (1 × 1) structure (Figure 9) in which the Cu atoms occupy the 4-fold hollow sites. XSW measurements also indicated that the Cu adatoms occupy the 4-fold hollow sites.[58] However, SEXAFS measurements suggested a different picture of the adlayer at full coverage.[52,56] In the model proposed from experimental data (which is, however, incompatible with STM and AFM images), the Cu−Cu distance is shorter than the Au−Au distance in the unreconstructed

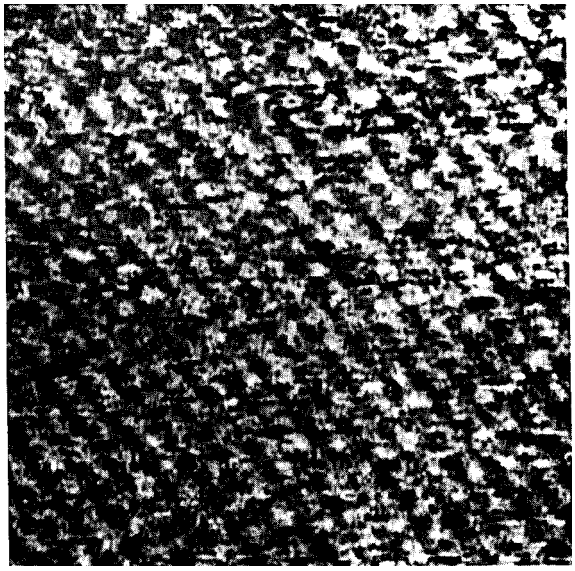

Figure 9. STM image of the Au(100) in 0.01 M H_2SO_4 + 1 mM $CuSO_4$. Reproduced with permission from ref 30. Copyright 1995 The American Physical Society.

Au(100) surface and the Cu adatoms occupy atop sites.[52,56] This would imply that the topmost gold layer is rearranged or reconstructed. As on Au(111) electrodes, the Cu oxidation state is close to +1.[52,56]

The presence of intermediate coverage structures in sulfuric acid is doubtful. The quasi-hexagonal structures identified by STM[27,28] were due to chloride contamination from the reference electrode.[30] Another structure, with $\Theta_{Cu} = 0.66$ and a $\begin{pmatrix} 2 & 2 \\ 0 & 3 \end{pmatrix}$ unit cell has been found at potentials within the broad peak[42] and is quite similar to that found in chloride media.[30] In fact, the voltammetric profile for Cu UPD on Au(100) in sulfuric acid shown in this particular work[42] is different from those previously reported and was similar to the one found in the presence of chloride.[30]

As before, the presence of chloride in the solution changes the behavior of the Cu UPD system. The voltammetric profile shows a pair of sharp peaks followed by a broad shoulder (Figure 8). After the sharp peak, the Cu adopts an ($n \times 2$) structure, which is a distorted hexagonal structure.[30] The Cu−Cu distance in the adlayer ranges between 3.6 and 4.1 Å, close to the distance found in Au(111) electrodes,[30] where the "(5×5)" structure is found.[29] This suggests that, in this case as well, the adlayer structure is determined mainly by Cu−Cl interactions, and a bilayer is also probably formed.

For Au(110) electrodes, two different structures have been found, with a (1×1) structure found in sulfuric acid media and a (2×1) structure formed in chloride media.[31] The model for the (2×1) structure is based on a CuCl(111) bilayer, in which, as in the previous cases, the adlayer structure in mainly determined by the Cu−Cl interactions.[31] A possible Cu−Au alloy formation was also detected.[31]

2. Ag UPD on Au(*h*,*k*,*l*) Electrodes

Although the UPD effect was discovered in 1949 studying silver deposition on gold,[91] Ag UPD on gold

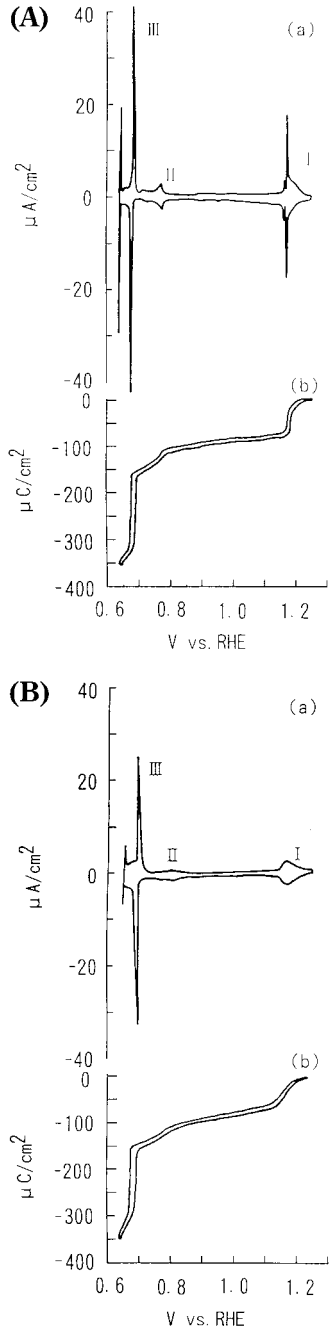

Figure 10. Cyclic voltammogram for a Au(111) electrode (A) in 0.05 M H_2SO_4 + 1 mM Ag_2SO_4 and (B) in 0.1 M $HClO_4$ + 1 mM $AgClO_4$. Scan rate: 2 mV·s^{-1}. Reproduced with permission from ref 104. Copyright 1995 Elsevier Science Ltd.

single crystal electrodes has only been extensively studied since the late 80's. Apart from an early study from Lorenz and co-workers,[92] this system has been studied by in situ SEXAFS,[93,94] X-ray diffraction,[95−100] STM,[101−111] AFM,[112−114] EQCM,[115] SHG,[62] and ex situ UHV techniques.[114,116]

The voltammetric profile for Ag UPD on Au(111) electrodes both in perchloric and sulfuric acid media shows three well-defined pairs of peaks (Figure 10) at approximately the same potentials. Peaks in sulfuric acid media, especially those at the most positive potentials, are sharper that those in perchloric acid. Some studies failed to report the existence of the third peak for silver UPD on Au(111),

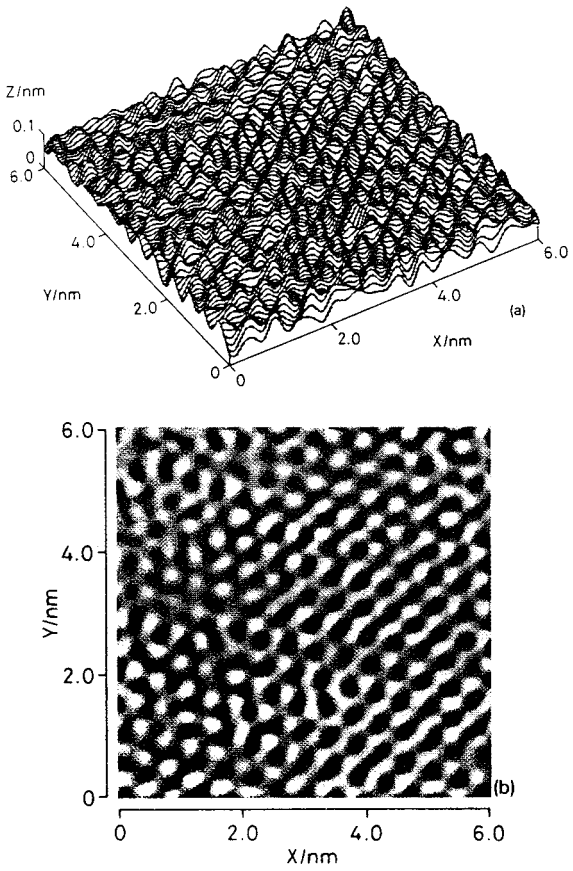

Figure 11. (a) STM topographic line scans and (b) top view of the $(\sqrt{3} \times \sqrt{3})R30°$ structure obtained in 0.05 M H_2SO_4 + 1 mM Ag_2SO_4 on Au(111) at +0.5 V vs Ag/Ag^+. Reproduced with permission from ref 102. Copyright 1992 Elsevier Science Publishers BV.

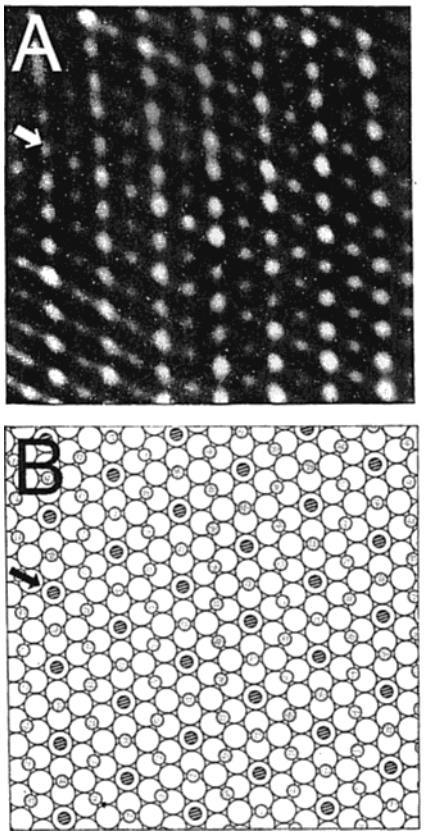

Figure 12. (A) 5 × 5 nm^2 AFM image of the $p(3 \times 3)$ structure obtained in 0.1 M H_2SO_4 + 0.77 mM Ag_2SO_4 on Au(111) at +0.42 V vs Ag/Ag^+. (B) Schematic representation of the $p(3 \times 3)$ structure (striped and shadowed circles represent the Ag atoms). Reproduced with permission from ref 112. Copyright 1992 American Chemical Society.

probably because it was mistakenly interpreted as the onset of bulk deposition.[106,112−114] The charge involved in the entire UPD process is 270−285 $\mu C \cdot cm^{-2}$,[104] whereas the charge required for the deposition of a (1 × 1) layer of silver (assuming that silver exchanges 1 electron upon deposition) would be 222 $\mu C \cdot cm^{-2}$, 50−65 $\mu C \cdot cm^{-2}$ lower than the experimental value. Since the measured charge also has contributions due to the adsorption/desorption of anions, it would be expected that some anions desorb upon silver deposition. EQCM[115] measurements have indeed shown that anions are desorbed during the first UPD deposition peak, probably giving rise, at least in part, to the excess charge found in the coulometry.

After the first UPD peak, EQCM measurements in sulfuric acid media have shown that the silver coverage is approximately 1/3,[115] which would suggest that the silver adlayer has a $(\sqrt{3} \times \sqrt{3})R30°$ structure. Two different structures have been found between the first and second UPD peaks by different groups using different techniques: a $(\sqrt{3} \times \sqrt{3})R30°$ ($\Theta_{Ag} = 0.33$) structure was observed by STM at potentials just after the first deposition peak[102,104] (Figure 11), and a $p(3 \times 3)$ (probably incommensurate with the gold substrate) (Figure 12) ($\Theta_{Ag} = 0.44$) structure was found by AFM at potentials slightly negative of those in the previous case.[112−114] EQCM[115] and coulometric[104] measurements revealed that the silver coverage increased slowly but gradually after the first peak. In fact, a faint peak can be observed in this region[114] that could correspond to a surface transition between both structures. This explanation, although probable, does not preclude other possibilities; i.e., AFM and STM are probing different species on the interface: silver and (bi)sulfate (recall Cu UPD on Au(111)). UHV studies of silver UPD on Au(111) in sulfuric acid media found two different structures: a $p(3 \times 3)$ at low sulfate concentrations (0.5 mM) and a $p(5 \times 5)$ at higher concentrations (50 mM),[114] also suggesting the possibility of several surface structures between first and second UPD peaks. No ordered structures have been observed between the second and third peaks.

In perchloric acid solution, only a (4 × 4) structure was found in the region between the first and second peaks.[104,109] A similar structure (although not unambiguously resolved) was observed by AFM.[112] UHV measurements for this system in hydrofluoric acid medium (fluoride, as well as perchlorate, are weakly adsorbing anions) revealed the existence of several intermediate structures: $p(3 \times 3)$; $p(5 \times 5)$; (5×5); (6×6).[116] This fact would suggest that the (4 × 4) structure found in the in-situ studies is incommensurate with the gold substrate and probably undergoes compression as the electrode potential is shifted negatively. STM measurements indicated that the silver adlayer, after the first deposition peak, grows through a step growth mechanism.[106] The

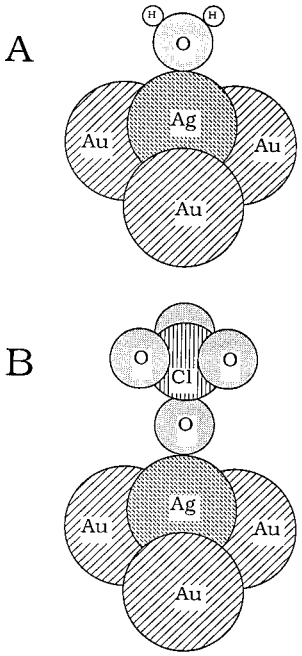

Figure 13. Model for the structure of an underpotentially deposited monolayer of silver on an Au(111) electrode with either (A) water or (B) perchlorate bonded to the silver adatoms through the oxygen. Reproduced with permission from ref 93. Copyright 1988 American Chemical Society.

same (4 × 4) structure is found in nitric acid medium.[112]

After the third UPD peak, a (1 × 1) commensurate structure is observed by STM both in perchloric and sulfuric acid media.[104] In perchloric acid, the Ag−Ag distance in the adlayer measured by SEXAFS is 2.88 ± 0.03 Å,[94] which is, within the error limits, the same as the Au−Au distance. The existence of a commensurate layer in these cases is not unexpected since silver and gold have atomic radii that differ only by 0.3%. SEXAFS studies suggested the existence of additional oxygen atoms on the adlayer[93,94] (Figure 13) probably form adsorbed water or perchlorate. These studies also revealed that silver, unlike copper,[49,54] is fully reduced[93,94] and occupies the 3-fold hollow sites.[94] The 3-fold geometry is also suggested by SHG.[62] Some changes in the Ag−Au distance have been observed in sulfuric acid solutions by differential X-ray diffraction,[96] probably induced by the presence of adsorbing (bi)sulfate. Upon completion of the first silver layer, the adlayer grows by the Stranski−Krastanov growth mode (island growth).[101,104,105] Surface interdiffusion between Au and Ag has been detected for bulk deposits.[98]

Silver UPD has also been studied on iodine-coated Au(111).[103] The structure, after the first deposition peak, is a (3 × 3) structure, in which silver adatoms are deposited underneath the iodine adlayer. This structure is the same as that found for silver deposition on iodine coated Pt(111),[117−119] suggesting that the Ag−I interactions dominate the adlayer structure.

Silver UPD on Au(100) also exhibits three pairs of peaks in perchloric and sulfuric acid media. In both supporting electrolytes, the surface structures appear to be the same. After the first UPD peaks, a $c(\sqrt{2} \times 5\sqrt{2})R45°$ structure is found, whereas after the second peak the (1 × 1) structure is found.[108,109] After the completion of the first monolayer, the adlayer grows with a Frank−Van der Merwe growth mode (layer-by-layer) at low overpotentials,[107,108] whereas a Stranski−Krastanov growth mode is observed at high overpotentials.[107]

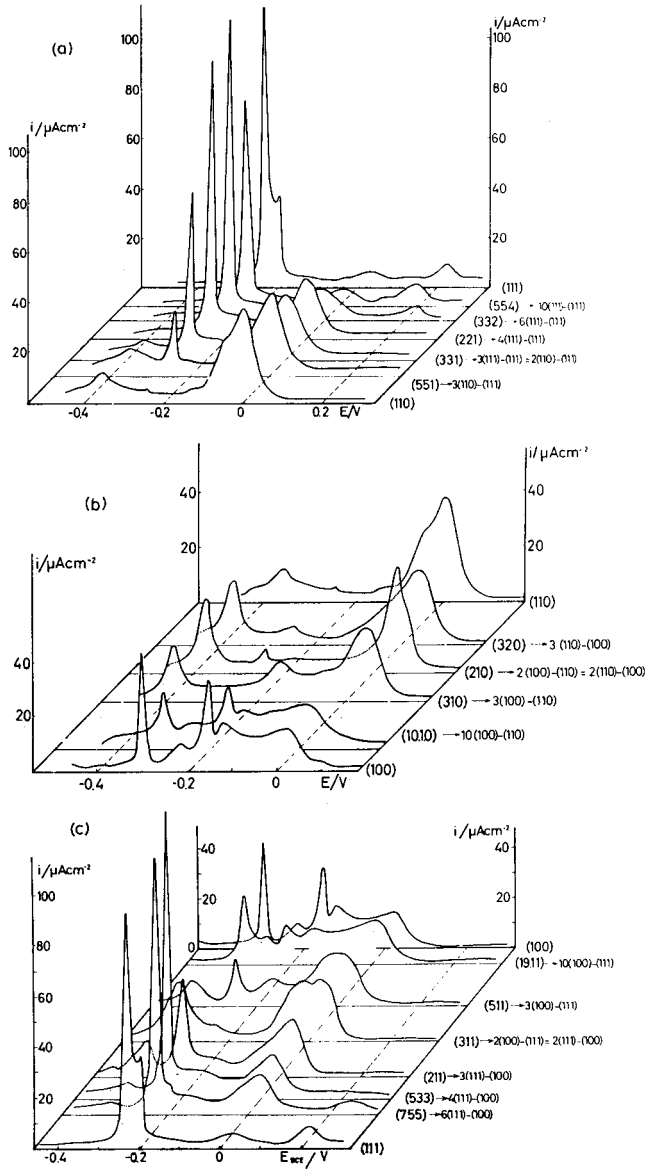

Figure 14. Cyclic voltammograms for the stripping of Pb UPD on Au(*h*,*k*,*l*) electrodes on the three main zones of the projected stereographic triangle in 10 mM $HClO_4$ + 1 mM PbF_2: (a) (111)−(110) zone; (b) (110)−(100) zone; (c) (100)−(111) zone. All surfaces are identified with Miller index notation as well as compact step notation. Reproduced with permission from ref 123. Copyright 1984 Elsevier Sequoia SA.

3. Pb UPD on Au(*h*,*k*,*l*) Electrodes

Unlike the rest of metal UPD processes on gold-(*h*,*k*,*l*) electrodes, a complete study of the effects of surface structure and steps on the Pb UPD process has been carried out.[120−123] These studies allowed the assignment of the voltammetric peaks for the different surfaces to deposition processes occurring on (111), (110), or (100) terraces or steps (Figure 14) and to observe the influence of the terrace width on the

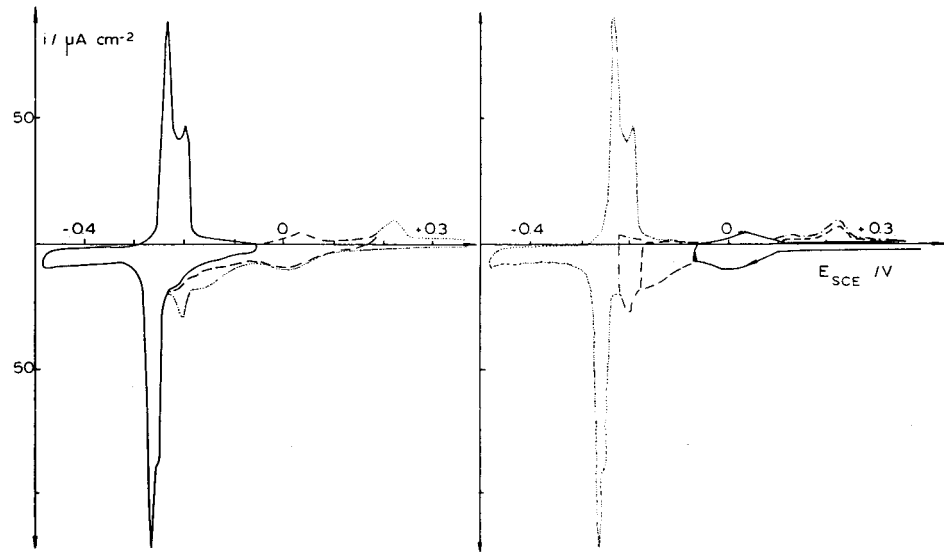

Figure 15. Cyclic voltammogram for a Au(111) electrode in 10 mM $HClO_4$ + 1 mM PbF_2. Different lines represent different potential scan ranges. Reproduced with permission from ref 120. Copyright 1979 Elsevier Sequoia SA.

shape of the voltammetric peaks. Apart from these studies, this system has also been studied by electrochemical methods[12,124−127] and in-situ UV-vis reflectance,[124] STM,[128−135] AFM,[136,137] X-ray diffraction,[138−140] and SHG.[62]

Lead UPD processes take place at potentials that overlap with the onset of hydrogen evolution on gold electrodes. However, the presence of lead on the electrode surface greatly inhibits the hydrogen evolution reaction, as would be expected given the high overpotential for hydrogen evolution on bulk lead electrodes. The voltammetric profile of lead UPD on Au(111) presents a pair of peaks (which splits in two) and a series of small and irreversible peaks at high underpotentials (Figure 15). The splitting is the result of the kinetics of the process; i.e., the peak at higher underpotentials corresponds to the growth of the lead deposited island, whereas the one at lower underpotentials corresponds to the coalescence process.[133]

In the presence of lead cations in solution, the voltammetric profile for all gold electrodes in the oxide region changes slightly.[120,127] Studies of electrode resistance have suggested that this change in the oxide region could be due to the presence of residual lead on the electrode surface,[127] which, in turn, could be the result of an irreversible adsorption process of lead species on the gold electrode surface, similar to the behavior found on platinum single-crystal electrodes.[141,142] At potentials positive of the main UPD peaks, the height of the adlayer, determined by AFM,[136] is higher than that corresponding to a single layer of one metallic lead. This would indicate the presence of hydroxide species at these potentials, again in agreement with the results on Pt(111) electrodes.[141,142] Electroreflectance studies also indicate that partially charged lead adspecies are present at these potentials.[124]

Lead and gold have very different atomic sizes (lead is ca. 20% larger than gold), which favors the formation of incommensurate adlayers. In fact, at potentials negative of the main UPD peaks, a hexagonal

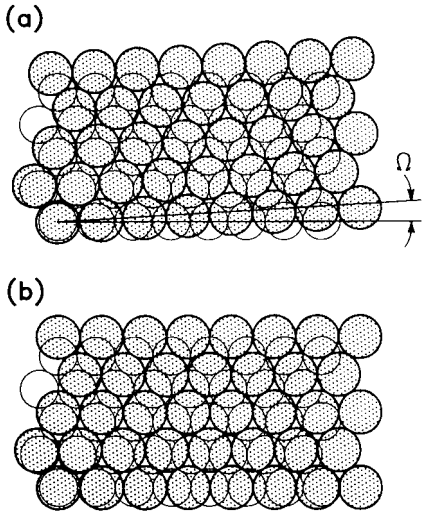

Figure 16. Schematic representation of the hexagonal structure of lead (shadowed circles) on Au(111) (open circles) with (a) a 2.5° rotation angle between the Pb and Au lattices and (b) 0° rotation angle between the Pb and Au lattices. Reproduced with permission from ref 139. Copyright 1995 American Chemical Society.

incommensurate structure has been found using X-ray diffraction techniques.[138,139] The presence of an incommensurate adlayer was also predicted from SHG studies.[62] This structure was also observed by STM[130,131,133] and AFM.[136] In this structure, the lead−lead distances are compressed 0.7% with respect to bulk lead.[138,139] The lead adlayer is rotated with respect to the Au(111) plane with an angle that varies between 2.5 and 0° depending on the applied potential[139] (Figure 16), which is consistent with the change in lead−gold distance over the same potential region observed with another X-ray diffraction technique, surface differential diffraction.[140] Over the same potential region, a change in the surface stress has also been observed.[137] The presence of an incommensurate adlayer causes the appearance of Moiré fringe patterns on the STM[133] and AFM[136] images. EQCM measurements on polycrystalline gold indi-

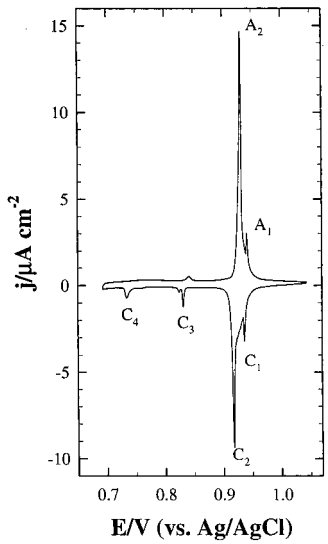

Figure 17. Cyclic voltammogram for a Au(111) electrode in 0.1 M H_2SO_4 + 1 mM Hg^{2+}. Scan rate: 1 mV·s^{-1}. Reproduced with permission from ref 145. Copyright 1997 American Chemical Society.

cate that the adlayer is completely discharged at these potentials.[143,144]

No other additional structures or phase transitions are found for this system, as predicted by thermodynamic and kinetic measurements.[125,126] The initial stages of lead deposition take place on terrace edges and are then dependent on the crystal quality.[129,130]

It is still not clear whether lead UPD deposits form alloys with the gold substrate. In some studies no alloy formation was observed,[120−123,133,139] whereas in others a roughening of the surface was observed.[129−132,135] The different behavior obtained could be the result of different negative limits in the voltammetric scans or differences in the quality of the Au(111) samples. For instance, in the related system of mercury UPD (see below and refs 145−147), the deposit only forms an alloy with the gold substrate at potentials lower than +0.50 V vs Ag/AgCl. It is also worth noting that alloy formation has always been observed in the proximity of edges and in roughened surfaces,[129−132,135] which would suggest that alloy formation is restricted only to edges and defect sites.

On Au(100) electrodes three different lead structures have been found, $c(2 \times 2)$,[134,135] $c(3\sqrt{2} \times \sqrt{2})$,[135] and an incommensurate hexagonal structure which also shows the presence of Moiré patterns in STM.

4. Hg UPD on Au(*h*,*k*,*l*) Electrodes

The behavior of mercury UPD on Au(111) electrodes resembles in some cases that of copper UPD on the same electrodes. This UPD system has been studied by electrochemical methods,[145,146] STM,[147] AFM,[113,148] and X-ray diffraction techniques.[149−154]

The voltammetric profile of mercury UPD on Au(111) electrodes in 0.1 M H_2SO_4 shows several pairs of peaks (Figure 17). The voltammogram shows a main deposition/stripping peak (centered at around +0.90 V vs Ag/AgCl) that splits into two. At positive (E > +0.80 V Ag/AgCl) potentials (bi)sulfate adsorbed on the electrode surface forms an ordered $(\sqrt{7} \times \sqrt{3})$ structure,[82,83,84] This ordered structure has also been observed in the presence of Hg^{2+} in the supporting electrolyte at potentials prior to the onset of mercury UPD.[147] The initial stages of mercury UPD appear to trigger an order−disorder transition in the (bi)-sulfate adlayer that gives rise to the first pair of peaks (C_1/A_1)[145] (Figure 17). After the second pair of peaks (C_2/A_2) an ordered surface structure is found. STM measurements have shown the existence of two different ordered structures after this peak:[147] $\begin{pmatrix} 2 & 0 \\ 3 & 3/2 \end{pmatrix}$ and $\begin{pmatrix} 1 & 1 \\ 4 & 4 \end{pmatrix}$ (Figure 18A). (In $HClO_4$, however, the structure found by in-situ STM (Figure 18B) was $\begin{pmatrix} 0 & 2 \\ 2 & 1 \end{pmatrix}$ pointing to the effects of anions.) The first structure found in 0.1 M H_2SO_4 was later observed by in situ X-ray diffraction and identified as a $(\sqrt{3} \times \sqrt{19})$ surface structure.[149] CTR[149] and coulometric[145] measurements indicated that the adlayer is likely constituted by Hg_2^{2+} cations and (bi)-sulfate anions. On the basis of the atomic distances derived form the CTR measurements, an adlayer structure similar (although distorted) to the honeycomb structure observed for copper UPD in the same medium was proposed (Figure 19).[149] At +0.82 V vs Ag/AgCl, the ordered structure disappears, giving rise to peak C_3.[149] Potential step measurements indicate that the kinetics for formation/dissolution of the mercury−(bi)sulfate adlayer follows a progressive nucleation and growth mechanism.[146]

In addition to the surface processes of mercury UPD, a process controlled by diffusion also appears in the voltammogram at potentials around +0.54 V vs Ag/AgCl. This redox process corresponds to the oxidation−reduction of mercury species in solution according to the following reaction:

$$2Hg^{2+} + 2e^- \leftrightarrow Hg_2^{2+} \quad E° = +0.698 \text{ V vs Ag/AgCl} \tag{2}$$

Coinciding with this solution process other additional ordered structures have been found. AFM measurements have identified a hexagonal structure.[113,148] X-ray diffraction studies identified two different hexagonal adlayers in this region: one at potentials between +0.63 and +0.68 V (vs Ag/AgCl) with a Hg−Hg distance of 3.84 Å and another at potentials below +0.63 V (vs Ag/AgCl) with a Hg−Hg distance of 3.33 Å.[150] The first hexagonal adlayer appears to be metastable and evolves, with time, to give the second adlayer.[150]

The last peak of mercury UPD on Au(111) appears at +0.52 V (vs Ag/AgCl) and corresponds to the formation of a mercury−gold amalgam that leads to the roughening of the electrode surface[145] (Figure 20). When mercury is stripped from the surface, pits of 2−5 nm in depth are created on the surface.[155] The roughening of the surface gives rise to the irreversible modification of the voltammetric profile of the Au(111) electrode (Figure 20B).

The effect of anions is also evident in the case of mercury UPD. In perchloric acid solutions the main UPD peak is not split and has a quasi-Gaussian shape (Figure 21), suggesting a Langmuir type

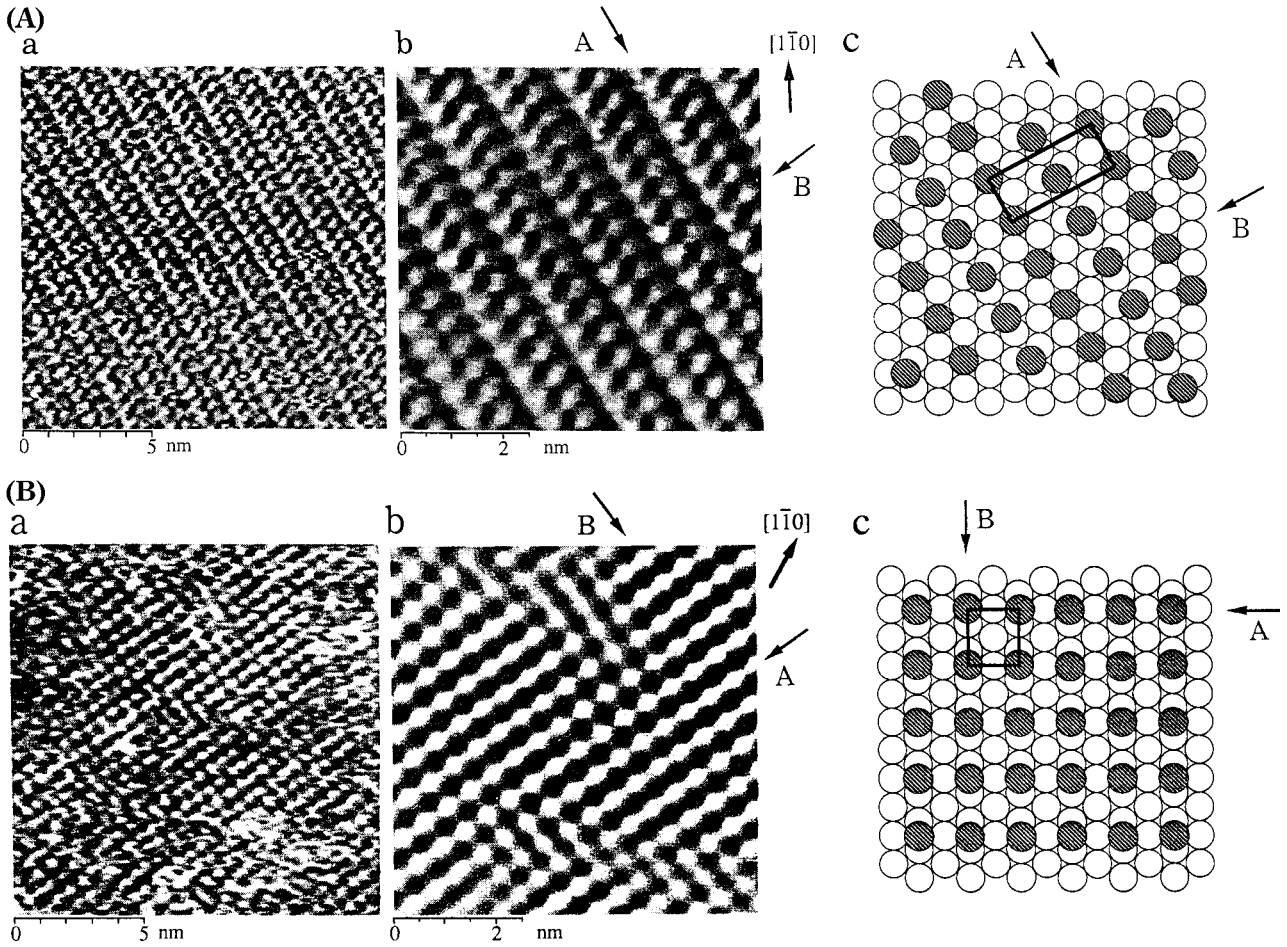

Figure 18. (A) STM images obtained in 0.05 M H_2SO_4 + 1 mM Hg^{2+} on Au(111): (a) 14 × 14 nm^2 at +1.05 V vs RHE showing the $\begin{pmatrix} 1 & \bar{1} \\ 4 & 4 \end{pmatrix}$ structure; (b) filtered image of (a); (c) structural model of (a). (B) STM images obtained in 0.10 M $HClO_4$ + 1 mM Hg^{2+} on Au(111): (a) 14 × 14 nm^2 at 1.05 V vs RHE, showing the $\begin{pmatrix} 0 & 2 \\ 2 & 1 \end{pmatrix}$ structure; (b) filtered image of (a); (c) structural model of (a). Adapted with permission from ref 147. Copyright 1996 Elsevier Science SA.

isotherm for the mercury adsorption/desorption process. STM[147] and AFM[113,148] studies have shown the formation of a $\begin{pmatrix} 0 & 2 \\ 2 & 1 \end{pmatrix}$ and hexagonal structures, respectively. However, due to the unavoidable presence of chloride in perchloric acid solutions and the relatively long times required to acquire the images, these results probably reflect the adlayer structure in the presence of chloride, in a way similar to what happened for copper UPD in perchloric acid media (see above). In fact, CTR measurements in perchloric acid after the first UPD peak revealed that the interface is constituted by chloride and mercury species.[151]

Unlike copper UPD, the voltammetric profile for mercury UPD on Au(111) in the presence of chloride resembles that observed in sulfuric acid media alone (Figure 22).[145] This would indicate that in both chloride and sulfuric acid media the UPD process is governed by mercury−substrate interactions. The main UPD peak also appears split, with the peak at higher underpotentials corresponding to an order−disorder/transition of the chloride adlayer.[145] After the main UPD peaks, a Hg_2Cl_2 bilayer is formed[151] in which mercury is bonded to the gold surface and chloride is deposited on top of the mercury adatoms. The main difference relative to the behavior observed in sulfuric acid is that bulk Hg_2Cl_2 deposition takes place instead of the amalgam formation.[145]

In acetic acid media, the UPD process is hindered due to the formation of Hg^{2+}-acetic acid complexes in solution.[145] After the main UPD peak, hexagonal structures have been observed with AFM[148] and X-ray diffraction.[151] The X-ray studies showed a compression in the hexagonal lattice as the potential became increasingly negative.

5. Other UPD Systems on Au(*h*,*k*,*l*) Electrodes

There have also been studies of UPD processes of other metals onto Au(*h*,*k*,*l*) electrodes including thallium,[12,62,139,140,156−162] bismuth,[12,163,164] nickel,[56,68,165] zinc,[166−169] cadmium,[170−175] tin,[176] selenium,[177] tellurium,[172,173,178−182] and antimony.[12,183] These systems have not been studies in as much detail as those discussed above but are included for the sake of completeness. Of particular note, however, has been the use of UPD methods for the deposition of semiconductors via a process that Stickney et al. have dubbed electrochemical atomic layer epitaxy (ECALE).[172,173,177,178,184−188]

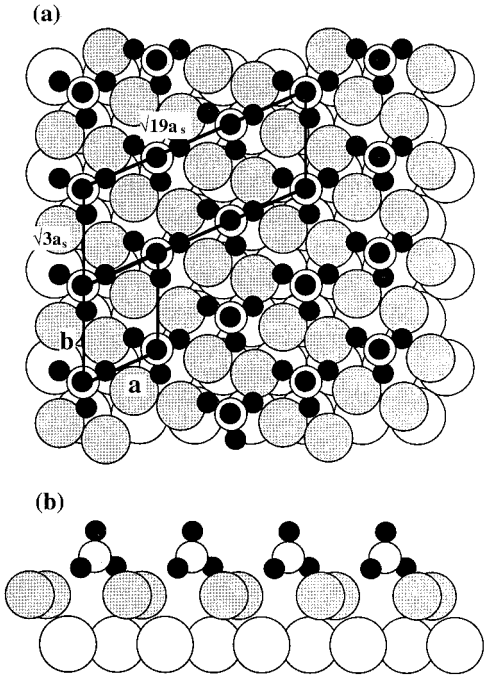

Figure 19. Distorted honeycomb structure of the coadsorbed Hg_2-SO_4 overlayer after C_2/A_2: (a) top view; (b) side view. Reproduced with permission from ref 149. Copyright 1997 American Chemical Society.

III. UPD on Platinum Surfaces

1. Cu UPD on Pt(*h*,*k*,*l*) Electrodes

Platinum single-crystal surfaces have been among the most widely studied within the context of underpotential deposition. From the systems studied the one that has received the most attention is, without a doubt, copper. Many of the initial studies performed were in an effort to describe the mechanism of electrodeposition at polycrystalline substrates through studies on the three low-index planes. As a large fraction of the body of literature dealing with copper UPD on platinum single crystals has been on the Pt(111) surface, we shall begin with that one, followed by a discussion of copper UPD on the (100) and (110) surfaces. Copper UPD has been studied by a wide variety of techniques including electrochemical,[189−213] reflectance spectroscopy,[214,215] radioactive labeling,[216,217] in-situ STM,[35,36,218−220] IR spectroscopy,[219,221] XAS,[203,222−226] X-ray surface scattering,[199,227−231] and ex-situ UHV techniques (such as LEED, AES, and XPS).[193,194,196−199,219,221,232−237] Even today, there continues to be a great deal of research done on copper UPD onto platinum substrates.

A. Copper UPD on Pt(111) in Perchloric Acid Media

It has been found that the cyclic voltammogram of copper UPD onto Pt(111) in the presence of perchloric acid shows two deposition peaks before the onset of bulk deposition but only one stripping peak[193,198] (Figure 23). The coulometrically determined copper coverage varied with scan rate indicating that copper deposition was a slow process. The coverage determined from the charge transferred (340 μC/cm^{-2}) was found to be lower than the theoretical coverage for a full copper monolayer (480 μC/cm^{-2}) in registry with the surface.[193] Coverages determined by UHV techniques such as LEED and AES do confirm that a complete monolayer is formed prior to bulk deposition.[193,194] This charge discrepancy is explained as the UPD copper monolayers in the electrochemical environment near their stripping potentials being partially charged. It was found that, for copper coverages greater 0.5 monolayers, the coulometrically determined copper coverage was too low by up to 30%. For coverages less than 0.5 monolayers, the coverage was too high by up to 50%.[194] This discrepancy is explained as due to partial discharge of coadsorbed perchlorate anions during desorption of copper.

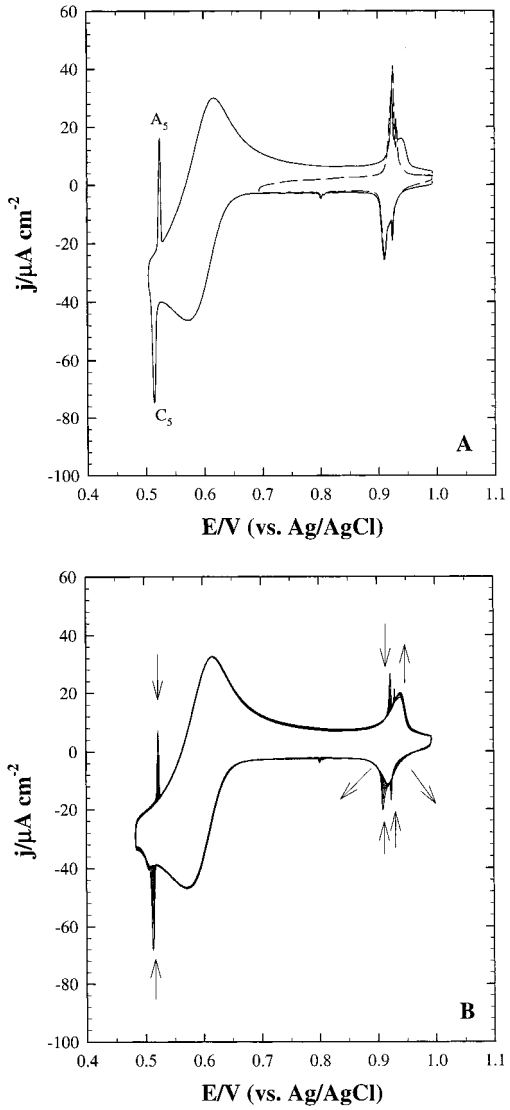

Figure 20. Modification of the voltammetric profile of Au(111) electrode in 0.10 M H_2SO_4 + 1 mM Hg^{2+} electrode after a potential excursion to +0.50 V: (A) first scan (full line) and comparison with the stable voltammetric profile over the range from +0.70 to +1.05 V (dashed line); (B) Evolution of the voltammetric profile upon cycling. Scan rate: 5 mV s^{-1}. Reproduced with permission from ref 145. Copyright 1997 American Chemical Society.

B. Copper UPD on Pt(111) in Sulfuric Acid Media

In contrast to the voltammetry of copper UPD in perchloric acid on Pt(111) electrodes, the deposition

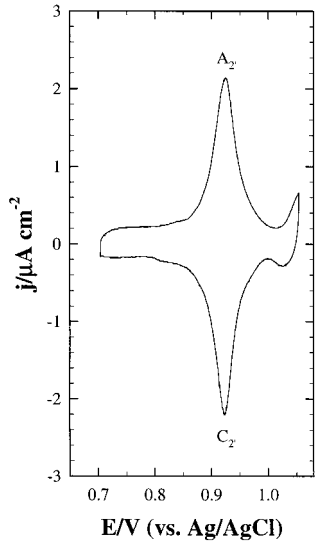

Figure 21. Voltammetric profile of a Au(111) electrode in 0.10 M $HClO_4$ + 10^{-3} M Hg^{2+}. Scan rate: 1 mV·s^{-1}. Reproduced with permission from ref 145. Copyright 1997 American Chemical Society.

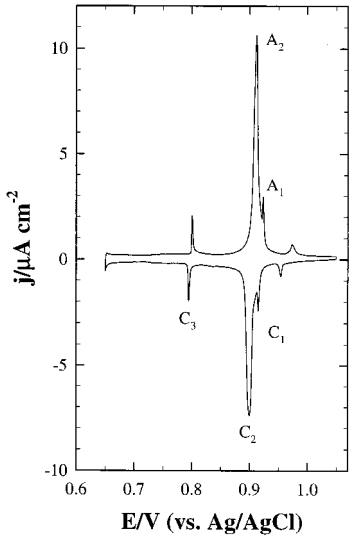

Figure 22. Voltammetric profile of a Au(111) electrode in 0.10 M $HClO_4$ + 1 mM NaCl +1 mM Hg^{2+}. Scan rate: 1 mV·s^{-1}. Reproduced with permission from ref 145. Copyright 1997 American Chemical Society.

peaks in the presence of high levels (0.1 M) of sulfuric acid are generally much sharper, showing that the deposition is facilitated by the presence of sulfate/bisulfate anions, leaving the stripping profile basically unchanged[198,216,222,223] (Figure 23). There has been much controversy surrounding the deposition profile in sulfuric acid. Some works show a deposition profile similar to that in perchloric acid with two deposition peaks, although these peaks are generally much sharper than in perchloric media.[216,223,224] Sometimes the voltammograms show just one deposition peak, although, at very slow sweep rates and with very high quality crystals, there is a splitting of the deposition/stripping peaks into two sets of peaks that are very close together.[198,209] The potentials of these peaks vary with sweep rate; as the sweep rate was increased, the cathodic and anodic

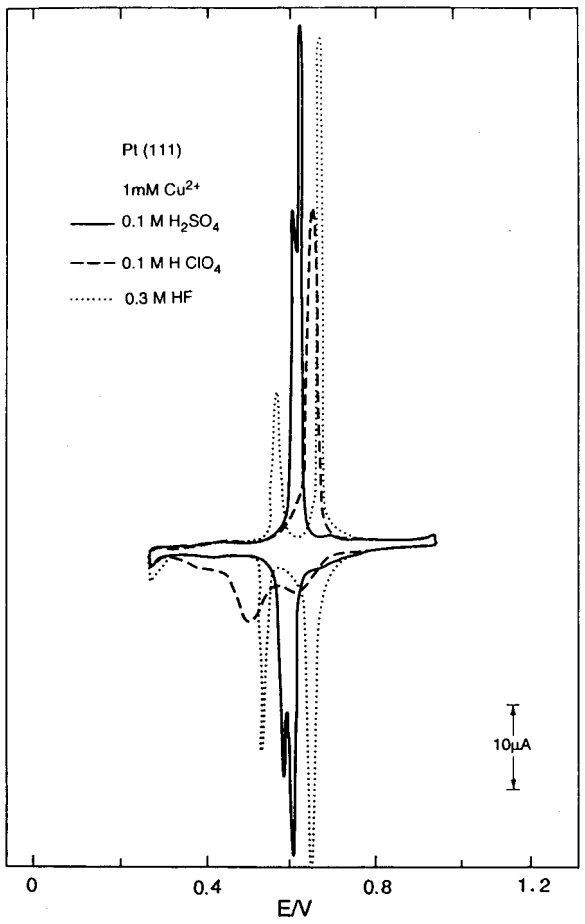

Figure 23. Cyclic voltammetry of Cu UPD at 1 mM Cu^{2+} ion concentration on a Pt(111) electrode in different supporting electrolytes. Reproduced with permission from ref 198. Copyright 1993 American Chemical Society.

peaks shift in negative and positive directions, respectively, suggesting that copper UPD in sulfuric acid media is also a slow process.[209] Given the differing concentrations of both copper and sulfuric acid and different experimental conditions, it is not possible to distinguish a general trend for the voltammetry of copper in sulfuric acid media beyond what is stated here.

It has also been reported that the deposition of a small amount of copper onto the platinum surface cause a redistribution in the states of adsorbed hydrogen in the voltammogram. This redistribution has been explained as the initial copper deposition inducing the adsorption of a small amount of sulfate/bisulfate anions on the platinum surface in the vicinity of the deposited copper. This enhanced anion adsorption in the vicinity of the deposited copper has also been observed through AES[198] and radioactive labeling methods.[216]

EXAFS studies (Figure 24) have shown that just as in perchloric acid media, the copper layer in sulfuric acid media is not completely discharged on the surface.[222,223] The effective charge of the copper species on the Pt(111) surface is close to +1 and not 0 as expected on the basis of complete charge transfer. The platinum surface appears to retain some negative charge so that the Cu−Pt bond is

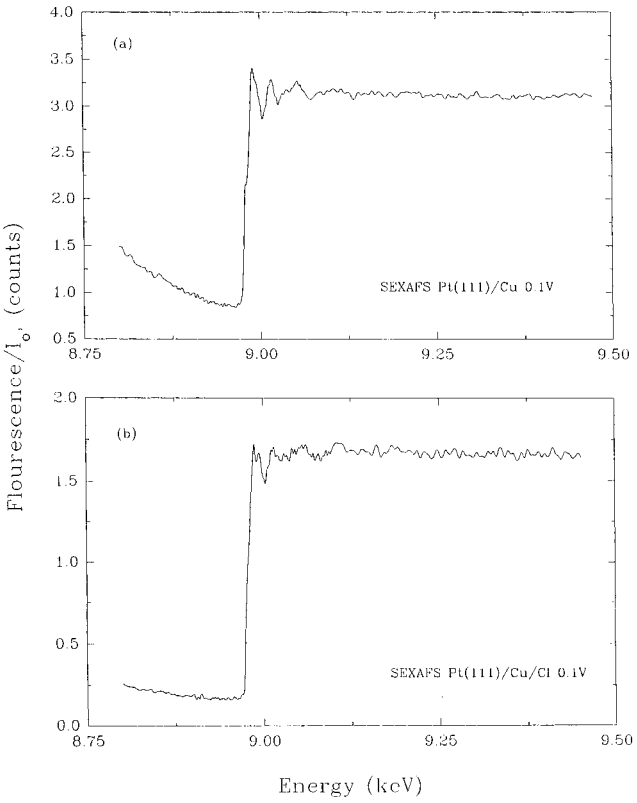

Figure 24. In-situ X-ray absorption spectra of copper UPD on Pt(111) from 0.1 M H_2SO_4 + 50 μM Cu^{2+} solution in the (a) absence and (b) presence of 10^{-3} M Cl^-. Potential was held at +0.1 V. Scan rate: 2 mV·s^{-1}. Reproduced with permission from ref 225. Copyright 1993 American Chemical Society.

highly polar. The Cu^+ species could then represent the site for bisulfate adsorption.[216]

In-situ IRAS has also shown that bisulfate anions are adsorbed on the platinum surface prior to copper deposition.[219] LEED and STM studies have shown that these anions have a $(\sqrt{3} \times \sqrt{3})R30°$ structure on the platinum surface.[219] After the deposition of copper, the in-situ STM images show a $\begin{pmatrix} 2 & 1 \\ 1 & 2 \end{pmatrix}$ structure for sulfate atop the deposited copper.[219] This structure is very close to a $(\sqrt{3} \times \sqrt{3})R30°$ structure which has been observed by ex-situ LEED[221] and previously by in-situ STM.[218] SEXAFS results show that the copper layer, at full coverage, has a close-packed structure with a copper−copper distance of 2.77 ± 0.03 Å. This structure corresponds to the copper residing in the 3-fold hollow sites of the Pt(111) surface.[222]

A possible mechanism for the copper deposition onto Pt(111) in the presence of sulfuric acid is as follows. Initially bisulfate anions are adsorbed on the copper-free platinum surface in a $(\sqrt{3} \times \sqrt{3})R30°$ structure. As the copper is initially deposited, the bisulfate is converted to sulfate and the first UPD peak has copper and sulfate coadsorbed. The evidence for the bisulfate/sulfate conversion is based largely on in-sutu IRAS studies.[219] Further copper deposition causes sulfate desorption from the Pt(111) surface in the second UPD peak. At full copper coverage, the sulfate is adsorbed on the copper surface in a $\begin{pmatrix} 2 & 1 \\ 1 & 2 \end{pmatrix}$ structure.

C. Copper UPD on Pt(111) in the Presence of Other Anions

As it has already been shown with sulfate/bisulfate, the presence of adsorbing anions greatly affects the UPD of copper onto platinum single-crystal surfaces (Figure 25). A great deal of the work on the effects of anions on the UPD of copper on Pt(111) has been centered mostly on the halides, with the first such works concentrating on iodide, in particular. Those studies involved the use of UHV spectroscopic and electrochemical techniques to investigate the electrodeposition of copper on Pt(111) surfaces that had been pretreated with I^- to form a Pt(111)($\sqrt{7} \times 7$)-*R*19.1°-I superlattice.[196] It was found that deposition took place in two steps. The more positive UPD peak produced a LEED pattern corresponding to a (3 × 3) lattice. After the second peak, a (10 × 10) lattice structure was found. The intensity of the iodine AES signal was not greatly affected by the deposited copper (Figure 26), suggesting that iodine resides as the topmost layer at all copper coverages.[196] In contrast, in-situ STM studies have shown that when iodide is in the depositing solution as KI instead of on the surface as a pretreatment, the STM images show a $(\sqrt{3} \times \sqrt{3})R30°$ structure after copper deposition (Figure 27).[35,36] The cyclic voltammogram of the copper deposition from a KI-containing solution only shows the presence of one set of voltammetric peaks (Figure 25), as opposed to two sets from the iodide covered electrode suggesting either structural or kinetic differences when copper is co-deposited with the iodide. The ex-situ UHV studies were done with perchloric acid as a supporting electrolyte while the in-situ STM experiments were performed with sulfuric acid as the electrolyte which may have also changed the final structure(s). It has also been found by SEXAFS measurements that under certain circumstances, which depend on the structure of the iodine layer pretreatment, the deposited copper may form 2-D clusters on the surface.[224]

Bromide and chloride anions also show a dramatic effect on copper UPD onto platinum single crystals. As in the presence of sulfuric acid, the deposition and stripping again take place in two distinct steps on Pt(111) (Figure 25).[36,195,197−202,225,227−232] It has been found that the potential for copper UPD on Pt(111) decreases in the order of $Cl^- > Br^- > I^- > S^{2-}$ and that there is also partial charge transfer from the adsorbed copper to the coadsorbate.[201] The order of these potentials correlates well with the half-cell reaction corresponding to

$$CuX + e^- \rightarrow Cu^0 + X^- \quad X = Cl^-, Br^-, I^-, S^{2-}$$

suggesting that the copper, as in the previous cases, is partially charged. Because of this partial charge transfer, any measurement of the total charge in a coverage determination is suspect due to the difficulty in interpreting surface coverage values in the presence of coadsorbed anions.[227]

There has been some controversy regarding the mechanism for copper UPD onto Pt(111) in the

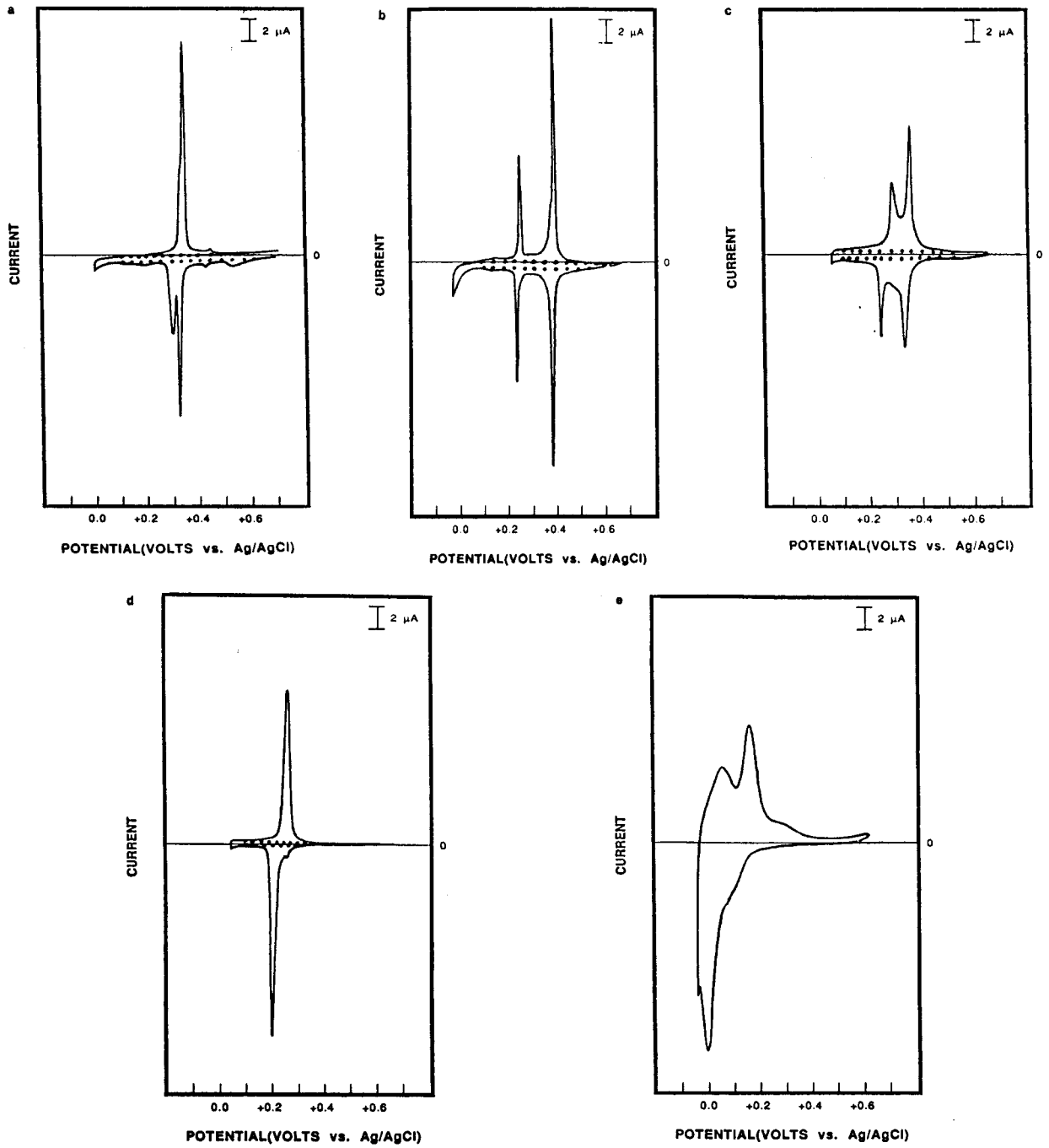

Figure 25. Voltammograms for copper UPD on Pt(111) from 1 mM Cu^{2+} and (a) 0.1 M H_2SO_4, (b) 0.1 M H_2SO_4 + 1 mM NaCl, (c) 0.1 M H_2SO_4 + 1 mM NaBr, (d) 0.1 M H_2SO_4, pretreated with 1 mM NaI in 0.1 M H_2SO_4, and (e) 0.1 M H_2SO_4, pretreated with 1 mM Na_2S in water. (Dotted lines refer to background currents.) Scan rate: 1 $mV \cdot s^{-1}$. Reproduced with permission from ref 201. Copyright 1990 American Chemical Society.

presence of chloride (or bromide) anions. Initial studies suggested that the more positive set of deposition/stripping peaks was due to deposition/stripping of a full monolayer of copper and that the second set of peaks was due to chloride adsorption/desorption from atop this copper layer.[232] Ex-situ LEED patterns with chloride present in solution showed a (4 × 4) structure after the first deposition peak. When bromide was present in solution, a (7 × 7) structure was found after the first copper deposition peak. This was attributed to a densely packed incommensurate structure of the halides atop the copper which was in registry with the surface.[232]

In more recent studies, and using a RRDE (in a shielding mode) with a Pt(111) single-crystal disk and a Pt ring,[199,200,227,228] it was determined that both sets of voltammetric peaks for copper UPD in the presence of halides were due to copper deposition/stripping (Figure 28). The more positive set of peaks was due to deposition of half a monolayer of copper into a copper−chloride lattice structure. The full copper monolayer was then formed by displacement of the chloride from the superlattice. They determined that the second set of peaks accounted for nearly half of the copper deposition charge and that only about 0.1 monolayer of halide was desorbed/adsorbed in this

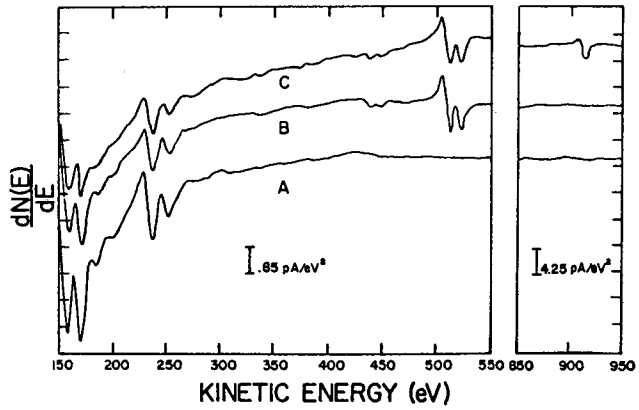

Figure 26. Auger spectra of (A) a Pt(111) clean surface, (B) Pt(111)-($\sqrt{7} \times \sqrt{7}$)*R*19.1°−I, and (C) between first and second copper UPD peaks for an iodine-treated Pt(111). Reproduced with permission from ref 196. Copyright 1984 The Electrochem. Society.

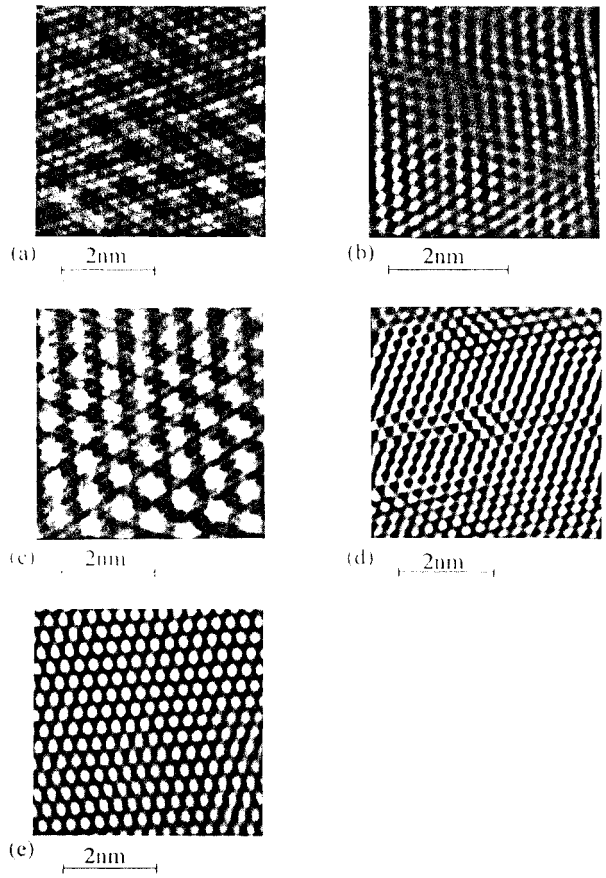

Figure 27. STM images of copper−halide structures on Pt(111) in 0.05 M H_2SO_4 + 1 mM $CuSO_4$ + 0.1 mM KCl, KBr, or KI: (a) (4 × 4) structure of CuCl after the first cathodic current peak (sample potential, +0.55 V vs SHE); (b) Pt(111)-(1 × 1) substrate structure taken before the cathodic peak of Cu + Cl co-deposition (sample potential, +0.75 V vs SHE); (c) (4 × 4) structure of Cu + Br after the first cathodic current peak; (sample potential, 0.54 V vs SHE); (d) ($\sqrt{3} \times \sqrt{3}$)*R*30° structure of Cu + Br after the second cathodic current peak (sample potential, +0.40 V vs SHE); (e) ($\sqrt{3} \times \sqrt{3}$)*R*30° structure of Cu + I after the cathodic current peak (sample potential, 0.38 V vs SHE). Reproduced with permission from ref 36. Copyright 1994 Elsevier Science SA.

voltammetric peak. They were also able to determine that, after the first copper deposition peak, there is

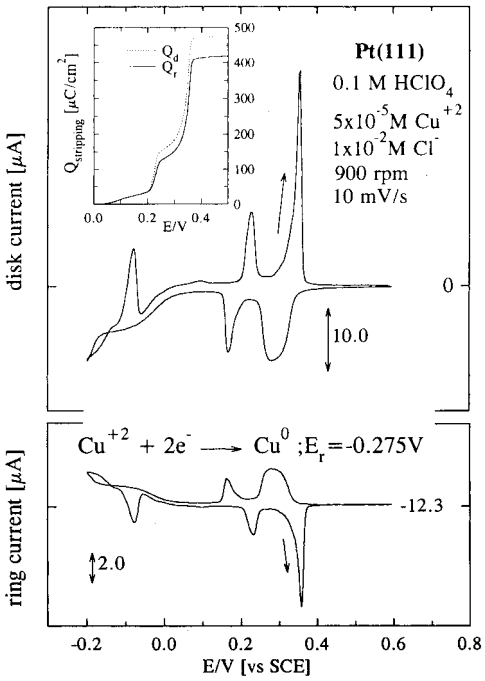

Figure 28. Cyclic voltammogram on a Pt(111) disk electrode in a RRDE assembly at 900 rpm: (top) Cu UPD on Pt(111) at 10 mV·s^{-1}; (bottom) ring electrode currents recorded with the ring being potentiostated at −0.275 V; (inset) Coulombic charging currents on the disk, Q_d, and the ring, Q_r (divided by N: $Q_r = Q_R/N$), electrodes during the positive-going sweep. Reproduced with permission from ref 199. Copyright 1995 Elsevier Science BV.

a copper−halide bilayer structure on the surface that is incommensurate with the platinum surface.[227,228] This appears to correspond to what was previously described as a (4 × 4) structure.

At full copper coverage, and in agreement with the previously proposed mechanism,[232] the copper layer is in registry with the platinum surface.[197,198] It has also been found that, at submonolayer coverages, the copper deposition induced the adsorption of chloride and bromide on Pt(111).[198,202]

In-situ STM measurements (Figure 27) of the UPD of copper onto Pt(111) in the presence of halides shows that when chloride is present there is a (4 × 4) structure.[35,36] This (4 × 4) structure is in disagreement with in-situ X-ray surface scattering results which show that the copper−halide lattice structure is not commensurate with the Pt(111) surface.[227,228] For the case of bromide, the in-situ STM image shows a ($\sqrt{3} \times \sqrt{3}$)*R*30° structure after the second UPD peak as well as a distorted (4 × 4) structure after the first peak.[35,36]

In agreement with the recently proposed mechanism, SEXAFS findings[225] (Figure 24) also indicated that, in the presence of chloride, the copper−copper bond distance of the deposited layer was close to that of bulk copper, unlike that of copper deposited in the absence of chloride. A mechanism was proposed for copper deposition in the presence of halides[203] which included a preadsorbed state, the transient formation of a copper−halide adlayer which led to a copper monolayer covered, in turn, by a halide layer.

Most recently, the dynamics of Cu UPD on Pt(111) electrodes in the presence of chloride (in 0.1 M $HClO_4$

supporting electrolyte) were studied in real time using time-resolved surface X-ray diffraction in conjunction with potential step cronoamperometry.[229] In these experiments, the acquisition of the X-ray data was synchronized with the potential step so that the dynamics of the surface structure formation or dissolution could be followed in real time. A most significant finding of this work was the great time difference that was observed for the decay of the current transient (typically less than about 0.5 s) and the development of long-range order (typically on the order of seconds) suggesting that these two processes take place on significantly different time scales. More recently the same authors reported on a more extensive time-resolved surface X-ray diffraction study which included nucleation behavior.[230]

D. Copper UPD on Other Platinum Single-Crystal Surfaces

Copper UPD has also been studied on the other low-index planes of platinum. The first such studies were done by Scortichini and Reilley[189−191,207] and Kolb,[214] but their surface pretreatment was probably not the most appropriate and their results will not be discussed here. For copper UPD onto the Pt(100) surface in perchloric acid media, the mechanism of copper deposition has been controversial. The discrepancies appear to arise from the reconstruction of the Pt(100) surface prior to copper deposition. When the Pt(100) electrode has a (1 × 1) surface, the corresponding copper UPD voltammetry gives rise to sharp reversible peaks.[198,208] If the measurements are performed on the reconstructed Pt(100)-hex-*R*0.7° surface, the corresponding copper UPD voltammetry is much less reversible and the copper stripping peak appears at a much more positive value.[208,234] From the Pt(100)-(1 × 1) electrode, there is a stripping charge of 446 μC/cm^2, which is in good agreement with the theoretical value of 420 μC/cm^2.[208] SEXAFS experiments performed on the Pt(100)-hex-*R*0.7° have shown that copper deposition takes place in two steps of one-half monolayer each into a *c*(2 × 2) structure.[226] LEED studies of the same system, on the other hand, have the copper forming compact planar islands.[234]

When there are chloride anions present in the depositing solution, the voltammetric profile for copper deposition onto Pt(100)-(1 × 1) is split into two stages just as in the case of Pt(111).[197,198] In this case the voltammetric splitting is much greater than in the case of deposition onto Pt(111) and the more negative peak is spread over a 200 mV range. This greater split is attributed to the stronger binding of chloride to the Pt(100) than to the Pt(111) surface. The first deposition peak corresponds to the formation of a *c*(2 × 2) copper structure with possibly randomly adsorbed chloride, as derived from LEED experiments.[197,198] At this potential, AES showed the presence of half a monolayer of copper which is consistent with the *c*(2 × 2) structure[197] (Figure 29). At full monolayer coverage, LEED studies again show the *c*(2 × 2) structure (Figure 29).

In-situ STM studies of this system also show a *c*(2 × 2) structure of the halide when either chloride or bromide is present.[36] It has been found that the structures for the chloride layers on the full copper monolayer on Pt(100)[210,215] closely match structures of chloride on copper single-crystal surfaces.[197,198]

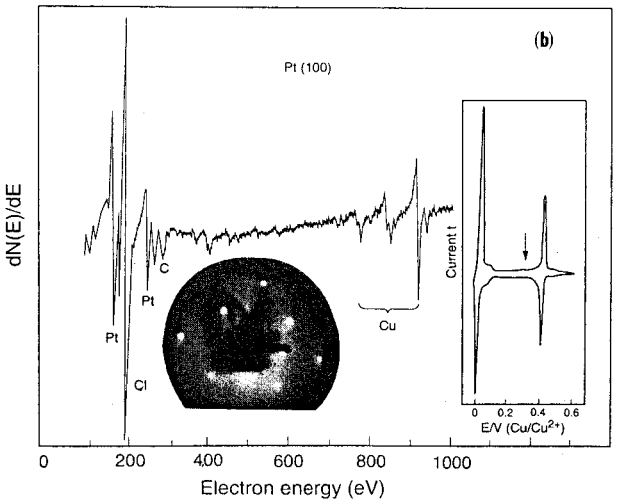

Figure 29. AES spectrum and LEED pattern (62 eV) for the emersion on the anodic sweep of a Pt(100) electrode (insert) from 0.3 M HF (containing 5 × 10^{-5} M Cl$^-$). Reproduced with permission from ref 197. Copyright 1993 Vacuum Society.

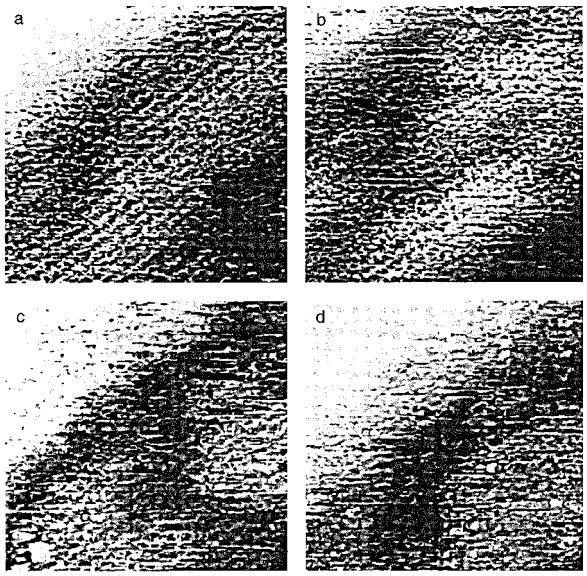

Figure 30. STM images of Pt(110) in 0.1 M H_2SO_4 + 10^{-3} M $CuSO_4$ recorded at increasing potentials: (a) 0.1; (b) 0.2; (c) 0.35; (d) 0.4 V (110 × 110 Å^2, I_t = 63 nA). Reproduced with permission from ref 220. Copyright 1995 Elsevier Science BV.

It has also been found that copper deposition from sulfuric acid solution onto the Pt(110) surface takes place in two distinct steps of about half of a monolayer (Figure 30).[215,233] The data have been interpreted in terms of copper deposition along the substrate grooves, with every second row being occupied until half of a monolayer has been deposited and then completion of the copper monolayer by filling in of the resulting troughs. UHV studies of copper UPD on Pt(110) found that the deposited copper exhibited the same (2 × 1) periodicity as the clean platinum (110) surface.[235] In contrast, in-situ STM experiments revealed a (1 × 1) structure

throughout the entire copper UPD range.[36] In agreement with the others, they found that the copper is deposited and stripped in two distinct steps. There has been little systematic work done on copper deposition onto Pt(110) in the presence of halides.

Studies of copper deposition onto surfaces other than the low index planes of platinum have also been conducted. On platinum-stepped surfaces consisting of (111) terraces of varying width and (100) steps,[209,210] it was found that, at low coverages, copper preferentially adsorbs at the step sites. In contrast to these results, studies of copper UPD on Pt(311), a highly stepped platinum surface, indicated that copper stripping occurred in two distinct peaks, corresponding to stripping from the (111) and the (100) sites, with the more negative peak corresponding to stripping from the (100) step sites (Figure 31).[211] On stepped surfaces with (110) step sites and (111) terraces of varying width, it has been shown that the (110) step sites induce the adsorption of sulfate/bisulfate by submonolayer amounts of copper.[212] It was also found that the maximum amount of induced adsorption took place on the (221) surface which has a 3-atom-wide (111) terrace with a (110) step. It appears that this represents the minimum amount of space necessary to accommodate both the copper and the sulfate/bisulfate.

There has been a limited amount of work on the higher index planes of platinum for copper deposition in the presence of halides. One such study dealt with copper deposition in the presence of chloride and bromide on the Pt(311) surface.[211] In each case, there were four distinct peaks that are ascribed to copper and halide adsorption/desorption processes on the steps and terraces. It was also determined that copper deposition on the (111) terrace sites was preferred over the (100) steps (Figure 31B).

In copper deposition on stepped surfaces with (111) terraces (of varying width) and (110) steps and in the presence of chloride it was found that there could be induced adsorption of chloride by electrodeposited copper and that the site of adsorption ((111) terraces or (110) steps) was dependent on the electrode's surface structure. Induced adsorption on the terrace sites was only observed on terraces that were wider than 9 atoms. Induced adsorption on the (110) steps sites was always observed when steps were present.[238]

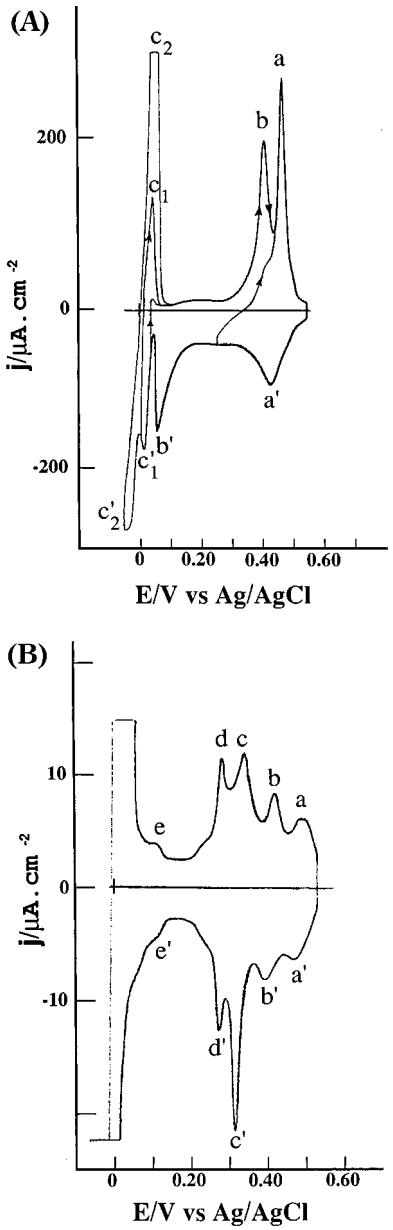

Figure 31. (A) Voltammogram corresponding to the UPD of copper on Pt(311). Test electrolyte: 0.1 M H_2SO_4 + 1 × 10^{-3} M Cu^{2+}. Scan rate: 50 mV·s^{-1}. (B) Steady-state voltammogram corresponding to the UPD of copper on Pt-(311). Test electrolyte: 0.1 M M H_2SO_4 + 1 × 10^{-3} M Cu^{2+} + 1 × 10^{-3} M NaCl. Scan rate: 5 mV·s^{-1}. Letters refer/identify corresponding peaks. Reproduced with permission from ref 211. Copyright 1994 American Chemical Society.

2. Ag UPD on Pt(*h*,*k*,*l*) Electrodes

Although copper deposition is by far the most studied UPD system onto single-crystal platinum surfaces, there has also been substantial work done on silver UPD onto the low-index planes of platinum. These studies have used mainly electrochemical,[117,119,239−244] radiochemical,[243] electrochemical STM,[245,246] X-ray scattering,[247,248] and UHV techniques.[117−119,239,242,249−253]

A. Silver Deposition onto Pt(111)

The initial studies of silver deposition onto polycrystalline samples had led researchers to believe that two monolayers of silver were deposited prior to bulk deposition. When studies were initiated on the Pt(111) surface, this was proven to be true. On Pt(111), the voltammetric profiles are complicated by the fact that the initial deposition begins in the region where oxygen electrosorption would occur in the absence of silver cations. It was found that, at relatively high silver ion concentrations (1 mM), the deposition could be divided into 4 distinct steps[240,242,243] (Figure 32). The first is deposition of 1.25 monolayers between +0.85 and +0.69 V (vs Ag/Ag/Cl). Next was the deposition of 0.2 monolayers between +0.69 and +0.45 V. The third was a very sharp process accounting for 0.75 monolayers between +0.45 and +0.36 V, and finally there was bulk deposition below +0.36 V. There has been some controversy regarding the voltammetric features of the first step. In one study, there was evidence of a sharp voltammetric spike

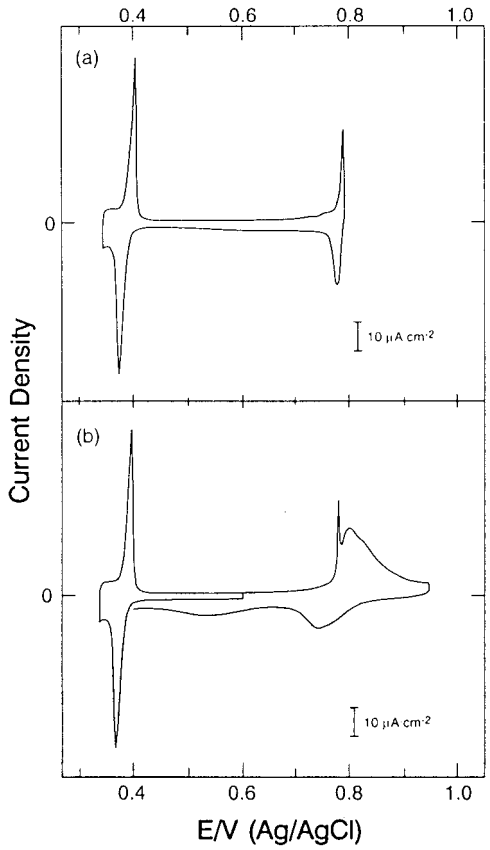

Figure 32. Cyclic voltammetry of Pt(111) in 0.5 M H_2SO_4 solution containing 10^{-3} M $AgClO_4$. Scan rate: 5 $mV \cdot s^{-1}$. The reversal potentials were (a) 0.80 and (b) 0.95 V. Reproduced with permission from ref 243. Copyright 1993 Elsevier Sequoia SA.

observed before development of the broad peak in the very positive potential region (Figure 32).[243] This feature is present only as a shoulder in other studies[240,242] and could probably be attributed to differences in crystal quality. This sharp spike resembled the silver stripping peak in the same potential region when iodine was present on the surface indicating the possibility of anion interactions.[243]

It has also been found that initially, after the immersion of the electrode into the cell, there is already the presence of a small amount of silver on the surface.[240] If the potential is adjusted to more positive values in order to desorb this small amount of silver, the presence of irreversible oxygen adsorption complicates any further silver deposition.[240] At high silver concentrations (1 mM), the silver monolayer formation is via a well-defined manner and the LEED patterns from this system showed a (1 × 1) pattern at all emersion potentials, suggesting a commensurate silver layer.[242] However, when the silver concentration was lowered to 0.005 mM, the silver deposition was found to be via three-dimensional nucleation and island formation.

Studies performed by angular distribution auger microscopy (ADAM) indicated that, after the second monolayer has been deposited, the ADAM image has 6-fold symmetry[252] which could mean that either the outer silver atoms are deposited atop the first layer or the outer silver atoms are in one of the two possible 3-fold hollow sites. STM images of silver deposition seem to indicate that the first two monolayers grow layer-by-layer rotationally commensurate with the Pt(111) substrate.[245] However, recent X-ray scattering studies have demonstrated that a commensurate-to-incommensurate phase transition takes place upon the electrodeposition of the second silver layer.[247,248]

Similar to copper deposition onto iodine pretreated platinum crystals, studies of silver deposition on iodine pretreated samples of Pt(111) have also been carried out. When Pt(111) is pretreated with iodide, there are several different structures that can form on the surface. The easiest pretreatment and therefore the most studied iodide structure is the $(\sqrt{7} \times \sqrt{7})R19.1°-I$ superlattice. This structure is formed by exposure of the electrode to an I_2 vapor beam for several minutes.[117,118,241,246] A cyclic voltammogram for silver UPD onto this surface shows three distinct regions prior to bulk deposition.[117,118,241,246] The most positive deposition peak resulted in 0.44 monolayers of silver being deposited which is virtually equal to the coverage of iodine on the surface: 0.46. At the end of second region, almost 1 full monolayer of silver has been deposited with a silver coverage of 0.84 monolayers. The third distinct region corresponds to deposition of almost a complete additional monolayer of silver. The total coverage of silver equals 1.60 monolayers. Auger studies show that the iodine signal intensity remains nearly constant throughout silver deposition indicating that the iodine layer was always the topmost layer and that the deposited silver lies beneath this iodine layer.[117,118] After completion of the first UPD peak, the LEED showed a (3 × 3) pattern with a unit cell containing four silver and four iodine atoms. During the second voltammetric peak, the (3 × 3) pattern was transformed into a $(\sqrt{3} \times \sqrt{3})R30°$. This structure is also seen at the end of the third UPD peak.[117,118] Bulk silver deposition also produced this same pattern. In-situ STM studies of this system confirm these structures[246] (Figure 33).

There exist other possible structures for the initial iodine layer on Pt(111).[119] This base structure, the $(3\sqrt{3} \times 9\sqrt{3})R30°-I$ structure, is formed by annealing the platinum sample in iodine vapor at atmospheric pressure. Other surface iodine structures can be formed from this structure through thermal desorption. The voltammetry for silver deposition onto these more disordered surface structures gives profiles similar to silver deposition onto a $(\sqrt{7} \times \sqrt{7})$-$R19.1°-I$ superlattice but with differing peak heights, widths, and potentials.[119]

The kinetics of the deposition of the first silver layer were found to be slower on more ordered surfaces, suggesting that surface defects accelerate the deposition possibly by providing nucleation sites.[241] Also, the presence of previously adsorbed organic molecules has been shown to affect the silver deposition.[244] Pyridine-like adsorbates that bind primarily through the ring nitrogen inhibit the deposition of the second silver monolayer but not the first.

B. Silver Deposition onto Other Platinum Surfaces

The voltammetric profile for silver deposition onto Pt(100) shows just two distinct potential regions[240,250,251] (Figure 34). In the more positive region,

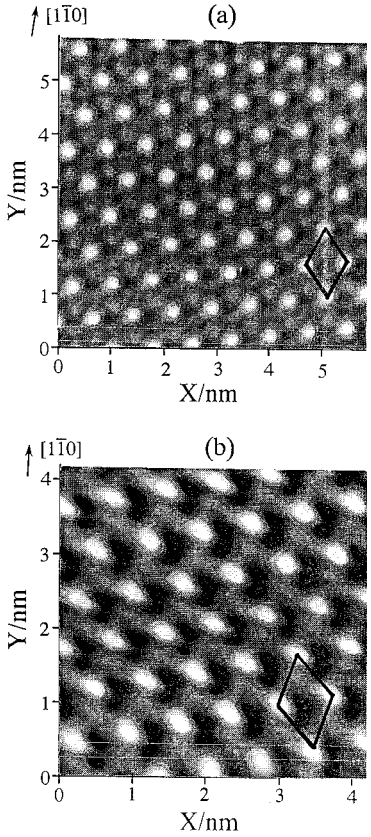

Figure 33. STM top views obtained at the Pt(111)($\sqrt{7} \times \sqrt{7}$)R19.1°−I electrode: (a) in air with a bias voltage of 50 mV; (b) in 1 M $HClO_4$ + 1 mM $AgClO_4$. The electrode potentials of Pt(111) and the tip were 1.05 and 1.2 V versus RHE, respectively. The [110] direction of the Pt(111) lattice is indicated by an arrow. Reproduced with permission from ref 246. Copyright 1995 Elsevier Science BV.

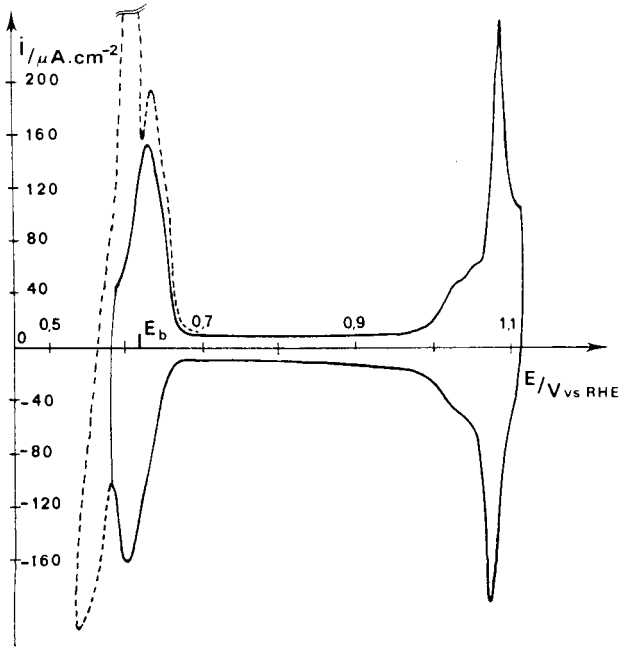

Figure 34. Study of Ag deposition on a Pt(100) electrode. Solution: 1 M H_2SO_4 + 10^{-3} M Ag_2SO_4. Scan rate: 5 mV·s^{-1}. Reproduced with permission from ref 240. Copyright 1984 Elsevier Sequoia SA.

deposition of the first monolayer takes place in the platinum oxidation region without actual oxidation of the surface. As with silver deposition onto Pt(111), if the potential is moved to more positive values, oxygen adsorption occurs, hindering further silver deposition. There is also formation of a second monolayer just prior to bulk deposition although it is not as well defined as on the (111) surface.

On Pt(100), it has been determined that if potential cycling is done in the region including the second monolayer deposition, the second UPD peak moves gradually toward the bulk deposition and a new peak appears in the vicinity of this second UPD peak.[250,251] Incidence-dependent Auger electron spectroscopy has confirmed that repeated cycling of the potential into the region of the second monolayer does induce alloying of the silver and platinum.

On the Pt(110) surface, the adsorption/desorption of silver and oxygen are not distinguishable in the more positive region of the voltammogram. There is also formation of a second layer of silver prior to bulk deposition as there was on the other low-index faces[240] (Figure 35).

Silver deposition has also been studied on Pt(100) surfaces containing iodine adlattices.[239,249] The presence of iodine on the Pt(100) can result in three different lattice structures. Each of these structures showed different responses to the silver deposition. Some of the possible initial structures include a [$c\sqrt{2} \times \sqrt{2}$]$R$45°−I structure, an incommensurate layer, and a [$c\sqrt{2} \times 5\sqrt{2}$]$R$45°−I structure.[249] Again, Auger studies confirm that, after silver deposition, the iodine remains the topmost layer.[249] Cyclic voltammograms of silver deposition onto the [c($\sqrt{2} \times 2\sqrt{2}$)]$R$45°−I structure showed two sharp sets of peaks.[249] When the silver deposition was performed onto the incommensurate structure, the voltammetric peaks became 10 times broader. Deposition onto the [c($\sqrt{2} \times 5\sqrt{2}$)]$R$45°−I lattice covered a range of potentials and formed polycrystalline deposits rather than monatomic layers.[239,249]

3. Irreversible Adsorption of Adatoms on Platinum Electrodes and Other UPD Process

Electrochemical experiments have also been performed to study bismuth deposition onto platinum single-crystal electrodes.[142,254−261] It was found that bismuth exhibits not only a UPD process but also an irreversible adsorption process. In irreversible adsorption, adsorbed adatoms remain on the surface substrate even in the absence of the depositing cation. In some cases, the adsorbed adatom can undergo a redox surface reaction where both species remain adsorbed onto the substrate. The species remain adsorbed and no dissolution occurs, so that the surface coverage is independent of potential. For the irreversible adsorption of bismuth onto Pt(111), it has been found that each bismuth adatom blocks three hydrogen adsorption sites and involves a two electron transfer.[142,254] The voltammetric profile of this irreversible adsorption is shown in Figure 36. In the voltammetric profile there is a reversible charge-transfer process at +0.62 V due to adsorbed bismuth atoms. The maximum bismuth coverage obtained was 0.33 monolayers which would correspond well to a ($\sqrt{3} \times \sqrt{3}$)R30° structure that was found in gas

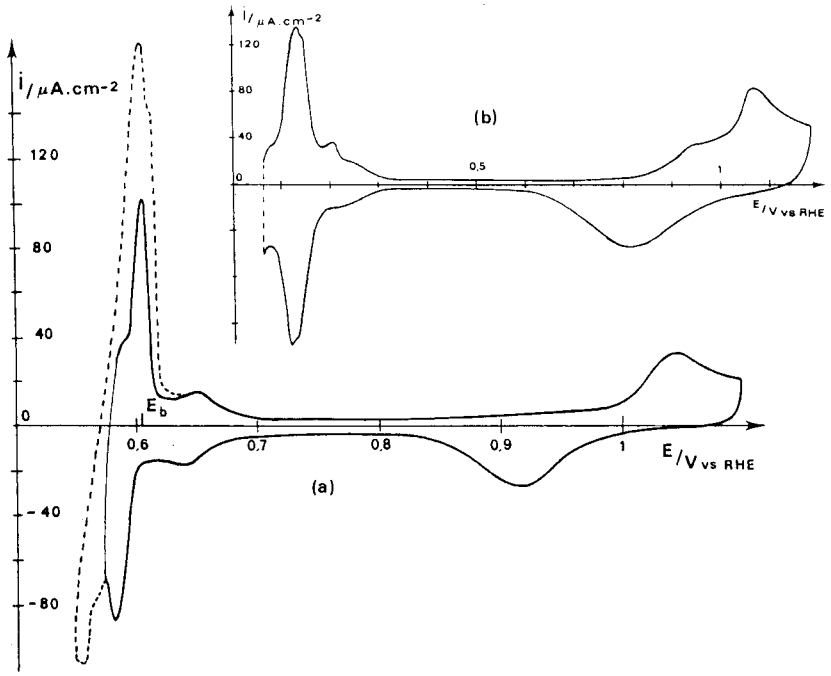

Figure 35. Voltammetric studies of a Pt(110) electrode: (a) solution 1 M H_2SO_4 + 0.5 × 10^{-3} M Ag_2SO_4, scan rate 5 mV/s; (b) solution 1 M H_2SO_4, scan rate 50 mV·s^{-1}. Reproduced with permission from ref 240. Copyright 1984 Elsevier Sequoia SA.

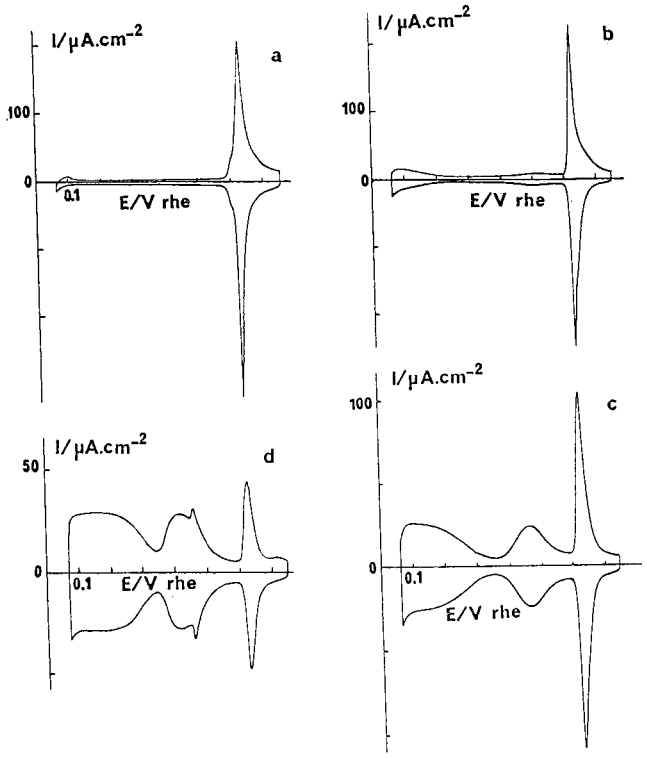

Figure 36. Voltammetric profiles for irreversibly adsorbed bismuth on Pt(111) in 0.5 M H_2SO_4, at various Bi coverages: (a) 0.33; (b) 0.27; (c) 0.14; (d) 0.06. Sweep rate: 50 mV·s^{-1}. Reproduced with permission from ref 142. Copyright 1991 Elsevier, Paris.

dosing LEED measurements.[262] In addition to the irreversible adsorption of bismuth onto Pt(111), there is also evidence of a bismuth UPD process, as shown in Figure 37. This process can be studied when the deposition is done from a 10^{-5} M Bi(III) solution.[142] The first few cycles show the irreversible adsorption peaks at +0.67 V vs RHE. On subsequent cycles, the charge associated with the adsorption process increases and the charge associated with adsorption/desorption of adsorbed hydrogen decreases until its complete disappearance. At this point, bismuth UPD begins at +0.61 V vs RHE. With increasing number of cycles, the charge associated with this new peak increases until it becomes the most important process. There is a 30% increase in the charge obtained when the UPD process is combined with the irreversible adsorption as opposed to irreversible adsorption alone. Possible explanations for this process include either a second layer being formed over the first layer, masking the redox process, or possibly a partial formation of an unstable higher coverage compact layer, as has been observed for irreversible adsorption of bismuth on Pt(111) electrodes.[258] When the bismuth covered electrode is removed from solution, rinsed, and placed in supporting electrolyte only, the voltammograms show a decrease of the process at +0.61 V and an increase in the one at +0.67 V, which is associated to the 0.33 coverage layer.[142]

Bismuth deposition onto Pt(100) is less reversible than on Pt(111) in addition to being shifted to higher potentials.[254] Each bismuth adatom undergoes a two electron transfer and blocks two hydrogen adsorption/desorption sites. There is no evidence of formation of a second layer or other compact structures. Bismuth deposition shows two oxidation peaks and a single reduction peak with a shoulder.[254] It has also been found that the stability of the adsorbed layer depends on surface order.[254,255] The surface defects appear to be preferential sites for dissolution of the bismuth at high potentials, and the steps may be blocked preferentially leaving terrace sites free.

There are several other cations that show irreversible adsorption properties when deposited onto platinum single-crystal surfaces which will not be discussed here. These include tin,[263−265] selenium,[266]

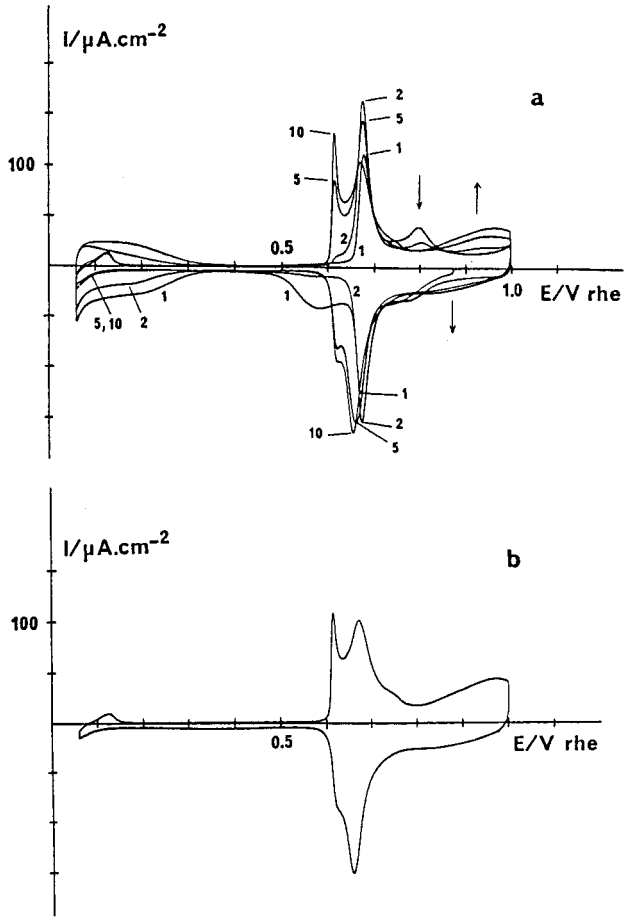

Figure 37. Voltammetric profiles obtained for Pt(111) in bismuth UPD conditions ([Bi(III)] = 10^{-5} M) in 0.1 M $HClO_4$: (a) evolution in first, second, fifth, and tenth cycles; (b) after 20 cycles. Reproduced with permission from ref 142. Copyright 1991 Elsevier, Paris.

arsenic,[258,267,268] antimony,[256,267,269] germanium,[270] thallium,[271−273] palladium,[274−277] lead,[141,142,215,278−284] and cobalt.[285] In addition to these cations and the species mentioned previously, both zinc[286,287,288] and cadmium[289] also show UPD processes on platinum single-crystal electrodes.

4. Hydrogen UPD on Pt(*h*,*k*,*l*) Electrodes

Although not a metal cation as the other UPD species are, hydrogen is also considered to be an ion which displays UPD properties on platinum single-crystal surfaces. Hydrogen UPD has been extensively studied [290−321] since the first results on it were published by Will in 1965.[290] The initial studies performed were all electrochemical, and the electrode probably did not have the crystal quality that is now possible. It was because of this lack of long-range order that the combined techniques of UHV surface preparation and electrochemistry were performed. However, contamination was still a problem on the highly sensitive platinum surfaces. One technique often utilized to rid the surface of contaminants was cycling the potential into the oxygen adsorption/desorption region. However, this has been found to disturb the crystallinity of the platinum surface. In 1980, a new thermal treatment for the preparation of platinum surfaces was introduced.[300] This technique opened up new venues for studies of hydrogen adsorption (and other studies as well) as it did away with the need for UHV chambers. The reproducibility of results from laboratory to laboratory increased dramatically. The voltammetry of the single-crystal surfaces was affected by the long-range order of the surface. With this, hydrogen adsorption/desorption voltammetric profiles on the platinum surfaces became a probe and test of surface quality. The work done since then on hydrogen adsorption on Pt(111) electrodes has been extensive and deserves attention beyond the scope of this review. However, as a general trend, it can be said that hydrogen UPD is a structure sensitive reaction, in which anion desorption takes place simultaneously with hydrogen adsorption. The only exception is the Pt(111) electrode where, depending on the anion adsorption strength and concentration, both processes can be separated. This gives rise to the appearance of the so-called "butterfly pattern" (aslo referred to as "unusual states") which correspond to the process of anion adsorption/desorption (Figure 38). The existence of these states is also tied to the long-range order of the Pt(111) surface. Many studies have also been performed on the other low-index planes as well as stepped surfaces of platinum.

IV. UPD on Silver Surfaces

1. Pb UPD on Ag(*h*,*k*,*l*) Electrodes

Several different types of single-crystal silver surfaces have been used for studying UPD processes on silver electrodes. Crystals cut from bulk silver have obviously been very prevalent, but silver surfaces formed from evaporation onto mica or grown in a Teflon capillary have also been used. These surfaces, especially the capillary grown electrodes, pioneered by Budevski and co-workers, have been found to give responses quite close to an ideal Ag(111) single-crystal surface, and in many cases, they give a far better response than bulk silver single crystals. By far, the most studied UPD system on silver single crystals has been lead deposition. This process has been studied by a wide variety of techniques including electrochemical,[16,322−343] optical reflectivity,[323] SHG,[344] STM,[135,345,346−353] X-ray absorption spectroscopy,[354] X-ray scattering,[355−361] and UHV techniques such as low-energy electron diffraction and Auger electron spectroscopy.[328,362,363] Theoretical models of lead deposition on silver single crystals have also been proposed and studied.[364−366]

A. Pb UPD on Ag(111) Electrodes

Cyclic voltammetry of lead deposition onto Ag(111) in perchloric acid media shows the presence of three voltammetric peaks prior to bulk deposition (Figure 39).[323−325,335,342] The characteristics of both the first and the third peak are highly dependent on the surface pretreatment and degree of order on the surface. It has been proposed that the first peak is due to adsorption at defect sites and that, additionally, the third peak is also associated with some process at defect sites.[323] On crystals grown in Teflon capillaries, there is little presence of the first and

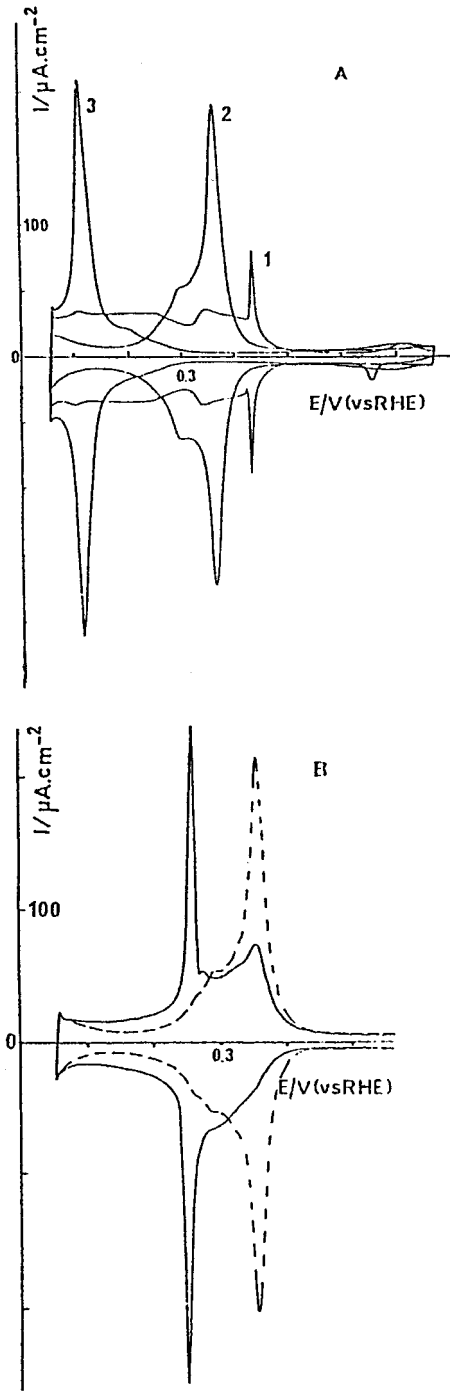

Figure 38. (A) Voltammograms of (1) Pt(111), (2) Pt(100), and (3) Pt(110) cooled in H_2 + Ar atmosphere after flame annealing. (B) Voltammograms of Pt(100) cooled in air (—) or in H_2 + Ar atmosphere (---) (0.5 M H_2SO_4). Sweep rate: 50 mV·s^{-1}. Reproduced with permission from ref 304. Copyright 1991 Elsevier, Paris.

third peaks, suggesting an extremely well-ordered sample.[334] The middle peak is generally quite sharp and contains the majority of the lead deposition charge. This peak appears to be due to a first-order phase transition.[323]

When the lead deposition is performed from chemisorbing electrolytes such as acetate, chloride, bromide, and iodide, the corresponding cyclic voltammograms show only the presence of a single deposition/stripping peak prior to bulk deposition.[362] The disappearance of the additional peaks has been

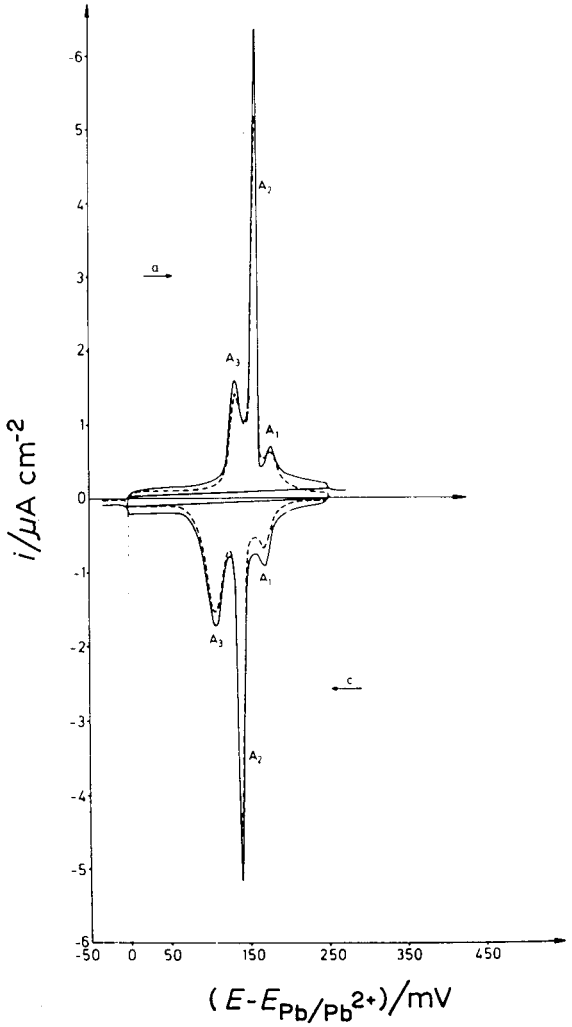

Figure 39. Cathodic (c) and anodic (a) current density–potential curves. System: Ag(111)/Pb^{2+}, ClO_4^-; $E_{Pb/Pb^{2+}}$ = −900 mV vs RHE; $|dE/dt|$= 0.42 mV s^{-1}; T = 298 K. Reproduced with permission from ref 324. Copyright 1978 Elsevier Sequoia SA.

attributed to the blocking of surface defects by the strongly adsorbing anions.[323,334,337] This deposition peak shifted negative from chloride through bromide to iodide.[362]

Considerable effort has been expended in an attempt to elucidate the structure of the lead overlayer on the Ag(111) surface. In-situ SEXAFS has been performed in acetate medium.[354] These studies have found that the deposited lead is in a zerovalent state and that the deposited lead layer is incommensurate with the silver substrate. There is also scattering observed from an atom which is most likely oxygen from water or acetate. This scattering implies that these molecules are chemisorbed on the deposited lead layer.

Additional structural information has been gained from in-situ STM studies.[346−348] A Ag(111)-hcp Pb superlattice structure has been observed, although originally there were reports of a "filled honeycomb Ag(111)-3(2 × 2)Pb" layer.[347,348] Such a structure would require a higher atomic density on the Pb(111) plane, which would introduce a high internal strain within the adlayer.[349] The final lead structure was rotated with respect to the Ag(111) surface by a value

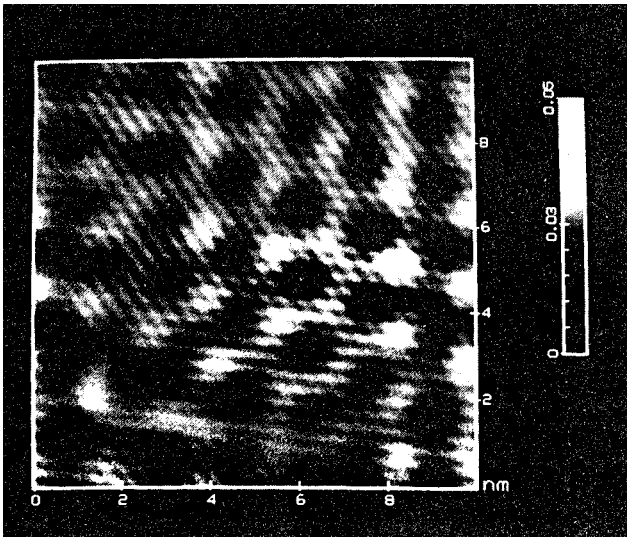

Figure 40. In-situ STM image (filtered) of a Moiré pattern of a Pb monolayer on a quasi-perfect Ag*(111) substrate at $\Delta E = 28$ mV and $T = 298$ K ($I_{tun} = 20$ nA, Pt−Ir tip). System: Ag(111)/5 × 10^{-3} M $Pb(ClO_4)_2$ + 10^{-2} M $HClO_4$. Reproduced with permission from ref 350. Copyright 1994 Pergamon Press.

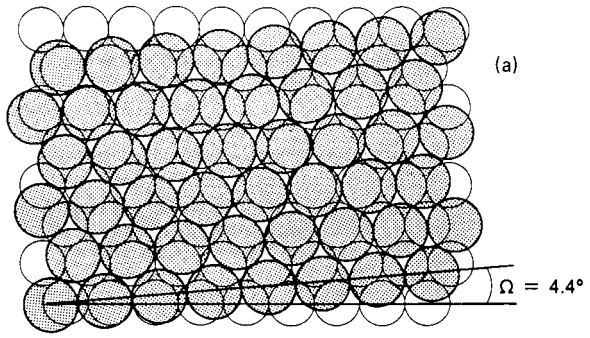

Figure 41. Schematic representation of one domain of UPD lead on silver (111). Open circles represent the silver atoms of the (111) surface, and shaded circles represent the lead atoms. The Pb monolayer is incommensurate, and the rotational epitaxy angle Ω is 4.4°. Reproduced with permission from ref 356. Copyright 1988 American Chemical Society.

of ∼4.4−4.5°. The STM images also indicated the presence of a distinct Moiré pattern,[346,348,349] which gives evidence for a higher order commensurate hcp lead superlattice structure. Moiré patterns of enhanced atomic interaction between the substrate and the overlayer can be distinguished at regular intervals as seen in Figure 40.[349] This Moiré structure has a characteristic length of approximately 1.7 nm and is rotated 24−29° against the lead layer.[348,349]

Surface X-ray scattering techniques have also been employed in structural studies.[356−361] Depositions done from either perchloric acid or acetate media show the presence of peaks in the azimuthal scans at $\phi = \pm 4.5°$ (Figure 41).[357,358,361] This marks the presence of two equivalent domains of an incommensurate lead overlayer with each being rotated ∼4.5° from the Ag[011] direction as confirmed by STM measurements. Grazing Incidence X-ray Scattering (GIXS) has also shown that lead deposited onto Ag(111) at full monolayer coverage undergoes a compression of 1.4% relative to bulk lead.[357−359] The

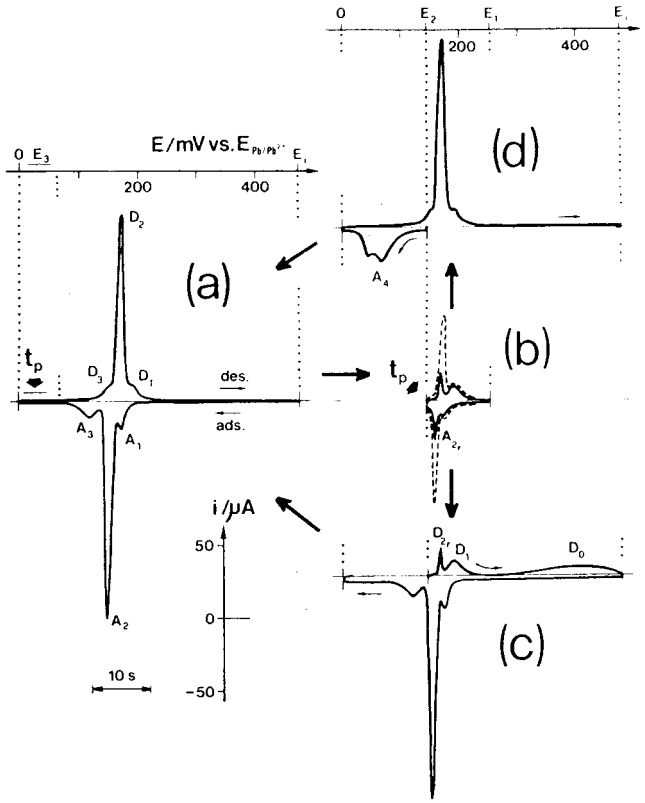

Figure 42. Nonequilibrium phenomena of Pb adsorbates on Ag(111): qualitative investigation by semi-infinite linear sweep voltammetry. $[Pb^{2+}] = 1.43 \times 10^{-3}$ M. Scan rate: 10 mV·s^{-1}. $E_{Pb/Pb^{2+}} = -475$ mV vs SCE. $E_i = E_{Pb/Pb^{2+}} + 475$ mV. (a) Cyclic voltammogram starting at E_i and covering the potential range $E_i \geq E(t) \geq E_3$, where $E_{Pb/Pb^{2+}} \leq E_3 < E_{Pb/Pb^{2+}} + 70$ mV, with and without extended polarization at E_3. (b) Effect of extended polarization t_p at $E = E_2 = E_{Pb/Pb^{2+}} + 140$ mV, following a cathodic potential sweep from E_i to E_2. Cyclic test scans were recorded after $t_p \approx 400$ s (---) and $t_p \approx 2000$ s (—) within the potential range $E_2 \leq E(t) \leq E_1$, where $E_1 = E_{Pb/Pb^{2+}} + 260$ mV. (c) Desorption scan $E_2 \leq E(t) \leq E_i$ after extensive polarization ($t_p \approx 2000$ s) at $E = E_2$, followed by cathodic readsorption sweep [$E_i \geq E(t) > E_{Pb/Pb^{2+}}$]. (d) Adsorption scan [$E_2 \geq E(t) > E_{Pb/Pb^{2+}}$] after extensive polarization ($t_p \approx 2000$ s) at $E = E_2$, followed by anodic desorption sweep [$E_{Pb/Pb^{2+}} < E(t) \leq E_i$]. Reproduced with permission from ref 327. Copyright 1979 Pergamon Press.

compression increases linearly with the applied potential until the onset of bulk deposition where the compression is 2.8%. X-ray studies employing surface differential diffraction have found that the distances measured for the lead layer were between 3.00 ± 0.05 and 3.2 ± 0.1 Å.[360] These distances can be ascribed to lead atoms being adsorbed between the a-top and bridge sites.

When lead UPD onto silver single crystals is done under a voltammetric routine which includes extended long-time polarization at certain potentials, the structure of the overlayer in relation to the silver surface is known to change.[327,330,334,336,338−341,352] These changes have been studied extensively using electrochemical techniques and include, among them, some of the first studies performed on lead deposition onto silver single-crystal surfaces grown in capillaries. Cyclic voltammetric evidence of the structural transformation is shown in Figure 42. The "standard" voltammogram for lead UPD in perchloric acid media

onto Ag(111) has been reported previously, and shows the presence of three sets of voltammetric peaks, labeled A_1-A_3/D_1-D_3.[327,336,338] Extended polarization at the most negative potential does not change any subsequent cyclic voltammetric scans, which suggests that the saturation coverage can be considered stable.

If the extended polarization takes place at a potential value that is located between the second and third peak, A_2 and A_3, subsequent voltammetric scans are significantly altered.[327,330,334,338] There is a gradual decrease of the A_2/D_2 peaks with polarization and after a polarization of 2000 seconds, only residual peaks remain, while peaks A_1/D_1 remain unchanged.[327,330,338] In a subsequent anodic scan to the initial starting point, an additional, broad desorption peak, D_0, is now present.[327,330,338] In contrast, if a subsequent cathodic scan is made from the polarization potential, an additional broad adsorption peak, A_4, is present at more negative values.[327,330] All subsequent voltammetric scans are the same as the "standard", suggesting that the original monolayer structure is again reestablished.

These changes may be ascribed to the extended polarization inducing the slow transformation of the overlayer into a more stable coverage accompanied by partial desorption into solution.[327,330] These transformations may include a partial exchange between the sites of the substrate and the deposit, leading to incorporation of the lead into the silver substrate.[330,338] This incorporation has been ascribed to the lead atoms creating incorporated agglomerates close to growth steps. If the step density is high, the structural transformation takes place at a much faster rate than if the step site density is low.[334,341] The peak D_0 is assigned as due to destruction of the agglomerates located close to the growth steps.[338] It was found that at coverages less than 20%, the incorporation of one lead atom into the crystal lattice gives rise to the blocking of six neighboring adsorption sites, and at coverages greater than 60%, all of the remaining adsorption sites are blocked for subsequent adsorption.[365] Given the extended polarization time needed for this restructuring to occur, the rearrangement of the substrate must be quite slow and also the rate-determining step.[330] Any excess deposit is subsequently desorbed, leaving, in the final state, about one lead atom for every four surface atoms of silver.

If the extended polarization is carried out at a more positive potential; between peaks A_1 and A_2, where the initial lead coverage is much lower, there are some subtle changes.[336,339] Following polarization, if the potential is swept anodically, a broad desorption peak, D_0, occurs, as before. This new peak is assigned to the desorption of lead incorporated into the silver lattice, but unlike before where the desorption occurred at the growth steps, now the desorption is ascribed to unstable agglomerates located farther from the growth steps. It is assumed that all lead particles adsorbed prior to polarization are transformed into the silver surface instead of being desorbed into solution. It has been proposed that the structural transformations of the lead layer on Ag(111) at low coverages are a result of incorporation of lead atoms mainly on the terraces, while at high coverage, the incorporation takes place mainly at steps.[336,338,341] If extended polarization is done at an intermediate coverage, aspects of both low and high coverage are seen.[338] The incorporation processes at step sites and terrace sites do not interfere with each other as the processes at the step sites are much faster than that on terraces.[341]

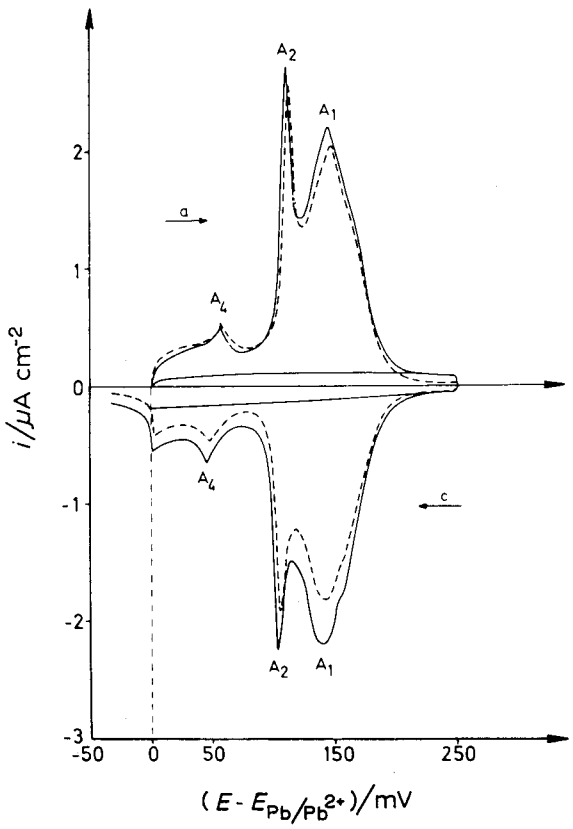

Figure 43. Cathodic (c) and anodic (a) current density–potential curves in a twin electrode thin layer cell. System: Ag(100)/Pb^{2+}, ClO_4^-; $E_{Pb/Pb^{2+}} = -900$ mV vs RHE; $|dE/dt| = 0.42$ mV s^{-1}; $T = 298$ K (solid line, global current; dashed line, generator current). Reproduced with permission from ref 324. Copyright 1978 Elsevier Sequoia SA.

B. Pb UPD on Ag(100) Electrodes

Lead UPD on Ag(100) surfaces from perchloric acid media has been studied by cyclic voltammetric methods, and different profiles have been reported.[323,324,325,334,335,342] The voltammetric profile shows two main peaks with a shoulder on the more positive one at slow sweep rates, in addition to an extra, smaller peak at more negative potentials (Figure 43).[323] It has been proposed that the first peak is due to a simple adsorption process which fills all favorable adsorption sites. The second peak would then correspond to a filling in of the remaining sites to a close-packed monolayer and a phase transition.[323]

In-situ STM studies have confirmed this mechanism structurally.[135,346,347,349] The initial stages of deposition occur at the step sites.[135] From the images taken at higher coverages, the interatomic distance of first nearest neighbors was determined to be 0.40 $\pm$ 0.02 nm and that of the second nearest neighbors was 0.59 $\pm$ 0.02 nm. This corresponds well to the top layer of a Ag(100)–$c(2 \times 2)$Pb–$c(2 \times 2)$Pb bilayer structure (Figure 44).[135,346,347,349] The underlying

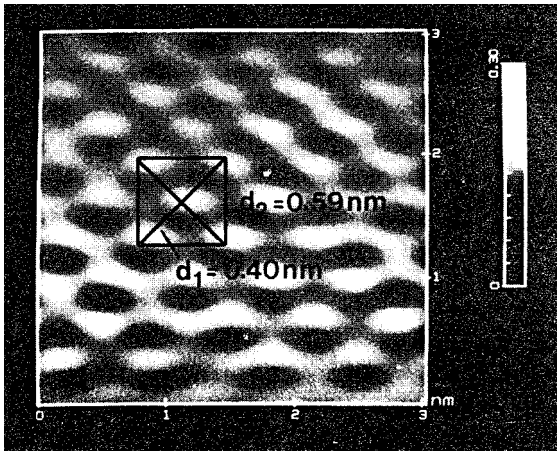

Figure 44. In-situ STM image of UPD lead monolayer on Ag(100). System: Ag(100)/5 × 10^{-3} M $Pb(ClO_4)_2$ + 1 × 10^{-2} M $HClO_4$ (pH = 2); ΔE = 40 mV; T = 298 K. Reproduced with permission from ref 347. Copyright 1992 Pergamon Press.

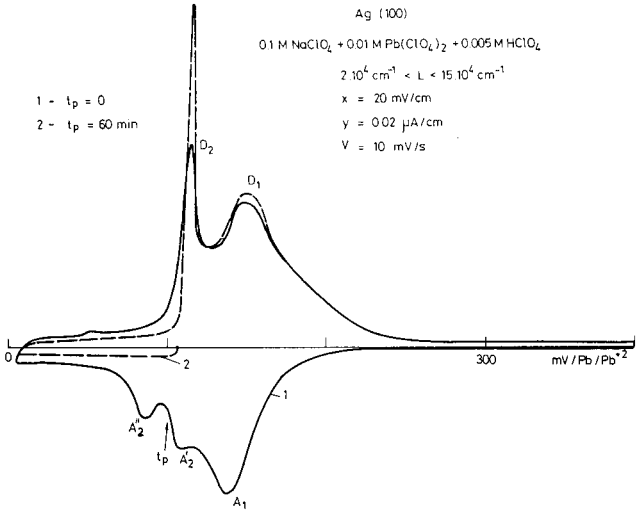

Figure 45. Cyclic voltammograms on Ag(100) (2 × 10^4 < L < 15 × 10^4 cm^{-1}): (1) standard curve; (2) curve after t_p = 60 min. Reproduced with permission from ref 334. Copyright 1986 Pergamon Press.

Ag(100)−c(2 × 2)Pb superlattice could not be observed. This is explained as being due to the relatively high exchange current density of adatoms at medium coverages.[135,346,349] Transient measurements and electrochemical impedance spectroscopy confirmed the enhanced mobility.[349] In-situ STM experiments have also shown the existence of a Moiré pattern for the lead layer on the Ag(100) surface.[135]

If the lead deposited on the Ag(100) surface is subjected to extended polarization, a transformation occurs.[334] However, the potential chosen for extended polarization is quite crucial. If the extended polarization is performed at a potential that lies between the first two peaks, the subsequent voltammetric profiles show no change. The extended polarization must be performed at a potential that lies between the two more negative peaks.[334] Once this requirement is met, there is a significant alteration in subsequent voltammetric profiles as seen in Figure 45. The most negative adsorption peak disappears, while the first desorption peak becomes much sharper and higher.[334] These results suggest a kinetic hindrance to the formation of the lead adsorbate which occurs after a partial formation of the layer. These alterations in the voltammetric profiles have been ascribed not to a structural transformation as seen on the Ag(111) but rather to either a phase transformation in the adsorption layer or the competitive adsorption of anions.[334]

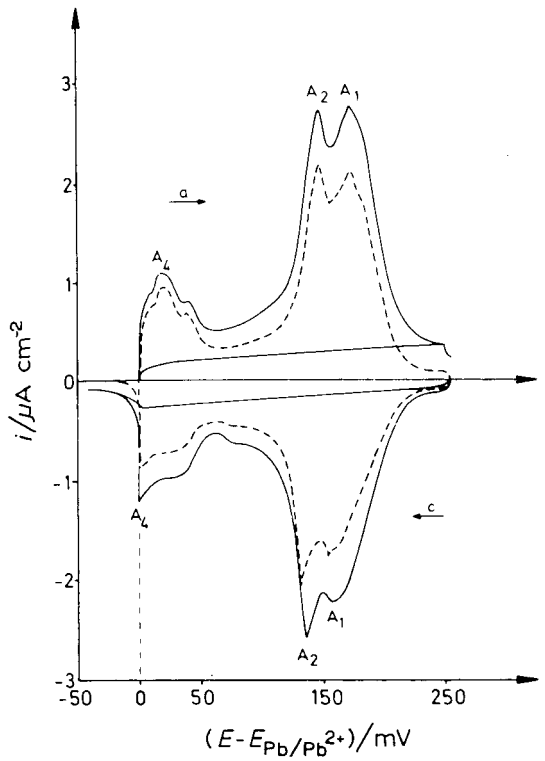

Figure 46. Cathodic (c) and anodic (a) current density−potential curves in a twin electrode thin layer cell. System: Ag(110)/Pb^{2+}, ClO_4^-; $E_{Pb/Pb^{2+}}$ = −900 mV vs RE; |dE/dt| = 0.42 mV s^{-1}; T = 298 K (solid line, global current; dashed line, generator current). Reproduced with permission from ref 324. Copyright 1978 Elsevier Sequoia SA.

C. Pb UPD on Ag(110) Electrodes

Cyclic voltammograms of lead deposition onto a Ag(110) surface show the presence of three peaks as shown in Figure 46.[323,324,335] It is believed that the first two peaks represent adsorption and a phase transformation, respectively.[323] The third peak has been attributed to deposition occurring atop the previously formed monolayer.[323] This is the only low-index plane of silver which shows the presence of the initial stages of second-monolayer deposition prior to bulk deposition.

2. Tl UPD on Ag(*h*,*k*,*l*) Electrodes

In addition to lead UPD onto silver single crystal surfaces, thallium UPD has also been extensively investigated. Thallium UPD has been studied by electrochemical techniques,[11,322,329,330,332,335,337,367−371] radiotracer,[372] optical methods,[368] in-situ STM,[352] X-ray scattering,[361,362,373−375] SHG[344,374,376] and UHV techniques.[362] Theoretical studies have also been performed.[377]

Cyclic voltammetric measurements of the UPD of thallium onto Ag(111) show the presence of two

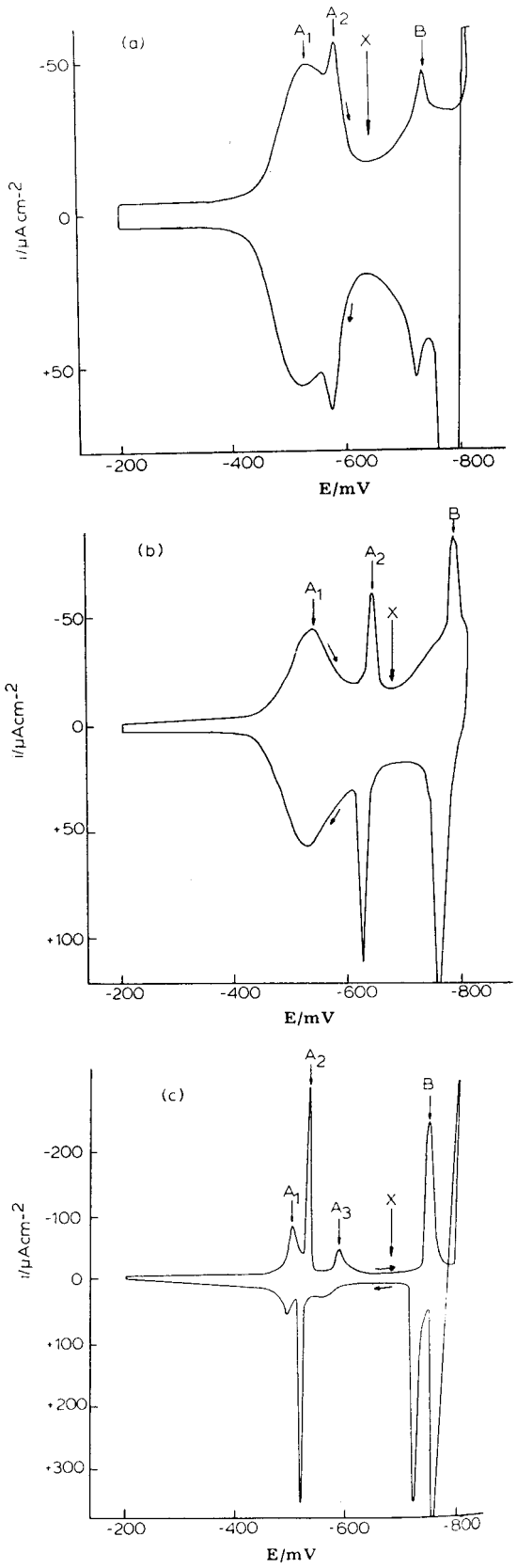

Figure 47. Cyclic voltammograms for thallium deposition onto chemically polished single crystals of silver: (a) 110; (b) 100; (c) 111 (0.74 mM Tl_2SO_4/0.5 M Na_2SO_4/1 mM $HClO_4$). Sweep rate: 30 mV·s^{-1}. Reproduced with permission from ref 368. Copyright 1974 Elsevier Sequoia SA.

distinct regions (Figure 47).[335,368,370] The more positive region contains three adsorption/desorption peaks

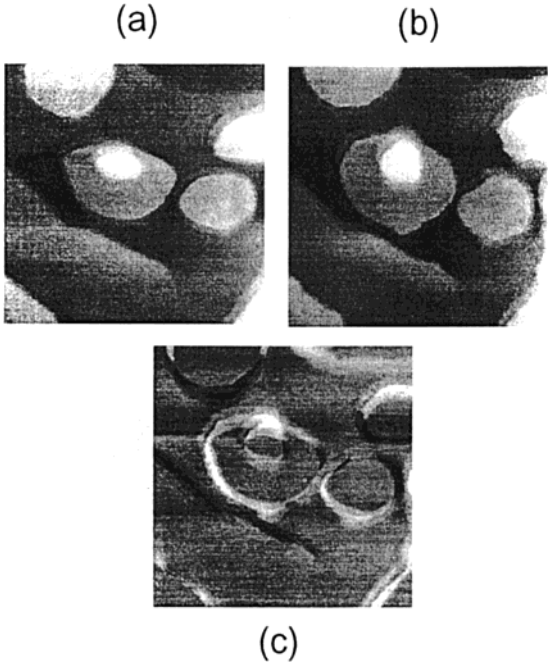

Figure 48. Effect of Tl adsorption in the voltammetric peak A_1 upon the nanometer-scale morphology. Images were recorded in 0.01 M $HClO_4$ + 0.005 M Tl^+. Window size: 146 × 146 nm. Gray scale range: 1.1 nm. Tunneling current: 25 nA. Key: (a) image of the Tl-free surface, ΔE = 436 mV; (b) image of the surface after Tl adsorption in peak A_1, ΔE = 324 mV; (c) difference pattern between images (a) and (b). Reproduced with permission from ref 352. Copyright 1995 Pergamon Press.

and corresponds to the deposition of one monolayer. The sharpness of the middle peak of this region suggests a two-dimensional nucleation and crystal growth process.[368] The second region, consisting of one voltammetric peak just prior to bulk deposition, also corresponds to the deposition/stripping of one monolayer. After deposition of one complete monolayer onto the silver surface, there are no favorable sites for adsorption to occur and nucleation and crystal growth of the second layer starts without any initial adsorption.[368]

Attempts to elucidate the structure of the thallium overlayers on Ag(111) have been made using several in-situ techniques. STM studies have been performed before and after the initial adsorption at voltammetric peak A_1. These images, seen in Figure 48, show that the Tl adsorption decorates the step-sites of Ag(111).[352] This confirms the assumption that the first voltammetric peak corresponds to adsorption at defect sites. Upon completion of adsorption of the first monolayer, STM images show a hexagonally close-packed thallium adlayer structure which is compressed in relation to bulk thallium.[352] The thallium overlayer is also rotated with respect to the silver surface by an angle of ~2.3 ± 0.3°. Upon completion of the second monolayer of thallium, STM images again show the presence of a hexagonally close-packed structure with nearly the same Tl−Tl nearest-neighbor distance as seen in the first layer.[352]

Many of the in-situ STM measurements have been confirmed by in-situ X-ray scattering studies.[361,373,374] These measurements have shown that, after complete deposition of one monolayer, there is an incom-

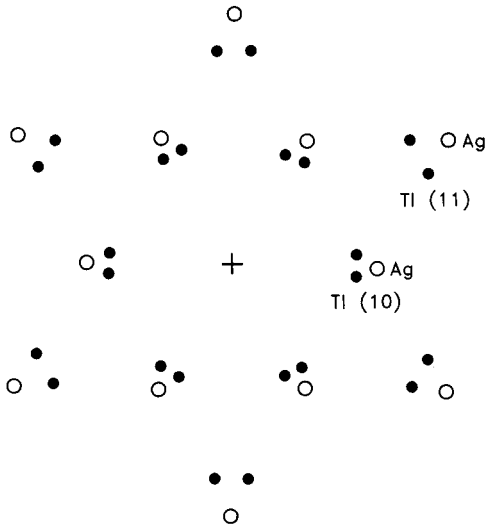

Figure 49. In-plane X-ray diffraction pattern ($Q_z = 0$) for a monolayer of Tl on Ag(111). The center of the pattern is illustrated with a plus sign, the Ag reflections are illustrated with open circles, and the Tl reflections are illustrated with solid circles. There are two observed domains, oriented ±4.6° from the Ag substrate. Reproduced with permission from ref 374. Copyright 1992 American Physical Society.

mensurate, hexagonal structure on the surface. This structure is compressed relative to bulk thallium by 1.4−3.0% and rotated from the Ag[01$\bar{1}$] direction by Ω ca. 4−5°, which depends on potential.[361,373,374] The diffraction pattern is shown in Figure 49. This structure is the same as vapor deposited thallium onto Ag(111), suggesting that the solvent molecules do not affect the structure.[374] Upon completion of deposition of the second monolayer, the thallium forms a bilayer that is also an incommensurate hexagonal structure.[361,373,374] The second layer is commensurate with the layer beneath it, and the newly deposited thallium atoms sit in the 3-fold hollow sites of the bottom layer.[374] In this structure, the compression is 1.0% relative to bulk thallium and the rotation is 3.9°.[373,374] Differential X-ray diffraction showed that, during thallium deposition, there is a gradual increase in the intensity of the diffraction peaks, suggesting that thallium deposition seems to be a gradual adsorption as opposed to a first-order phase transition which Pb deposition appears to be.[360]

As with lead UPD, thallium UPD also shows structural changes on Ag(111) with extended polarization.[330,370] If the extended polarization is performed after the completion of either the first or second monolayer, there are no apparent changes in any subsequent voltammetric scan suggesting that, upon completion of the monolayer, the resulting structure is stable.[330,370] If the extended polarization is performed at potentials that reside between the second and third adsorption peaks, E_2, the overlayer structure changes significantly. As seen in Figure 50, subsequent cyclic voltammograms exhibit a decrease in peaks A_2/D_2 until their complete disappearance, while peaks A_1/D_1 remain nearly constant.[370] If the polarization is followed by an anodic voltammetric

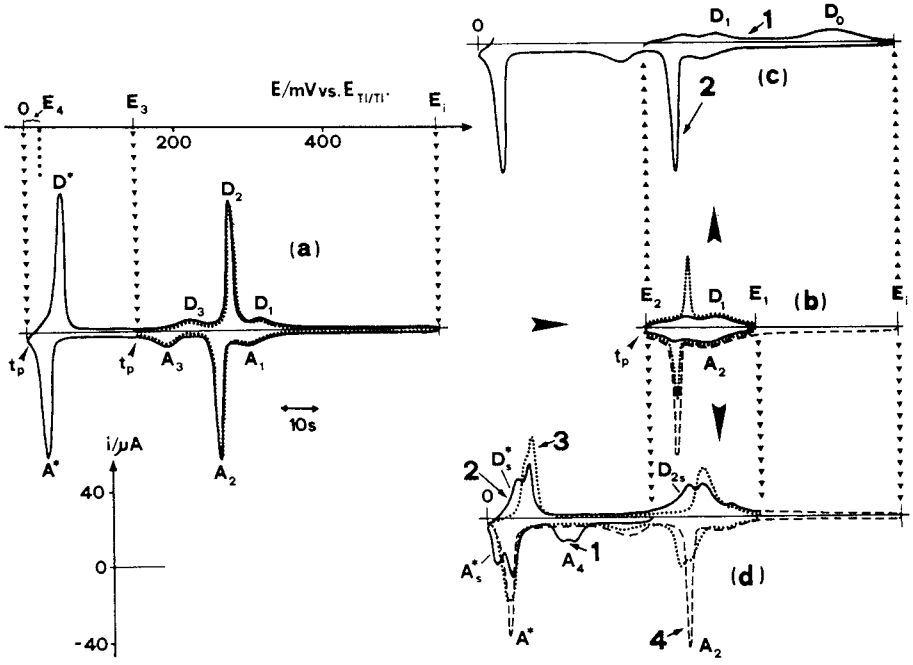

Figure 50. Nonequilibrium phenomena of Tl adsorbates on Ag(111): Qualitative investigation by semi-infinite cyclic voltammetry. $[Tl^+] = 1.5 \times 10^{-3}$, $v = 10$ mV·s^{-1}, and $E_i = E_{Tl/Tl^+} + 570$ mV. Key: (a) cyclic voltammograms starting at E_i and covering the potential ranges $E_i \geq E(t) \geq E_{Tl/Tl^+}$ (—) and $E_i \geq E(t) \geq E_2$} (····), with and without extended polarization at $E = E_4 \approx E_{Tl/Tl^+}$ and $E = E_3 = E_{Tl/Tl^+} + 150$ mV, respectively; (b) effect of extended polarization at $E = E_2 = E_{Tl/Tl^+} + 230$ mV with initial cathodic scan (---), $E_i \geq E(t) \geq E_2$, followed by extended polarization of various duration t_p at $E = E_2$ and subsequent cyclic scans within the range $E_2 \leq E(t) \leq E_1$, e.g. after $t_p \approx 1000$ s (····) and $t_p \approx 2000$ s (—) ($E_1 = E_{Tl/Tl^+} + 350$ mV); (c) desorption scan (curve 1), $E_2 \leq E(t) \leq E_i$, after extended polarization ($t_p > 2000$ s) at E_2, followed by readsorption sweep (curve 2); (d) adsorption scan (curve 1, —), $E_2 \geq E(t) \geq E_{Tl/Tl^+}$, after extended polarization ($t_p > 2000$ s) at E_2 followed by desorption sweep (curve 2, —) and subsequent potential cycling within the range $E_{Tl/Tl^+} \leq E(t) \leq E_1$. Curve 3 (····): cyclic voltammogram recorded after potential cycling during ≈500 s. Curve 4 (—): Readsorption sweep following potential shift to E_i. Reproduced with permission from ref 370. Copyright 1978 Pergamon Press.

scan, the presence of a new desorption peak, D_0, can be observed. Subsequent voltammetric scans indicate that the original profile is reestablished. Only one-third of the charge associated with peak A_2 is recovered in peak D_0, suggesting simultaneous desorption during polarization while the remaining thallium is bound to the substrate more strongly than before as seen in the case of lead adsorption. If, on the other hand, the polarization is followed by a cathodic scan, the presence of a new broad, adsorption double peak, A_4, is seen. Following this peak, the second monolayer adsorption is broadened and split into two peaks.[330,370] Repetitive potential cycling from this state will gradually reestablish the original profile.

A. Tl UPD on Ag(100) and Ag(110) Electrodes

When cyclic voltammetric scans of thallium deposition onto Ag(100) are performed at slow sweep rates, the presence of three distinct sets of peaks can be seen (Figure 47).[335,368,370] The coverage data suggest that this system is compatible with three successively built up Ag(100)−$c(2 \times 2)$Tl structures.[370] If the voltammetry is performed at sweep rates faster than $\sim$40 mV s^{-1}, an additional voltammetric peak is found at negative potentials.[368] In contrast to the Ag(111) surface, the Ag(100) substrate does not exhibit any changes with thallium coverage under extended polarization conditions.[370]

Thallium deposition onto Ag(100) has also been studied by surface X-ray scattering.[375] In these studies it has been found that, following deposition in the first voltammetric peak, there is a disordered phase until after deposition in the second voltammetric peak which leads to a full monolayer. These measurements indicated that the first monolayer of thallium forms a $c(p\times 2)$ close-packed structure which compresses uniaxially (p decreasing from 1.185 to 1.168) with decreasing potential.[375] With deposition of the second layer, it has been found that the first layer expands slightly and both layers form a $c(1.2 \times 2)$ bilayer.

Cyclic voltammograms of thallium deposition onto Ag(110) show the presence of three sets of adsorption/desorption peaks that are not as well defined as on the other low index faces of silver (Figure 47).[368] As on the other faces, the deposition of thallium probably gives total coverages of two monolayers.[368]

3. Other UPD Systems on Ag(*h*,*k*,*l*) Electrodes

UPD onto the low-index planes of silver has been studied using other cations although not as extensively as with lead and thallium. Studies of bismuth,[362,378,379] cadmium,[337,380−382] copper,[383−385] nickel,[165] and zinc[376] deposition have been performed.

V. Conclusions

In this review, we have explored structural aspects of the electrodeposition of metal monolayers onto well-ordered single-crystal electrode surfaces with emphasis on gold, platinum, and silver substrates. The electrodeposition appears to take place with the formation of well-defined surface structures at sub- and full-monolayer coverage. The kinetics of electrodeposition/desorption as well as the resulting structures are greatly dependent on the nature and concentration of anions. In the presence of weakly adsorbing anions (e.g. perchlorate), the kinetics of deposition/desorption are typically sluggish. The presence of strongly interacting anions (e.g. halides except fluoride) generally leads to much faster kinetics often ascribed to the formation of coadsorbed (M−X) layers. The formation of these layers is associated in some cases with phase transitions.

In the case of small lattice mismatch between the adsorbate and the substrate, the resulting structures are often commensurate. In systems with a large lattice mismatch, the deposits are generally incommensurate, especially at monolayer coverage. As a general mechanism for the monolayer formation one can postulate a sequence of events that involves electrodeposition of the metal being deposited coupled with the coadsorption of anions to form a 2-D metal anion layer. Further reduction results in the disruption of these layers with additional electrodeposition leading to the formation of a zerovalent metal adlayer. The presence of steps greatly modifies the structure and kinetics by providing sites of enhanced reactivity for adsorption of both metal and anions.

VI. Abbreviations and Acronyms

ADAM	angular distribution Auger microscopy
AES	Auger electron spectroscopy
AFM	atomic force microscopy
CTR	crystal truncation rod
EQCM	electrochemical quartz crystal microbalance
FTIR	Fourier transform infrared
GIXS	grazing incidence X-ray scattering
IRAS	infrared reflection absorption spectroscopy
LEED	low-energy electron diffraction
RHEED	reflection high-energy electron diffraction
RRDE	rotating ring-disk electrode
SEXAFS	surface-extended X-ray absorption fine structure
SGH	second harmonic generation
STM	scanning tunneling microscopy
UHV	ultrahigh vacuum
UPD	underpotential deposition
XANES	X-ray absorption near-edge structure
XAS	X-ray absorption spectroscopy

Acknowledgments

This work was supported by the National Science Foundation, the Office of Naval Research, the Cornell Center for Materials Research, and DGES of Spain. E.H. acknowledges the support by a Postdoctoral Fellowship from the Spanish government. H.D.A. acknowledges support by a sabbatical Fellowship from the Generalitat Valenciana.

References

(1) Somorjai, G. A. *Chemistry in Two Dimensions: Surfaces*; Cornell University Press: London, 1981.
(2) Rhodin, T. N.; Ertl, G. *The Nature of the Surface Chemical Bond*; North-Holland: Amsterdam, 1979.
(3) Adamson, A. W. *Physical Chemistry of Surfaces*, 4th ed.; Wiley: New York, 1982.
(4) Benard, J.; Ed. *Adsorption on Metal Surfaces*; Elsevier Scientific Publ.: Amsterdam, 1983.

(5) Gaebler, N.; Jacobi, K.; Ranke, W. *Surf. Sci.* **1978**, *75*, 355.
(6) Shmeisser, D.; Jacobi, K. *Surf. Sci.* **1979**, *88*, 138.
(7) Takasu, Y.; Bradshaw, A. M. In *Chemistry and Physics of Solids and their Surfaces*; 1978; Vol. 7, p 59.
(8) Kolb, D. M. In *Advances in Electrochemistry and Electrochemical Engineering*; Gerisher, H., Tobias, C. W., Eds.; Wiley-Interscience: New York, 1978; Vol. 11, p 125.
(9) Adzic, R. In *Advances in Electrochemistry and Electrochemical Engineering*; Gerisher, H., Tobias, C. W., Eds.; Wiley-Interscience: New York, 1984; Vol. 13.
(10) Juttner, K.; Lorenz, W. J. *Z. Phys. Chem.* **1980**, *122*, 163.
(11) Lorenz, W. J.; Hermann, H. D.; Wüthrich, N.; Hilbert, F. *J. Electrochem. Soc.* **1974**, *121*, 1167.
(12) Schultze, J. W.; Dickertmann, D. *Surf. Sci.* **1976**, *54*, 489.
(13) Szabos, S. *Int. Rev. Phys. Chem.* **1991**, *10*, 207.
(14) Aramata, A. In *Modern Aspects of Electrochemistry*; Bockris, J. O'M., White, R. E., Conway, B. E., Eds.; Plenum Press: New York, 1997; Vol. 31, p 181.
(15) Lorenz, W. J.; Budevski, E. B.; Staikov, G. T. *Electrochemical phase formation and growth*; Wiley-VCH: Weinheim, Germany, 1996.
(16) Dickertmann, D.; Koppitz, F. D.; Schultze, J. W. *Electrochim. Acta* **1976**, *21*, 967.
(17) Cappadonia, M.; Linke, U.; Robinson, K. M.; Schidberger, J.; Stimming, U. *J. Electroanal. Chem.* **1996**, *405*, 227.
(18) Hölze, M. H.; Zwing, V.; Kolb, D. M. *Electrochim. Acta* **1995**, *40*, 1237.
(19) Shi, Z.; Lipkowski, J. *J. Electroanal. Chem.* **1994**, *364*, 289.
(20) Shi, Z.; Lipkowski, J. *J. Electroanal. Chem.* **1994**, *365*, 303.
(21) Shi, Z.; Lipkowski, J. *J. Electroanal. Chem.* **1994**, *369*, 283.
(22) Shi, Z.; Lipkowski, J. *J. Phys. Chem.* **1995**, *99*, 417.
(23) Shi, Z.; Wu, S.; Lipkowski, J. *J. Electroanal. Chem.* **1995**, *384*, 171.
(24) Shi, Z.; Wu, S.; Lipkowski, J. *Electrochim. Acta* **1995**, *40*, 9.
(25) Hölze, M. H.; Retter, U.; Kolb, D. M. *J. Electroanal. Chem.* **1994**, *371*, 101.
(26) Omar, I. O.; Pauling, H. G.; Jüttner, K. *J. Electrochem. Soc.* **1993**, *140*, 2187.
(27) Magnussen, O. M.; Hotlos, J.; Nichols, R. J.; Kolb, D. M.; Behm, R. J. *Phys. Rev. Lett.* **1990**, *64*, 2929.
(28) Magnussen, O. M.; Hotlos, J.; Beitel, G.; Kolb, D. M.; Behm, R. J. *J. Vac. Sci. Technol. B* **1991**, *9*, 969.
(29) Hotlos, J.; Magnussen, O. M.; Behm, R. J. *Surf. Sci.* **1995**, *335*, 129.
(30) Möller, F. A.; Magnussen, O. M.; Behm, R. J. *Phys. Rev. B* **1995**, *51*, 2484.
(31) Möller, F. A.; Magnussen, O. M.; Behm, R. J. *Electrochim. Acta* **1995**, *40*, 1259.
(32) Hachiya, T.; Honbo, H.; Itaya, K. *J. Electroanal. Chem.* **1991**, *315*, 275.
(33) Batina, N.; Will, T.; Kolb, D. M. *Faraday Discuss.* **1992**, *94*, 93.
(34) Green, M. P.; Hanson, K. P. *J. Vac. Sci. Technol. A* **1992**, *10*, 3012.
(35) Matsumoto, H.; Oda, I.; Inukai, J.; Ito, M. *J. Electroanal. Chem.* **1993**, *356*, 275.
(36) Matsumoto, H.; Oda, I.; Inukai, J.; Ito, M. *J. Electroanal. Chem.* **1994**, *379*, 223.
(37) Kolb, D. M. *Ber. Bunsen-Ges. Phys. Chem.* **1994**, *98*, 1421.
(38) Haiss, W.; Sass, J. K. *Langmuir* **1996**, *12*, 4311.
(39) Haiss, W.; Sass, J. K. *J. Electroanal. Chem.* **1996**, *410*, 119.
(40) Manne, S.; Hansma, P. K.; Massie, J.; Elings, V. B.; Gewirth, A. A. *Science* **1991**, *251*, 183.
(41) Ikemiya, N.; Miyaoka, S.; Hara, S. *Surf. Sci.* **1994**, *311*, L641.
(42) Ikemiya, N.; Miyaoka, S.; Hara, S. *Surf. Sci.* **1995**, *327*, 261.
(43) Toney, M. F.; Howard, J. N.; Richer, J.; Borges, G. l.; Gordon, J. G.; Melroy, O. R. *Phys. Rev. Lett.* **1995**, *75*, 4472.
(44) Gordon, J. G.; Melroy, O. R.; Toney, M. F. *Electrochim. Acta* **1995**, *40*, 3.
(45) Chabala, E. D.; Cairns, J.; Rayment, T. *J. Electroanal. Chem.* **1996**, *412*, 77.
(46) Herrero, E.; Glazier, S.; Buller, L. J.; Abruña, H. D. *J. Electroanal. Chem.* **1999**, *461*, 121.
(47) Herrero, E.; Glazier, S.; Abruña, H. D. *J. Phys. Chem B* **1998**, *102*, 9825.
(48) Cappadonia, M.; Robinson, K. M.; Schmidberger, J.; Stiming, U. *J. Electroanal. Chem.* **1997**, *436*, 73.
(49) Blum, L.; Abruña, H. D.; White, J.; Gordon, J. G., II; Borges, G. L.; Samant, M. G.; Melroy, O. R. *J. Chem. Phys.* **1986**, *82*, 6732.
(50) Melroy, O. R.; Borges, G. L.; Blum, L.; Abruña, H. D.; Albarelli, M. J.; Samant, M. G.; McMillan, M.; White, J. H.; Gordon, J. G., II. *Langmuir* **1988**, *4*, 728.
(51) Abruña, H. D.; White, J. H.; Albarelli, M. J.; Bommarito, G. M.; Bedzyk, M. J.; McMillan, M. *J. Phys. Chem.* **1988**, *92*, 7045.
(52) Tourillon, G.; Guay, D.; Tadjeddine, A. *J. Electroanal. Chem.* **1990**, *289*, 263.
(53) Tadjeddine, A.; Guay, D.; Landouceur, M.; Tourillon, G. *Phys. Rev. Lett.* **1991**, *66*, 2235.
(54) Tadjeddine, A.; Tourillon, G.; Guay, D. *Electrochim. Acta* **1991**, *36*, 1859.
(55) Tadjeddine, A.; Tourillon, G. *Analusis* **1992**, *20*, 309.
(56) Tadjeddine, A.; Lahrichi, A.; Tourillon, G. *J. Electroanal. Chem.* **1993**, *360*, 261.
(57) Wu, S.; Lipkowski, J.; Tyliszczak, T.; Hitchcock, A. P. *Prog. Surf. Sci.* **1995**, *50*, 227.
(58) Abruña, H. D.; Gog, T.; Mateerlik, G.; Uelhoff, W. *J. Electroanal. Chem.* **1993**, *360*, 315.
(59) Borges, G. L.; Kanazawa, K. K.; Gordon, J. G., II; Ashley, K.; Richer, J. *J. Electroanal. Chem.* **1994**, *364*, 281.
(60) Watanabe, M.; Uchida, H.; Miura, M.; Ikeda. N. *J. Electroanal. Chem.* **1995**, *384*, 191.
(61) Uchida, H.; Hiei, M.; Watanabe, M. *J. Electroanal. Chem.* **1998**, *452*, 97.
(62) Koos, D. A.; Richmond, G. L. *J. Phys. Chem.* **1992**, *96*, 3770.
(63) Nakay, Y.; Zei, M. S.; Kolb, D. M.; Lehmpfuhl, G. *Ber. Bunsen-Ges. Phys. Chem.* **1984**, *88*, 340.
(64) Kolb, D. M. *Z. Phys. Chem. (Munich)* **1987**, *154*, 179.
(65) Zei, M. S.; Qiao, G.; Lehmpfuhl, G.; Kolb, D. M. *Ber. Bunsen-Ges. Phys. Chem.* **1987**, *91*, 349.
(66) Zhang, J.; Sung, Y. E.; Rikvold, P. A.; Wieckowski, A. *J. Chem. Phys.* **1996**, *104*, 5699.
(67) Bludau, H.; Wu, K.; Zei, M. S.; Eiswirth, M.; Over, H.; Ertl, G. *Surf. Sci.* **1998**, *402*−*4*, 786.
(68) Magnussen, O. M.; Behm, R. J. *J. Electroanal. Chem.* **1999**, *467*, 258.
(69) Huckaby, D. A.; Blum, L. *J. Electroanal. Chem.* **1991**, *315*, 255.
(70) Blum, L.; Huckaby, D. A. *J. Electroanal. Chem.* **1994**, *375*, 69.
(71) Huckaby, D. A.; Blum, L. *Langmuir* **1995**, *11*, 4583.
(72) Blum, L.; Huckaby, D. A.; Legault, M. *Electrochim. Acta* **1996**, *41*, 2207.
(73) Legault, M.; Blum, L.; Huckaby, D. A. *J. Electroanal. Chem.* **1996**, *409*, 79.
(74) Huckaby, D. A.; Legault, M. D.; Blum, L. *J. Chem. Phys.* **1998**, *109*, 3600.
(75) Xu, J. G.; Wang, X. W. *Surf. Sci.* **1998**, *408*, 317.
(76) Brow, G.; Rikvold, P. A.; Novotny, M. A.; Wieckowski, A. *J. Electrochem. Soc.* **1999**, *146*, 1035.
(77) Sánchez, C.; Leiva, E. P. M. *Electrochim. Acta* **1999**, *45*, 691.
(78) Horanyi, G.; Rizmayer, E. M.; Joo, P. *J. Electroanal. Chem.* **1977**, *152*, 211.
(79) Zelenay, P.; Rice-Jackson, L. M.; Wieckowski, A.; Gawlowski, J. *Surf. Sci.* **1991**, *256*, 253.
(80) Parry, D. B.; Samant, M. G.; Seki, H.; Philpott, M. R.; Ashley, K. *Langmuir* **1993**, *9*, 1878.
(81) Shi, Z.; Lipkowski, J.; Gamboa, M.; Zelenay, P.; Wieckowski. A. *J. Electroanal. Chem.* **1994**, *366*, 317.
(82) Magnussen, O. M.; Hageböck, J.; Hotlos J.; Behm, R. J. *Faraday Discuss. Chem. Soc.* **1992**, *94*, 329.
(83) Edens, G. J.; Gao, X, Weaver, M. J. *J. Electroanal. Chem.* **1994**, *375*, 357.
(84) Nishizawa, T.; Nakada, T.; Kinoshita, Y.; Miyashita, S.; Sazaki, G. *Surf. Sci.* **1996**, *367*, L73.
(85) Wyckhohh, R. G. W. *Crystal Structures*; Wiley: New York, **1963**; Vol. 1.
(86) Haiss, W.; Lackey, D.; Sass, J. K.; Meyer, H.; Nichols, R. J. *Chem. Phys. Lett.* **1992**, *200*, 343.
(87) Holzle, M. H.; Kolb, D. M. *Ber. Bunsen-Ges. Phys. Chem.* **1994**, *98*, 330.
(88) Holzle, M. H.; Apsel, C. W.; Will, T.; Kolb, D. M. *J. Electrochem. Soc.* **1995**, *142*, 3741.
(89) Adzic, G. D.; Scherson, D. A. *J. Electroanal. Chem.* **1989**, *263*, 421.
(90) Whelan, C. M.; Smyth, M. R.; Barnes, C. J. *J. Electroanal. Chem.* **1998**, *441*, 109.
(91) Rogers, A. T.; Krause, D. P.; Griess, J. C.; Ehrlinger, D. B. *J. Electrochem. Soc.* **1949**, *95*, 33.
(92) Lorenz, W. J.; Herman, H. D.; Wüthrich, N.; Hilbert, F. *J. Electrochem. Soc.* **1974**, *121*, 1167.
(93) White, J. H.; Albarelli, M. J.; Abruña, H. D.; Blum, L.; Melroy, O. R.; Sammant, M. G.; Borges, G. L.; Gordon, J. G., II. *J. Phys. Chem.* **1988**, *92*, 4433.
(94) Samant, M. G.; Borges, G.; Melroy, O. R. *J. Electrochem. Soc.* **1993**, *140*, 421.
(95) Chabala, E. D.; Rayment, T. *J. Chem. Soc., Faraday. Trans.* **1996**, *92*, 1277.
(96) Chabala, E. D.; Rayment, T. *J. Electroanal. Chem.* **1996**, *401*, 257.
(97) Chabala, E. D.; Ramadan, A. R.; Brunt, T.; Rayment, T. *J. Electroanal. Chem.* **1996**, *412*, 67.
(98) Chabala, E. D.; Rayment, T. *J. Chem. Soc., Faraday Trans.* **1996**, *92*, 4657.
(99) Lee, D.; Rayment, T. *Phys. Chem. Chem. Phys.* **1999**, *1*, 4389.
(100) Ramadan, A. R.; Chabala, E. D.; Rayment, T. *Chem. Phys. Phys. Chem.* **1999**, *1*, 1591.
(101) Endo, K.; Sugawara, Y.; Mishima, S.; Okada, T.; Morita, S. *Jpn. J. Appl. Phys.* **1991**, *30*, 2592.
(102) Hachiya, T.; Itaya, K. *Ultramicroscopy* **1992**, *42*, 445.
(103) Sugita, S.; Abe, T.; Itaya, K. *J. Phys. Chem.* **1993**, *97*, 8780.
(104) Ogaki, K.; Itaya, K. *Electrochim. Acta* **1995**, *40*, 1249.

(105) Corcora, S. G.; Chakarova, S. G.; Sieradzki, K. *Phys. Rev. Lett.* **1993**, *71*, 158.
(106) Corcora, S. G.; Chakarova, S. G.; Sieradzki, K. *J. Electroanal. Chem.* **1994**, *377*, 85.
(107) Garcia, S. J.; Salinas, D.; Mayer, C.; Vilche, J. R.; Pauling, H.-J.; Vinzelberg, S.; Staikov, G.; Lorenz, W. J. *Surf. Sci.* **1994**, *316*, 143.
(108) Ikemiya, N.; Yamada, K.; Hara, H. *Surf. Sci.* **1996**, *348*, 253.
(109) Garcia, S.; Salinas, D.; Mayer, C.; Schmidt, E.; Staikov, G.; Lorenz, W. J. *Electrochim. Acta* **1998**, *43*, 3007.
(110) Whelan, C. M.; Smyth, M. R.; Barnes, C. J.; Attard, G. A.; Yang, X. F. *J. Electroanal. Chem.* **1999**, *474*, 138.
(111) Esplandiu, M. J.; Schneeweiss, M. A.; Kolb, D. M. *Phys. Chem. Chem. Phys.* **1999**, *1*, 4847.
(112) Chen, C.-H.; Vesecky, S. M.; Gewirth; A. A. *J. Am. Chem. Soc.* **1992**, *114*, 451.
(113) Chen, C.-H.; Gewirth, A. A. *Ultramicroscopy* **1992**, *42*, 437.
(114) Mrozek, P.; Sung, Y.-E.; Han, M.; Gamboa-Aldeco, M.; Wieckowski, A.; Chen, C.-H.; Gewirth, A. A. *Electrochim. Acta* **1995**, *40*, 17.
(115) Uchida, H.; Miura, M.; Watanabe, M. *J. Electroanal. Chem.* **1995**, *386*, 261.
(116) Mrozek, P.; Sung, Y.-E.; Wieckowski, A. *Surf. Sci.* **1995**, *335*, 44.
(117) Stickney, J. L.; Rosasco, S. D.; Song, D.; Schardt, B. C.; Hubard, A. T. *Surf. Sci.* **1983**, *130*, 326.
(118) Hubard, A. T.; Stickney, J. L.; Rosasco, S. D.; Soriaga, M. P.; Song, D.; Schardt, B. C. *J. Electroanal. Chem.* **1983**, *150*, 165.
(119) Wieckowski, A.; Schardt, B. C.; Rosasco, S. D.; Stickney, J. L.; Hubard, A. T. *Surf. Sci.* **1984**, *146*, 115.
(120) Hamelin, A. *J. Electroanal. Chem.* **1979**, *101*, 285.
(121) Hamelin, A.; Katayama, A. *J. Electroanal. Chem.* **1981**, *117*, 221.
(122) Hamelin, A. *J. Electroanal. Chem.* **1984**, *165*, 167.
(123) Hamelin, A.; Lipkowski, J. *J. Electroanal. Chem.* **1984**, *171*, 317.
(124) Adzic, R.; Yeager, E.; Cahan, B. D. *J. Electrochem. Soc.* **1974**, *121*, 474.
(125) Engelsmann, K.; Lorenz, W. J.; Schmidt, E. *J. Electroanal. Chem.* **1980**, *114*, 1.
(126) Engelsmann, K.; Lorenz, W. J.; Schmidt, E. *J. Electroanal. Chem.* **1980**, *114*, 11.
(127) Rath, D. L. *J. Electroanal. Chem.* **1983**, *150*, 521.
(128) Green, M. P.; Lindau, I.; Carr, R.; Xing, X.; Hanson, K. J.; Scherson, D. A.; Richter, M.; Ross, P. N. *J. Microsc.* **1988**, *152*, 823.
(129) Green, M. P.; Hanson, K. J.; Scherson, D. A.; Xing, X.; Richter, M.; Ross, P. N.; Carr, R.; Lindau, I. *J. Phys. Chem.* **1989**, *93*, 2181.
(130) Green, M. P.; Hanson, K. J.; Carr, R.; Lindau, I. *J. Electrochem. Soc.* **1990**, *137*, 3493.
(131) Green, M. P.; Hanson, K. J. *Surf. Sci.* **1991**, *259*, L743.
(132) Binggeli, M.; Carnal, D.; Nyffenegger, R.; Siegenthaler, H.; Christoph, R.; Rohrer, H. *J. Vac. Sci. Technol. B* **1991**, *9*, 1985.
(133) Tao, N. J.; Pan, J.; Li, Y.; Oden, P. I.; Derose, J. A.; Lindsay, S. M. *Surf. Sci.* **1992**, *271*, L338.
(134) Robinson, K. M.; O'Grady, W. E. *Faraday Discuss.* **1993**, *95*, 55.
(135) Schmidt, U.; Vinzelberg, S.; Staikov, G. *Surf. Sci.* **1996**, *348*, 261.
(136) Chen, C.-H.; Washburn, N.; Gewirth, A. A. *J. Phys. Chem.* **1993**, *97*, 9754.
(137) Brunt, T. A.; Rayment, T.; O'Shea, S. J.; Welland, M. E. *Langmuir* **1996**, *12*, 5922.
(138) Samant, M. G.; Melroy, O. R.; Toney, M. F.; Borges, G. L.; Blum, L. *J. Phys. Chem.* **1988**, *92*, 220.
(139) Toney, M. F.; Gordon, J. G.; Sammant, M. G.; Borges, G. L.; Melroy, O. R.; Yee, D.; Sorensen, L. B. *J. Phys. Chem.* **1995**, *99*, 4733.
(140) Chabala, E. D.; Harji, B. H.; Rayment, T.; Archer, M. D. *Langmuir* **1992**, *8*, 2028.
(141) Clavilier, J.; Orts, J. M.; Feliu, J. M.; Aldaz, A. *J. Electroanal. Chem.* **1990**, *293*, 197.
(142) Feliu, J. M.; Fernández-Vega, A.; Orts, J. M.; Aldaz, A. *J. Chim. Phys.* **1991**, *88*, 1493.
(143) Melroy, O.; Kanazawa, K.; Gordon, J. G., II; Butry, D. *Langmuir* **1986**, *2*, 697.
(144) Deakin, M. R.; Melroy, O. *J. Electroanal. Chem.* **1988**, *239*, 321.
(145) Herrero, E.; Abruña, H. D. *Langmuir* **1997**, *13*, 4446.
(146) Herrero, E.; Abruña, H. D. *J. Phys. Chem. B* **1998**, *102*, 444.
(147) Inukai, J.; Sugita, S.; Itaya, K. *J. Electroanal. Chem.* **1996**, *403*, 159.
(148) Chen, C.-H.; Gewirth, A. A. *Phys. Rev. Lett.* **1992**, *68*, 1571.
(149) Li, J.; Abruña, H. D. *J. Phys. Chem. B* **1997**, *101*, 244.
(150) Li, J.; Abruña, H. D. *J. Phys. Chem. B* **1997**, *101*, 2907.
(151) Li, J.; Herrero, E.; Abruña, H. D. *J. Colloids Surf. A* **1998**, *134*, 113.
(152) Herrero, E.; Li, J.; Abruña, H. D. Structural and Kinetic Studies of Hg(UPD) On Au(111). In *The Electrochemical Double Layer*; Korzeniewski, C., Conway, B. E., Eds.; The Electrochemical Society: Pennington, NJ, 1997; Vol. 97-17, p 277.
(153) Abruña, H. D.; Feliu, J. M.; Brock, J. D.; Buller, L. J.; Herrero, E.; Li, J.; Gómez, R.; Finnefrock, A. *Electrochim. Acta* **1998**, *43*, 2899.
(154) Herrero, E.; Buller, L. J.; Li, J.; Finnefrock, A.; Salomón, A. B.; Alonso, C.; Brock, J. D.; Abruña, H. D. *Electrochim Acta* **1998**, *44*, 983.
(155) Yang, X.-M.; Tonami, K.; Nagahara, L. A.; Hashimoto, K.; Wei, Y.; Fujishima, A. *Surf. Sci.* **1995**, *324*, L363.
(156) Wang, J. X.; Adzic, R. R.; Ocko, B. M. *J. Phys. Chem.* **1994**, *8*, 7182.
(157) Wang, J. X.; Adzic, R. R.; Magnussen, O. M.; Ocko, B. M. *Surf. Sci.* **1995**, *335*, 120.
(158) Koos, D. A. *J. Electrochem. Soc.* **1989**, *136*, 218C.
(159) Koos, D. A.; Richmond, G. L. *J. Chem. Phys.* **1990**, *93*, 869.
(160) Adzic, R. R.; Wang, J. X. *J. Phys. Chem. B* **1998**, *102*, 6305.
(161) Wang, J. X.; Robinson, I. K.; Adzic, R. R. *Surf. Sci.* **1998**, *413*, 374.
(162) Niece, B. K.; Gewirth, A. A. *J. Phys. Chem. B* **1998**, *102*, 818.
(163) Chen, C.-H.; Gewirth, A. A. *J. Am. Chem. Soc.* **1992**, *114*, 5439.
(164) Chen, C.-H.; Kepler, K. D.; Gewirth, A. A.; Ocko, B. M.; Wang, J. *J. Phys. Chem.* **1993**, *97*, 7291.
(165) Morin, S.; Lachenwitzer, A.; Moller, F. A.; Magnussen, O. M.; Behm, R. J. *J. Electrochem. Soc.* **1999**, *146*, 1013.
(166) Moniwa, S.; Aramata, A. *J. Electroanal. Chem.* **1994**, *376*, 203.
(167) Nakamura, N.; Aramata, A.; Yamagishi. A.; Taniguchi, M. *J. Electroanal. Chem.* **1998**, *446*, 227.
(168) Aramata, A.; Taguchi, S.; Fukuda, T.; Nakamura, M.; Horanyi, G. *Electrochim. Acta* **1998**, *44*, 999.
(169) Takahashi, S.; Hasebe, K.; Aramata, A. *Electrochem. Commun.* **1999**, *1*, 301.
(170) Huang, H.; Zhao, M.; Xing, X.; Bae, I. T.; Scherson, D. A. *J. Electroanal. Chem.* **1990**, *293*, 279.
(171) Xing, X. K.; Scherson, D. A.; Mak, C. *J. Electrochem. Soc.* **1990**, *137*, 2166.
(172) Suggs, D. W.; Stickney, J. L. *Surf. Sci.* **1993**, *290*, 362.
(173) Suggs, D. W.; Stickney, J. L. *Surf. Sci.* **1993**, *290*, 375.
(174) Bondos, J. C.; Gewirth, A. A.; Nuzzo, R. G. *J. Phys. Chem.* **1996**, *100*, 8617.
(175) Gichuchi, A.; Boone, B. E.; Demir, U.; Shannon, C. *J. Phys. Chem. B* **1998**, *102*, 6499.
(176) Rodes, A.; Herrero, E.; Feliu, J. M.; Aldaz, A. *J. Chem. Soc., Faraday Trans.* **1996**, *92*, 3796.
(177) Lister, T. E.; Stickney, J. L. *J. Phys. Chem.* **1996**, *100*, 19568.
(178) Suggs, D. W.; Stickney, J. L. *J. Phys. Chem.* **1991**, *95*, 10056.
(179) Ikemiya, N.; Iwai, D.; Yamada, K.; Vidu, R.; Hara, S. *Surf. Sci.* **1996**, *369*, 199.
(180) Yagi, I.; Nakabayashi, S.; Uosaki, K. *Surf. Sci.* **1998**, *406*, 1.
(181) Yagi, I.; Nakabayashi, S.; Uosaki K. *J. Phys. Chem. B* **1998**, *102*, 2677.
(182) Hyden, B. E.; Nandhakuma, I. S. *J. Phys. Chem. B* **1998**, *102*, 4897.
(183) Jung, G.; Rhee, C. K. *J. Electroanal. Chem.* **1998**, *436*, 277.
(184) Villegas, I.; Stickney, J. *J. Electrochem Soc.* **1992**, *139*, 686.
(185) Villegas, I.; Stickney, J. *J. Vac. Sci. Technol. A* **1992**, *10*, 3032.
(186) Colleti, L. P.; Flowers, B. H.; Stickney, J. L. *J. Electrochem. Soc.* **1998**, *145*, 1442.
(187) Lister, T. E.; Colleti, L. P.; Stickney, J. L. *Isr. J. Chem.* **1997**, *37*, 287.
(188) Colleti, L. P.; Stickney, J. L. *J. Electrochem. Soc.* **1998**, *145*, 3594.
(189) Scortichini, C. L.; Reilley, C. N. *J. Electroanal. Chem.* **1982**, *139*, 247.
(190) Scortichini, C. L.; Reilley, C. N. *J. Electroanal. Chem.* **1982**, *139*, 265.
(191) Scortichini, C. L.; Reilley, C. N. *J. Electroanal. Chem.* **1983**, *152*, 255.
(192) Andricacos, P. C.; Ross, P. N. *J. Electroanal. Chem.* **1984**, *167*, 301.
(193) Leung, L. H.; Gregg, T. W.; Goodman, D. W. *Langmuir* **1991**, *7*, 3205.
(194) Leung, L. H.; Gregg, T. W.; Goodman, D. W. *Chem. Phys. Lett.* **1992**, *188*, 467.
(195) Kolb, D. M.; Al Jaaf-Golze, K.; Zei, M. S. *DECHEMA Monogr.* **1986**, *12*, 53.
(196) Stickney, J. L.; Rosasco, S.; Hubbard, A. T. *J. Electrochem. Soc.* **1984**, *131*, 260.
(197) Markovic, N. M.; Ross, P. N. *J. Vac. Sci. Technol.* **1993**, *11*, 2225.
(198) Markovic, N. M.; Ross, P. N. *Langmuir* **1993**, *9*, 580.
(199) Markovic, N. M.; Gasteiger, H. A.; Lucas, C. A.; Tidswell, I. M.; Ross, P. N. *Surf. Sci.* **1995**, *335*, 91.
(200) Markovic, N. M.; Gasteiger, H. A.; Ross, P. N. *Langmuir* **1995**, *11*, 4098.
(201) White, J. H.; Abruña, H. D. *J. Phys. Chem.* **1990**, *94*, 894.
(202) Gómez, R.; Feliu, J. M.; Abruña, H. D. *J. Phys. Chem.* **1994**, *98*, 5514.
(203) Gómez, R.; Yee, H. S.; Bommarito, G. M.; Feliu, J. M.; Abruña, H. D. *Surf. Sci.* **1995**, *335*, 101.
(204) White, J. H.; Abruña, H. D. *J. Electroanal. Chem.* **1991**, *300*, 521.

(205) Bhatt, D. P.; Twomey, T.; Plieth, W.; Schumacher, R.; Meyer, H. *J. Electroanal. Chem.* **1992**, *322*, 279.
(206) Dakkouri, A. S.; Batina, N.; Kolb, D. M. *Electrochim. Acta* **1993**, *38*, 2467.
(207) Scortichini, C. L.; Reilley, C. N. *J. Electroanal. Chem.* **1982**, *139*, 233.
(208) Al-Akl, A.; Attard, G.; Price, R.; Timothy, B. *J. Chem. Soc., Faraday Trans.* **1995**, *91*, 3585.
(209) Nishihara, C.; Nozoye, H. *J. Electroanal. Chem.* **1995**, *386*, 75.
(210) Nishihara, C.; Nozoye, H. *J. Electroanal. Chem.* **1995**, *396*, 139.
(211) Gómez, R.; Feliu, J. M.; Abruña, H. D. *Langmuir* **1994**, *10*, 4315.
(212) Buller, L. J.; Herrero, E.; Gómez, R.; Feliu, J. M.; Abruña, H. D. *J. Chem. Soc., Faraday Trans.* **1996**, *92*, 3757.
(213) Wang, C.; Chung, C.; Chang, S. *J. Electroanal. Chem.* **1995**, *395*, 317.
(214) Kolb, D. M.; Kotz, R.; Yamamoto, K. *Surf. Sci.* **1979**, *87*, 20.
(215) Kolb, D. M.; Kotz, R.; Rath, D. L. *Surf. Sci.* **1980**, *101*, 490.
(216) Varga, K.; Zelenay, P.; Wieckowski, A. *J. Electroanal. Chem.* **1992**, *330*, 453.
(217) Zelenay, P.; Wieckowski, A. *J. Electrochem. Soc.* **1992**, *139*, 2552.
(218) Sashikata, K.; Furuya, N.; Itaya, K. *J. Electroanal. Chem.* **1991**, *316*, 361.
(219) Shingaya, Y.; Matsumoto, H.; Ogasawara, H.; Ito, M. *Surf. Sci.* **1995**, *335*, 23.
(220) Beitel, G.; Magnussen, O. M.; Behm, R. J. *Surf. Sci.* **1995**, *336*, 19.
(221) Ogasawara, H.; Inukai, J.; Ito, M. *Surf. Sci.* **1994**, *311*, L665.
(222) Yee, H. S.; Abruña, H. D. *J. Phys. Chem.* **1993**, *97*, 6278.
(223) Yee, H. S.; Abruña, H. D. *J. Phys. Chem.* **1994**, *98*, 6552.
(224) White, J. H.; Abruña, H. D. *J. Electroanal. Chem.* **1989**, *274*, 185.
(225) Yee, H. S.; Abruña, H. D. *Langmuir* **1993**, *9*, 2460.
(226) Durand, R.; Faure, R.; Aberdam, D.; Salem, C.; Tourillon, G.; Guay, D.; Ladouceur, M. *Electrochim. Acta* **1992**, *37*, 1977.
(227) Lucas, C. A.; Markovic, N. M.; Tidswell, I. M.; Ross, P. N. *Physica B* **1996**, *221*, 245.
(228) Tidswell, I. M.; Lucas, C. A.; Markovic, N. M.; Ross, P. N. *Phys. Rev. B* **1995**, *51*, 10205.
(229) Finnefrock, A. C.; Buller, L. J.; Ringland, K.; Brock, J. D.; Abruña, H. D. *J. Am. Chem. Soc.* **1997**, *119*, 11703.
(230) Finnefrock, A. C.; Ringland, K. L.; Brock, J. D.; Buller, L. J.; Abruña, H. D. *Phys. Rev. Lett.* **1998**, *81*, 3459.
(231) Markovic, N. M.; Grgur, B. N.; Lucas, C. A.; Ross, P. N. *Electrochim. Acta* **1998**, *44*, 1009.
(232) Michaelis, R.; Zei, M. S.; Zhai, R. S.; Kolb, D. M. *J. Electroanal. Chem.* **1992**, *339*, 299.
(233) Michaelis, R.; Kolb, D. M. *J. Electroanal. Chem.* **1992**, *328*, 341.
(234) Aberdam, D.; Gauthier, Y.; Durand, R.; Faure, R. *Surf. Sci.* **1994**, *306*, 114.
(235) Aberdam, D.; Durand, R.; Faure, R.; El Omar, F. *Surf. Sci.* **1985**, *162*, 782.
(236) Zei, M. S.; Wu, K.; Eiswirth, M.; Ertl, G. *Electrochim. Acta* **1999**, *45*, 809.
(237) Zei, M. S. *Z. Phys. Chem.* **1999**, *208*, 77.
(238) Buller, L. J.; Herrero, E.; Gómez, R.; Feliu, J. M.; Abruña, H. D. *J. Phys. Chem. B* **2000**, *104*, 5932.
(239) Wieckowski, A.; Rosasco, S. D.; Schardt, B. C.; Stickney, J. L.; Hubbard, A. T. *Inorg. Chem.* **1984**, *23*, 565.
(240) El Omar, F.; Durand, R.; Faure, R. *J. Electroanal. Chem.* **1984**, *160*, 385.
(241) Gibson, N. C.; Saville, P. M.; Harrington, D. A. *J. Electroanal. Chem.* **1991**, *318*, 271.
(242) Rodriguez, J. F.; Taylor, D. L.; Abruña, H. D. *Electrochim. Acta* **1993**, *38*, 235.
(243) Zelenay, P.; Gamboa-Aldeco, M.; Horanyi, G.; Wieckowski, A. *J. Electroanal. Chem.* **1993**, *357*, 307.
(244) Taylor, D. L.; Abruña, H. D. *J. Electrochem. Soc.* **1993**, *140*, 3402.
(245) Kimizuka, N.; Itaya, K. *Faraday Discuss.* **1992**, *94*, 117.
(246) Shinotsuka, N.; Sashikata, K.; Itaya, K. *Surf. Sci.* **1995**, *335*, 75.
(247) Wang, J. X.; Marinkovic, N. S.; Adzic, R. R.; Ocko, B. M. *Surf. Sci.* **1998**, *398*, L291.
(248) Marinkovic, N. S.; Wang, J. X.; Marinkovic, J. S.; Adzic, R. R. *J. Phys. Chem.* **1999**, *103*, 139.
(249) Stickney, J. L.; Rosasco, S. D.; Schardt, B. C.; Hubbard, A. T. *J. Phys. Chem.* **1984**, *88*, 251.
(250) Durand, R.; Faure, R.; Aberdam, D.; Traore, S. *Electrochim. Acta* **1989**, *34*, 1653.
(251) Aberdam, D.; Salem, C.; Durand, R.; Faure, R. *Surf. Sci.* **1990**, *239*, 71.
(252) Frank, D. G.; Golden, T.; Chyan, O. M. R.; Hubbard, A. T. *Appl. Surf. Sci.* **1991**, *48/49*, 166.
(253) Frank, D. G.; Chyan, O. M. R.; Golden, T.; Hubbard, A. T. *J. Phys. Chem.* **1994**, *98*, 1895.
(254) Clavilier, J.; Feliu, J. M.; Aldaz, A. *J. Electroanal. Chem.* **1988**, *243*, 419.
(255) Clavilier, J.; Aldaz, A.; Feliu, J. M.; Fernández-Vega, A. *J. Electroanal. Chem.* **1989**, *269*, 175.
(256) Gómez, R.; Fernández-Vega, A.; Feliu, J. M.; Aldaz, A. *J. Phys. Chem.* **1993**, *97*, 4769.
(257) Dollard, L.; Evans, R. W.; Attard, G. A. *J. Electroanal. Chem.* **1993**, *345*, 205.
(258) Evans, R. W.; Attard, G. A. *J. Electroanal. Chem.* **1993**, *345*, 337.
(259) Smith, S. P. E.; Abruña, H. D. *J. Phys. Chem. B* **1998**, *102*, 3506.
(260) Smith, S. P. E.; Abruña, H. D. *J. Phys. Chem. B* **1999**, *103*, 6764.
(261) Hamm, U. W.; Kramer, D.; Zhai, R. S.; Kolb, D. M. *Electrochim. Acta* **1998**, *43*, 2969.
(262) Paffett, M. T.; Campbell, C. T.; Taylor, T. N. *J. Chem. Phys.* **1986**, *85*, 6176.
(263) Haner, A. N.; Ross, P. N. *J. Phys. Chem.* **1991**, *95*, 3740.
(264) Stickney, J. L.; Schardt, B. C.; Stern, D. A.; Wieckowski, A.; Hubbard, A. T. *J. Electrochem. Soc.* **1986**, *133*, 648.
(265) Campbell, S. A.; Parsons, R. *J. Chem. Soc., Faraday Trans.* **1992**, *88*, 833.
(266) Feliu, J. M.; Gómez, R.; Llorca, M. J.; Aldaz, A. *J. Electroanal. Chem.* **1993**, *289*, 152.
(267) Feliu, J. M.; Clavilier, J.; Aldaz, A.; Fernández-Vega, A. *J. Electroanal. Chem.* **1988**, *256*, 149.
(268) Clavilier, J.; Feliu, J. M.; Fernández-Vega, A.; Aldaz, A. *J. Electroanal. Chem.* **1990**, *294*, 193.
(269) Jung, G. Y.; Park, H. S.; Rhee, C. K. *J. Electroanal. Chem.* **1998**, *453*, 243.
(270) Gómez, R.; Llorca, M. J.; Feliu, J. M.; Aldaz, A. *J. Electroanal. Chem.* **1992**, *340*, 349.
(271) Clavilier, J.; Petit, M.; Ganon, J. P. *J. Electroanal. Chem.* **1989**, *265*, 231.
(272) Wheeler, D. R.; Wang, J. X.; Adzic, R. R. *J. Electroanal. Chem.* **1995**, *387*, 115.
(273) Marinkovic, N. S.; Fawcett, W. R.; Wang, J. X.; Adzic, R. R. *J. Phys. Chem.* **1995**, *99*, 17490.
(274) Attard, G. A.; Bannister, A. *J. Electroanal. Chem.* **1991**, *300*, 467.
(275) Clavilier, J.; Llorca, M. J.; Feliu, J. M.; Aldaz, A. *J. Electroanal. Chem.* **1991**, *310*, 429.
(276) Llorca, M. J.; Feliu, J. M.; Aldaz, A. *J. Electroanal. Chem.* **1993**, *351*, 299.
(277) Attard, G. A.; Price, R.; Al-Akl, A. *Electrochim. Acta* **1994**, *39*, 1525.
(278) El Omar, F.; Durand, R. *J. Electroanal. Chem.* **1984**, *178*, 343.
(279) Adzic, R. R.; Wang, J.; Vitus, C. M.; Ocko, B. M. *Surf. Sci.* **1993**, *293*, L876.
(280) Borup, R. L.; Sauer, D. E.; Stuve, E. M. *Surf. Sci.* **1993**, *293*, 10.
(281) Borup, R. L.; Sauer, D. E.; Stuve, E. M. *Surf. Sci.* **1993**, *293*, 27.
(282) Markovic, N. M.; Grgur, B. N.; Lucas, C. A.; Ross, P. N. *J. Electroanal. Chem.* **1998**, *448*, 183.
(283) Markovic, N. M.; Grgur, B. N.; Lucas, C. A.; Ross, P. N. *J. Chem. Soc., Faraday Trans.* **1998**, *94*, 3373.
(284) Nishihara, C.; Iwata, K.; Tai, T.; Yuasa, M.; Sekine, I.; Nozoye, H. *Electrochem. Commun.* **1999**, *1*, 104.
(285) Herrero, E.; Li, J.; Abruña, H. D. *Electrochim. Acta* **1999**, *44*, 2385.
(286) Taguchi, S.; Aramata, A.; Quaiyyum, M. A.; Enyo, M. *J. Electroanal. Chem.* **1994**, *374*, 275.
(287) Taguchi, S.; Aramata, A. *J. Electroanal. Chem.* **1995**, *396*, 131.
(288) Taguchi, S.; Aramata, A. *J. Electroanal. Chem.* **1998**, *457*, 73.
(289) Varga, K.; Zelenay, P.; Horanyi, G.; Wieckowski, A. *J. Electroanal. Chem.* **1992**, *327*, 291.
(290) Will, F. G. *J. Electrochem. Soc.* **1965**, *112*, 451.
(291) Woodard, F. E.; Scortichini, C. L.; Reilley, C. N. *J. Electroanal. Chem.* **1983**, *151*, 109.
(292) Markovic, N.; Hanson, M.; McDougall, G.; Yeager, E. *J. Electroanal. Chem.* **1986**, *214*, 555.
(293) Kita, H.; Ye, S.; Aramata, A.; Furuya, N. *J. Electroanal. Chem.* **1990**, *295*, 317.
(294) Ogasawara, H.; Ito, M. *Chem. Phys. Lett.* **1994**, *221*, 213.
(295) Love, B.; Seto, K.; Lipkowski, J. *J. Electroanal. Chem.* **1986**, *199*, 219.
(296) Adzic, R. R.; Feddrix, F.; Nikolik, B. Z.; Yeager, E. *J. Electroanal. Chem.* **1992**, *341*, 287.
(297) Clavilier, J.; Armand, D.; Sun, S. G.; Petit, M. *J. Electroanal. Chem.* **1986**, *205*, 267.
(298) Love, B.; Seto, K.; Lipkowski, J. *Rev. Chem. Intermed.* **1987**, *8*, 87.
(299) Al Jaaf-Golze, K.; Kolb, D. M.; Scherson, D. *J. Electroanal. Chem.* **1986**, *200*, 353.
(300) Clavilier, J.; Faure, R.; Guinet, G.; Durand, R. *J. Electroanal. Chem.* **1980**, *107*, 205.
(301) Armand, D.; Clavilier, J. *J. Electroanal. Chem.* **1989**, *263*, 109.
(302) Armand, D.; Clavilier, J. *J. Electroanal. Chem.* **1987**, *225*, 205.
(303) Nishihara, C.; Nozoye, H. *J. Electroanal. Chem.* **1994**, *379*, 527.
(304) Clavilier, J.; Rodes, A.; El Achi, K.; Zamakchari, M. A. *J. Chim. Phys.* **1991**, *88*, 1291.
(305) Clavilier, J.; Durand, R.; Guinet, G.; Faure, R. *J. Electroanal. Chem.* **1981**, *127*, 281.
(306) Clavilier, J.; Armand, D. *J. Electroanal. Chem.* **1986**, *199*, 187.
(307) Clavilier, J.; El Achi, K.; Rodes, A. *Chem. Phys.* **1990**, *141*, 1.

(308) Hubbard, A. T.; Ishikawa, R. M.; Katekaru, J. *J. Electroanal. Chem.* **1978**, *86*, 271.
(309) Adzic, R. R.; Tripkovic, A. V.; Vesovic, V. B. *J. Electroanal. Chem.* **1986**, *204*, 329.
(310) Clavilier, J. *J. Electroanal. Chem.* **1980**, *107*, 211.
(311) Yamamoto, K.; Kolb, D. M.; Kotz, R.; Lehmpfuhl, G. *J. Electroanal. Chem.* **1979**, *96*, 233.
(312) Homa, A. S.; Yeager, E.; Cahan, B. D. *J. Electroanal. Chem.* **1983**, *150*, 181.
(313) Ross, P. N. *J. Electrochem. Soc.* **1979**, *126*, 67.
(314) Parsons, R.; Ritzoulis, G. *J. Electroanal. Chem.* **1991**, *318*, 1.
(315) Ross, P. N. *Surf. Sci.* **1981**, *102*, 463.
(316) Motoo, S.; Furuya, N. *Ber. Bunsen-Ges. Phys. Chem.* **1987**, *91*, 457.
(317) Markovic, N. M.; Marinkovic, N. S.; Adzic, R. R. *J. Electroanal. Chem.* **1988**, *241*, 309.
(318) Furuya, N.; Koide, S. *Surf. Sci.* **1989**, *220*, 18.
(319) Rodes, A.; El Achi, K.; Zamakchari, M. A.; Clavilier, J. *J. Electroanal. Chem.* **1990**, *284*, 245.
(320) Clavilier, J.; El Achi, K.; Rodes, A. *J. Electroanal. Chem.* **1989**, *272*, 253.
(321) Angerstein-Kozlowska, H.; Conway, B. E. *J. Electroanal. Chem.* **1979**, *95*, 1.
(322) Bewick, A.; Thomas, B. *J. Electroanal. Chem.* **1976**, *70*, 239.
(323) Bewick, A.; Thomas, B. *J. Electroanal. Chem.* **1977**, *84*, 127.
(324) Bort, H.; Jüttner, K.; Lorenz, W. J. *J. Electroanal. Chem.* **1978**, *90*, 413.
(325) Lorenz, W. J.; Schmidt, E.; Staikov, G.; Bort, H. *Symp. Faraday Soc.* **1978**, *12*, 14.
(326) Staikov, G.; Jüttner, K.; Lorenz, W. J.; Budevski, E. *Electrochim. Acta* **1978**, *23*, 319.
(327) Siegenthaler, H.; Jüttner, K. *Electrochim. Acta* **1979**, *24*, 109.
(328) Takayanagi, K.; Kolb, D. M.; Kambe, K.; Lehmpfuhl, G. *Surf. Sci.* **1980**, *100*, 407.
(329) Klimmeck, M.; Jüttner, K. *Electrochim. Acta* **1982**, *27*, 83.
(330) Schmidt, E.; Siegenthaler, H. *J. Electroanal. Chem.* **1983**, *150*, 59.
(331) Jovicevic, J. N.; Jovic, V. D.; Despic, A. R. *Electrochim. Acta* **1984**, *29*, 1625.
(332) Batina, N.; Cosovic, B.; Adzic, R. *J. Electroanal. Chem.* **1985**, *184*, 427.
(333) Jovic, V. D.; Jovicevic, J. N.; Despic, A. R. *Electrochim. Acta* **1985**, *30*, 1455.
(334) Vitanov, T.; Popov, A.; Staikov, G.; Budevski, E.; Lorenz, W. J.; Schmidt, E. *Electrochim. Acta* **1986**, *31*, 981.
(335) Jüttner, K. *Electrochim. Acta* **1986**, *31*, 917.
(336) Popov, A.; Dimitrov, N.; Velev, O.; Vitanov, T.; Budevski, E.; Schmidt, E.; Siegenthaler, H. *Electrochim. Acta* **1989**, *34*, 265.
(337) Jovic, V. D.; Jovic, B. M.; Despic, A. R. *J. Electroanal. Chem.* **1990**, *288*, 229.
(338) Dimitrov, N.; Popov, A.; Vitanov, T.; Budevski, E. *Electrochim. Acta* **1991**, *36*, 2077.
(339) Dimitrov, N.; Popov, A.; Kashchiev, D.; Vitanov, T.; Budevski, E. *Electrochim. Acta* **1991**, *36*, 1259.
(340) Dimitrov, N.; Popov, A.; Kashchiev, D.; Vitanov, T. *Electrochim. Acta* **1994**, *39*, 957.
(341) Popov, A.; Dimitrov, N.; Vitanov, T.; Kashchiev, D.; Budevski, E. *Electrochim. Acta* **1995**, *40*, 1495.
(342) Popov, A. *Electrochim. Acta* **1995**, *40*, 551.
(343) Stevenson, K. J.; Hatchett, D. W.; White, H. S. *Langmuir* **1996**, *12*, 494.
(344) Koos, D. A.; Shannon, V. L.; Richmond, G. L. *J. Phys. Chem.* **1990**, *94*, 2091.
(345) Höpfner, M.; Obretenov, W.; Jüttner, K.; Lorenz, W. J.; Staikov, G.; Bostanov, V.; Budevski, E. *Surf. Sci.* **1991**, *248*, 225.
(346) Obretenov, W.; Schmidt, U.; Lorenz, W. J.; Staikov, G.; Budevski, E.; Carnal, D.; Müller, U.; Siegenthaler, H.; Schmidt, E. *Faraday Discuss.* **1992**, *94*, 107.
(347) Lorenz, W. J.; Gassa, L. M.; Schmidt, U.; Obretenov, W.; Staikov, G.; Bostanov, V.; Budevski, E. *Electrochim. Acta* **1992**, *37*, 2173.
(348) Müller, U.; Carnal, D.; Siegenthaler, H.; Schmidt, E.; Lorenz, W. J.; Obretenov, W.; Schmidt, U.; Staikov, G.; Budevski, E. *Phys. Rev. B* **1992**, *46*, 12899.
(349) Obretenov, W.; Schmidt, U.; Lorenz, W. J.; Staikov, G.; Budevski, E.; Carnal, D.; Müller, U.; Siegenthaler, H.; Schmidt, E. *J. Electrochem. Soc.* **1993**, *140*, 692.
(350) Staikov, G.; Jüttner, K.; Lorenz, W. J.; Budevski, E. *Electrochim. Acta* **1994**, *39*, 1019.
(351) Müller, U.; Carnal, D.; Siegenthaler, H.; Schmidt, E.; Lorenz, W. J.; Obretenov, W.; Schmidt, U.; Staikov, G.; Budevski, E. *Phys. Rev. B* **1994**, *49*, 7795.
(352) Carnal, D.; Oden, P. I.; Müller, U.; Schmidt, E.; Siegenthaler, H. *Electrochim. Acta* **1995**, *40*, 1223.
(353) Sackmann, J.; Bunk, A.; Potzschke, R. T.; Staikov, G.; Lorenz, W. J. *Electrochim. Acta* **1998**, *43*, 2863.
(354) Samant, M. G.; Borges, G. L.; Gordon, J. G.; Melroy, O. R.; Blum, L. *J. Am. Chem. Soc.* **1987**, *109*, 5970.
(355) Fleischmann, M.; Mao, B. W. *J. Electroanal. Chem.* **1988**, *247*, 297.
(356) Samant, M. G.; Toney, M. F.; Borges, G. L.; Blum, L.; Melroy, O. R. *J. Phys. Chem.* **1988**, *92*, 220.
(357) Samant, M. G.; Toney, M. F.; Borges, G. L.; Blum, L.; Melroy, O. R. *Surf. Sci.* **1988**, *193*, L29.
(358) Melroy, O. R.; Toney, M. F.; Borges, G. L.; Samant, M. G.; Kortright, J. B.; Ross, P. N.; Blum, L. *Phys. Rev. B* **1988**, *38*, 10 962.
(359) Melroy, O. R.; Toney, M. F.; Borges, G. L.; Samant, M. G.; Kortright, J. B.; Ross, P. N.; Blum, L. *J. Electroanal. Chem.* **1989**, *258*, 403.
(360) Chabala, E. D.; Rayment, T. *Langmuir* **1994**, *10*, 4324.
(361) Toney, M. F.; Gordon, J. G.; Samant, M. G.; Borges, G. L.; Melroy, O. R.; Yee, D.; Sorenson, L. B. *J. Phys. Chem.* **1995**, *99*, 4733.
(362) Laguren-Davidson, L.; Lu, F.; Salaita, G. N.; Hubbard, A. T. *Langmuir* **1988**, *4*, 224.
(363) Hanson, M. E.; Yeager, E. *ACS Symp. Series* **1988**, *378*, 398.
(364) Popov, A.; Dimitrov, N.; Kashchiev, D.; Vitanov, T.; Budevski, E. *Electrochim. Acta* **1989**, *34*, 269.
(365) Popov, A.; Dimitrov, N.; Kashchiev, D.; Vitanov, T.; Budevski, E. *Electrochim. Acta* **1993**, *38*, 387.
(366) Leiva, E.; Schmickler, W. *Electrochim. Acta* **1994**, *39*, 1015.
(367) Hilbert, F.; Mayer, C.; Lorenz, W. J. *J. Electroanal. Chem.* **1973**, *47*, 167.
(368) Bewick, A.; Thomas, B. *J. Electroanal. Chem.* **1975**, *65*, 911.
(369) Jüttner, K.; Siegenthaler, H. *Electrochim. Acta* **1978**, *23*, 971.
(370) Siegenthaler, H.; Jüttner, K.; Schmidt, E.; Lorenz, W. J. *Electrochim. Acta* **1978**, *23*, 1009.
(371) Mao, B. W.; Tian, Z. Q.; Fleischmann, M. *Electrochim. Acta* **1992**, *37*, 1767.
(372) Waszcsuk, P.; Wnuk, A.; Sobkowski, J. *Electrochim. Acta* **1999**, *44*, 1789.
(373) Toney, M. F.; Gordon, J. G.; Samant, M. G.; Borges, G. L.; Melroy, O. R.; Kau, L.-S.; Wiesler, D. G.; Yee, D.; Sorenson, L. B. *Phys. Rev. B* **1990**, *42*, 5594.
(374) Toney, M. F.; Gordon, J. G.; Samant, M. G.; Borges, G. L.; Melroy, O. R.; Yee, D.; Sorenson, L. B. *Phys. Rev. B* **1992**, *45*, 9362.
(375) Wang, J. X.; Adzic, R. R.; Magnussen, O. M.; Ocko, B. M. *Surf. Sci.* **1995**, *344*, 111.
(376) Miragliotta, J.; Furtak, T. E. *Surf. Interface Anal.* **1989**, *14*, 53.
(377) Leiva, E. *Surf. Sci.* **1995**, *335*, 83.
(378) Schultze, J. W.; Brenske, K. R. *J. Electroanal. Chem.* **1982**, *137*, 331.
(379) Toney, M. F.; Gordon, J. G.; Samant, M. G.; Borges, G. L.; Wiesler, D. G. *Langmuir* **1991**, *7*, 796.
(380) Bort, H.; Jüttner, K.; Lorenz, W. J.; Staikov, G. *Electrochim. Acta* **1983**, *28*, 993.
(381) Xing, X.; Scherson, D. A.; Mak, C. *J. Electrochem. Soc.* **1990**, *137*, 2166.
(382) Foreti, M. L.; Pezzatini, G.; Cavallini, M.; Aloisi, G.; Innocenti, M.; Guidelli, R. *J. Phys. Chem. B* **1998**, *102*, 7413.
(383) Dietterle, M.; Will, T.; Kolb, D. M. *Surf. Sci.* **1995**, *342*, 29.
(384) Dietterle, M.; Will, T.; Kolb, D. M. *Surf. Sci.* **1998**, *396*, 189.
(385) Delpopolo, M.; Leiva, E. *J. Electroanal. Chem.* **1997**, *440*, 271.

CR9600363